

Thermally driven phase transitions in biomolecular systems

Nathalie MERTENS

Promotor: Prof. C. Glorieux

Proefschrift ingediend tot het
behalen van de graad van
Master of Science in de Fysica

Academiejaar 2013-2014

© Copyright by KU Leuven

Without written permission of the promotor and the authors it is forbidden to reproduce or adapt in any form or by any means any part of this publication. Requests for obtaining the right to reproduce or utilize parts of this publication should be addressed to KU Leuven, Faculteit Wetenschappen, Geel Huis, Kasteelpark Arenberg 11 bus 2100, 3001 Leuven (Heverlee), Telephone +32 16 32 14 01.

A written permission of the promotor is also required to use the methods, products, schematics and programs described in this work for industrial or commercial use, and for submitting this publication in scientific contests.

Vulgariserende samenvatting

In deze masterproef wordt onderzoek gedaan naar faseovergangen in verschillende biomoleculaire systemen. Faseovergangen worden geobserveerd wanneer een systeem een temperatuursverandering ondergaat. Ijs zal bijvoorbeeld smelten wanneer het opgewarmd wordt en ondergaat dus een faseovergang van een vaste fase naar een vloeibare fase. Elke faseovergang gaat gepaard met een verandering in structuur en eigenschappen. Net zoals in water zijn er ook faseovergangen geobserveerd in biomoleculaire systemen zoals lipiden en proteïnen. Deze faseovergangen worden gemeten via een calorimeter die de warmtecapaciteit meet gedurende de experimenten. De warmtecapaciteit geeft weer hoeveel energie moet toegevoegd worden om de temperatuur met één Kelvin te veranderen. Wanneer het systeem een faseovergang ondergaat, zal een scherpe piek geobserveerd worden in de temperatuursevolutie van de warmtecapaciteit. Elke faseovergang bevat een hoeveelheid energie, weergegeven via de enthalpie, die overeenkomt met de oppervlakte onder de overgangspiek. Beide thermodynamische eigenschappen worden via de Peltier-gebaseerde adiabatisc scan techniek gemeten. Deze geeft, met een grote nauwkeurigheid, de temperatuur van de faseovergang weer, alsook de thermodynamische eigenschappen. Via deze nauwkeurige techniek worden faseovergangen in een membraan, bestaande uit een dubbele laag van lipiden, onderzocht. Deze lipiden bevatten een polair hoofd en een apolaire (dubbele) staart, drie verschillende (fosfo)lipiden (DMPC, DPPC en DSPC) worden geanalyseerd. Ze bevatten elk een fosfor-hoofd en een koolwaterstof-staart met een toenemende lengte volgens oplisting. Vier verschillende fasen zijn geobserveerd volgens toenemende temperatuur: een subgel fase, een gel fase, een rimpel-gel fase en een vloeibare fase. De orde in de structuur van deze membranen neemt af bij een toenemende temperatuur, bovendien worden de overgangen geobserveerd bij hogere temperaturen wanneer de staart van de lipiden langer is. Het onderzoek wordt uitgebreid wanneer de verschillende lipiden worden gemengd, waardoor de resultaten worden beïnvloed. De rimpel-gel fase wordt niet meer geobserveerd, en de overgang tussen de gel- en de vloeibare fase vindt plaats over een bredere temperatuursinterval. Tijdens deze overgang bevindt het mengsel zich in een tweefasen systeem (gel en vloeibaar). Naast deze mengsels wordt de invloed van cholesterol op de fasen van een lipidemembraan bestudeerd. Ook hier verdwijnt de rimpel-gel fase en wordt de overgang tussen de gel- en de vloeibare fase aangetast. Door de interactie tussen de lipiden en cholesterol ontstaat een nieuwe fase die noch in de zuivere lipidemembraan, noch in de lipide mengsels, geobserveerd wordt. Deze fase bevat zowel eigenschappen van de vloeibare (minder geordende) fase als van de gel (meer geordende) fase. Tenslotte wordt een onderzoek gedaan op menselijk bloedplasma, dat rijk is aan zowel lipiden als aan proteïnen. Elk onderdeel van dit complex systeem ondergaat een faseovergang bij een welbepaalde temperatuur, hierdoor worden verschillende pieken in de temperatuursevolutie van de warmtecapaciteit geobserveerd. De bepaling van al deze verschillende fasen, met een hoge nauwkeurigheid, in deze biomoleculaire systemen maakt deze thesis interessant. Zowel lipiden, proteïnen als bloedplasma zijn belangrijke componenten in het menselijk lichaam en dragen, afhankelijk van hun structuur, bij tot belangrijke biologische functies.

Preface

Motivation

This Master's thesis deals with phase transitions in biomolecular systems. The theory and the knowledge of physics are combined with the biological part of life. Both physics and biology are important topics in life, combining them makes this Master's thesis even more interesting. This work is up-to-date because of dealing with biomolecular systems such as lipids, cholesterol and blood plasma. These subjects concern people because they represent people's health which makes this investigation worthwhile and rewarding.

First, lipids and lipid mixtures are investigated. Most people link these systems, mostly known as fats, to some negative aspect in the human body. Nevertheless, lipids are both structural building blocks of the cell and an energy source for a good functioning of the cell. Even more, when dealing with cell membranes, lipids are essential to control several biological functions. Recent research places the functional role of membranes at the same level of the research of the proteins.

Also cholesterol (which is a special kind of lipid) is a very known subject, and is essential in the human body. These lipids are produced by the body itself and are required to build and maintain cell membranes. The cell wall around the membrane is also produced by cholesterol. Finally, this lipid takes also care about the production of vitamin D, bile and certain hormones. When too much cholesterol is collected in the body, several cardiovascular diseases possibly occur. The best way to avoid these diseases is to control the cholesterol in the body, so investigating the effects of cholesterol on a lipid bilayer possibly helps to understand and control cholesterol in the human body.

Furthermore, a closer look at blood plasma is taken, which is present in the human body for about 55 % of the total blood volume. This plasma contains, beyond the main amount of water, some important and interesting matter. By donating blood plasma, which becomes more often a hot topic, other people can be helped or products to save life can be produced out of it. Of course, it is important that the donating plasma is healthy, which can be checked by using the adiabatic scanning calorimetry. Finally, the features of the phase transitions observed, have been shown to be linked to some diseases such as cancer and Lyme disease.

Therefore, a deeper knowledge of the physical properties is essential for revealing the causes of malfunctioning and diseased conditions. Linked to the medical world, this is an important application which deals with the medical treatment.

Words of thanks

This thesis would not have been possible without the time and the support of many people, I couldn't have done it on my own. I am very grateful to a lot of people, helping me with the

writing of this Master's thesis.

First of all, I am grateful to the Kuleuven, the Department of Physics and Astronomy, and the laboratory of Acoustics and Thermal Physics (ATF) to give me the opportunity to gain insight in the physical part of life, day by day. I would like to express my gratitude to my promotor Professor Christ Glorieux for introducing the subject of this thesis, for the supervision during the months and the several new ideas and suggestions to enlarge the investigations.

I would like to express my sincere thanks to Jan Leys, I have very much appreciated your guidance and great support. I have been privileged to experience first-hand how a critical and passionate supervisor can make a difference. Thanks for all the explanations, ideas, remarks and suggestions. Thanks for the weekly travelling and the daily mails.

I want to say thanks to Eli Slenders, to supervise me during the first steps of this thesis, for introducing me in the practical work in the lab. Thanks for teaching the skills and tricks of the experiments. Also thanks to keep on measuring during my examinations in January.

I would like to thank Patricia Maria Losada Perez, for us known as Pati, to prepare the samples. Thanks for the scientific consultations, the travelling to Leuven and the positive, encouraging words.

Another thanks goes to Professor Jan Thoen, to keep an eye on my results and for involving me in several investigations, which was my first introduction to real research.

I would like to thank all the professors, all the (post-)doctoral researchers, all the workers and all the colleagues of the second floor of the ATF building. Thanks for the nice work atmosphere, the kindness and the daily smile encouraging my daily presence (*'ik ga gaan thesissen'*). An especially thanks goes to Tristan Putzeys for the samples and the discussions about the blood plasma. Another thanks goes to Werner Neefs for the technical support at the lab.

I certainly want to thank my family to give me the opportunity to study at the University and to support me every day in everything I would like to achieve. Thanks for the support during all the *thesisdagen* and during the many hours at my desk.

Finally, I want to say thanks to all my friends for the understanding and the support. Thanks for the entertainment, the Alma-visits, the thesis-visits and the pub-visits which diverts during the thesis stress.

Summary

In this Master's thesis, phase transitions in biomolecular systems are investigated, thermally induced by heating the system. Systems such as lipids, binary lipid mixtures, cholesterol and blood plasma are part of the research because of their various functions in the human body. By using Peltier-based adiabatic scanning calorimetry, the temperature evolution of the specific heat capacity and of the enthalpy are measured with a high temperature resolution. The exceptional temperature stability of ± 50 mK and the slow scanning rates bring the sample close to the thermal equilibrium, allowing the precise determination of the phase diagram.

The behaviour of three different pure lipids and two different lipids mixtures are examined. Heating a pure lipid results in several stable phases, visualised by a sharp peak in the temperature evolution of the specific heat capacity. Four different phases occur, as a function of the temperature: the subgel phase, the gel phase, the ripple-gel phase and the liquid phase, recognised by an increasing disorder. All three phase transitions are clearly first-order, since they exhibit a clear discontinuous jump in the enthalpy, presenting the total energy of the transition. Three types of pure phospholipids (lipids with a phosphor polar head and a carboxyl-double chain with a length of 14, 16 and 18 respectively) are measured: DMPC, DPPC and DSPC. The transition temperatures shift to higher temperatures with an increasing chain length and more energy is contained in the phase transition. To indicate the melting process in a lipid bilayer, the cooperativity unit (CU) estimates the degree of cooperativity at the transition. The sharper the transition peak, the larger the fraction of membrane molecules that go through the phase transition simultaneously.

The behaviour of the pure lipid bilayers has been expanded by measuring two types of binary mixtures of phospholipids, both DMPC with DPPC and DMPC with DSPC. The temperature evolution of the specific heat capacity reveals combined effects of the two respective individual main transitions. The contribution to these transition scales with the concentration of the additional lipid and a two-phase system is observed. At this coexistence phase, one type of phospholipid molecules has already undergone the gel to liquid phase transition, while the other type not yet. The subgel-gel transition of the binary mixtures shifts to higher temperatures, while the gel to ripple-gel transition is no longer observed. Possibly due to the difference in alkyl chain between the two components of the mixture, which prevents the formation of the ripple phase. For DMPC with DSPC mixtures, the phase coexistence region is delimited by two well defined peaks due to the less ideal mixing because of the higher dissimilarity.

Further, the influence of cholesterol on a pure lipid (DPPC) is investigated. Cholesterol is a rather bulky lipid, characterised by a large tail and a small polar head. This geometrical shape influences the position of cholesterol in the lipid bilayers and a new physical phase is observed. By adding cholesterol, the transition between the gel and the ripple-gel no longer occurs and the main transition is broadened because both the phospholipids-rich and the cholesterol-rich domains differ in melting temperature, causing a two-phase region. The melting occurs at lower transition temperatures and a liquid-ordered phase is observed. This phase is recognised by the

liquid-order of the polar heads and by gel-order caused by the alkyl chains.

Finally, blood plasma, containing several lipids and proteins, is investigated by pASC. The complex composition and the interactions of the components influence the phase transition. The temperature evolution observed is a complex thermogram containing a lot of peaks. Each lipid and protein present in the human plasma undergoes its phase transition at a particular temperature, the thermogram presents the superposition of all these components. The main peak observed is linked to the denaturation of the albumin protein which transition is, in contrast with lipids, not reversible. Both the thermogram of a platelet poor plasma (PPP) and a platelet rich plasma (PRP) are measured, observing a shift in denaturation temperature. The same transitions still occur, but a shift is caused because of the different interactions occurring in PPP and PRP. Based on some albumin measurements, the influence of the environment and the interactions on the transition temperature is examined.

All investigations based on pASC give some comparable results to the literature. A lot of insight in the biomolecular systems and their phase transitions are gained. The main deviations between the pASC results and the literature are caused by the method of analysis. In order to minimize arbitrary procedures, a systematic procedure is followed, mainly based on an equivalent approach to the methods used in previous studies.

Samenvatting

In deze masterproef worden thermisch gedreven faseovergangen in biomoleculaire systemen onderzocht. Systemen zoals lipiden, lipide mengsels, cholesterol en bloedplasma vormen een deel van het onderzoek door hun verscheidene functies in het menselijk lichaam. Aan de hand van Peltier gebaseerde scan calorimetrie wordt de temperatuursevolutie van de specifieke warmtecapaciteit en van de enthalpie gemeten met een hoge temperatuursresolutie. De gemeten systemen bevinden zich in thermodynamisch evenwicht door enerzijds de bijzondere temperatuursmeting van ± 50 mK, en anderzijds de trage scan snelheden. Op deze manier wordt het fase-diagram bepaald met een hoge precisie.

Het gedrag van drie verschillende zuivere lipiden en twee verschillende lipide mengsels worden onderzocht. Wanneer een zuiver lipide opgewarmd wordt, ontstaan verschillende stabiele fasen, geobserveerd via een scherpe piek in de temperatuursevolutie van de specifieke warmtecapaciteit. In functie van de temperatuur treden er vier verschillende fasen op: de subgel fase, de gel fase, de rimpel gel fase en de vloeibare fase, gekenmerkt door een toenemende orde. Alle faseovergang zijn eerste orde overgangen en leveren een duidelijke discontinue stap in de enthalpie, die de totale energie van de faseovergang weergeeft. Drie verschillende zuivere fosfolipiden worden gemeten (dit zijn lipiden met een polair hoofd bestaande uit fosfor en een apolaire dubbele staart bestaande uit koolwaterstof met een lengte van 14, respectievelijk 16 en 18): DMPC, DPPC en DSPC. De overgangstemperaturen van de zuivere lipiden verschuiven naar hogere temperaturen wanneer de lengte van de staart toeneemt, bovendien bevat de overgang meer energie. Om het fenomeen van smelten in een lipide membraan te duiden, wordt een maat voor samenwerking tijdens de faseovergang weergegeven via de coöperativiteit eenheid (CU). Hoe scherper de piek in de specifieke warmtecapaciteit, hoe meer moleculen uit het membraan gelijktijdig de faseovergang zullen ondergaan.

Het gedrag van de zuivere lipiden wordt uitgebreid aan de hand van lipide mengsels, bestaande uit twee zuivere lipiden (zowel DMPC met DPPC, als DMPC met DSPC). De temperatuursevolutie van de warmtecapaciteit geeft op deze manier de effecten weer van het smeltproces van de gecombineerde, zuivere lipiden. Afhankelijk van de concentratie van de toegevoegde lipide wordt een verschillende bijdrage geleverd aan de faseovergang, waarbij een tweefasen systeem geobserveerd wordt. In deze co-existentie fase bevindt de ene soort fosfolipiden zich reeds in de vloeibare fase, terwijl de andere nog geen faseovergang ondergaan is. Deze fase is afgebakend door twee duidelijke pieken voor het DMPC met DSPC mengsel, dit mengsel is minder ideaal dan het DMPC met DPPC mengsel door het grotere verschil in lengte van de keten. Tenslotte verschuift de overgang van een subgel fase naar een gel fase in de lipide mengsels naar hogere temperaturen en de overgang van de gel fase naar de rimpel gel fase vindt niet meer plaats. Dit is mogelijk te wijten aan het verschil in lengte van de koolwaterstofketen tussen de twee verschillende types van lipiden, waardoor deze fase niet langer meer gevormd wordt.

Vervolgens wordt de invloed van cholesterol op een zuiver lipide onderzocht. Cholesterol is een redelijk omvangrijk lipide, gekarakteriseerd door een lange staart en een eerder kleiner polair

hoofd. Deze geometrische structuur beïnvloedt de locatie in de dubbele membraan waardoor een nieuwe fysische fase geobserveerd wordt. De overgang van de gel fase naar de rimpel-gel fase treedt niet langer op wanneer cholesterol wordt toegevoegd. De hoofdovergang zal door de verschillende smelttemperaturen van de cholesterol-rijke gebieden en de fosfolipide-rijke gebieden verbreden, waarbij een tweefasen gebied optreedt. Het mengsel smelt bij lagere temperaturen en een vloeibare-geordende fase wordt geobserveerd. Deze fase is samengesteld door de ordening van de vloeibare fase veroorzaakt door de polaire hoofden, en de ordening van de gel-fase afkomstig van de koolwaterstof keten.

Als laatste wordt bloedplasma, bestaand uit verschillende lipiden en proteïnen, onderzocht met behulp van pASC. Door de complexe samenstelling en de verschillende interacties tussen de verschillende componenten, worden de faseovergangen beïnvloed. De temperatuursevolutie van de specifieke warmtecapaciteit geeft een thermogram weer, bestaande uit verschillende pieken. Ieder lipide en ieder proteïne in het bloedplasma ondergaat een faseovergang bij een welbepaalde temperatuur, op die manier geeft dit thermogram de superpositie weer van al deze componenten. De voornaamste piek geobserveerd, is afkomstig van de (in vergelijking met de lipiden, niet omkeerbare) denaturatie van het albumine proteïne. Zowel het thermogram voor bloedplasma zonder (PPP) en met (PRP) bloedplaatjes wordt opgesteld, waarbij een verschuiving in overgangstemperatuur is geobserveerd. Alle fasen blijven dus volledig behouden, maar een verandering in temperatuur vindt plaats door de verschillende interacties die optreden in beide plasma's. Gebaseerd op enkele albumine metingen worden de invloed van zowel de omgeving (pH en hoeveelheid ionen), als de interacties in het plasma onderzocht.

Alle experimenten aan de hand van pASC geven resultaten die vergelijkbaar zijn met de literatuur. Dankzij de metingen wordt er inzicht in de verschillende biomoleculaire systemen gecreëerd. De belangrijkste afwijking tussen de resultaten bekomen via pASC en de resultaten uit de metingen, zijn afkomstig van de analyse van de data. Om deze fouten te minimaliseren is steeds een systematische methode van analyse gebruikt, die hoofdzakelijk gebaseerd is op de verschillende methoden uit eerder onderzoek.

Abbreviations and Symbols	Explanation
ASC	Adiabatic Scanning Calorimetry
DSC	Differential Scanning Calorimetry
pASC	Peltier-based Adiabatic Scanning Calorimetry
ATF	Acoustics and Thermal Physics
NTC	Negative Temperature Coefficient
DC	Direct Current
PE	Peltier Element (or Piezo Element)
DLPC	1,2-dilauroyl-sn-glycero-3-phosphocholine
DMPC	1,2-dimyristoyl-sn-glycero-3-phosphocholine
DPPC	1,2-dipalmitoyl-sn-glycero-3-phosphocholine
DSPC	1,2-distearoyl-sn-glycero-3-phosphocholine
L_c	Subgel phase
L_β	Gel phase
P_β	Ripple-gel phase
L_α	Liquid phase
L_d	Liquid disordered
L_o	Liquid ordered
S_o	Solid ordered
S_d	Solid disordered
HEPES	4-(2-Hydroxyethyl)-1-piperazineethanesulfonic acid
QCM-D	Quartz Crystal Microbalance with Dissipation
pH	Potential Hydrogen
R_x	Rotator Phase
H-NMR	Proton Nuclear Magnetic Resonance
PID	Proportional Integral Derivative
CMC	Critical Micelle Concentration
PPP	Platelets Poor Plasma
PRP	Platelets Rich Plasma
EPR	Electron Paramagnetic Resonance
rpm	Rotations Per Minute
LDL	Low-Density Lipoprotein
HDL	High-Density Lipoprotein
HSA	Human Serum Albumin
BSA	Bovine Serum Albumin
DNA	Deoxyribonucleic Acid
ANS	Anilino-naphthalene Sulphonate
IgA (IgM, IgC)	Immunoglobulin A (Immunoglobulin B, Immunoglobulin C)
C_p	Heat Capacity [J/K]
H	Enthalpy [J]
c_p	Specific Heat Capacity [J/(g · K)]
h	Specific Enthalpy [J/g]
CU	Cooperative Unit [mole/cooperative unit]
U	Internal Energy [J]
F	Helmholtz Free Energy [J]
G	Gibbs Free Energy [J]
S	Entropy [J/K]
Q	Heat [J]
p	Pressure [mbar]
T	Temperature [K] or [°C]
P	Power [W]
S	Seebeck Coefficient [V/K]
K	Thermal Conductance [W/K]
ϕ	Volume Fraction []
PV	Peltier-voltage [V]
H_{VH}	van 't Hoff Enthalpy [J]
H_{cal}	Calorimetric Enthalpy [J]
f	Frequency [Hz]
D	Energy Dissipation Factor []

Contents

Vulgariserende samenvatting	iv
Preface	v
Summary	vii
Samenvatting	ix
1 About this work	1
2 Theoretical background	3
2.1 Thermodynamic concepts	3
2.1.1 The thermodynamic variables	3
2.1.2 The thermodynamic potentials	4
2.2 Phase transitions	4
3 Adiabatic scanning calorimetry	7
3.1 Why calorimetry?	7
3.2 Possible techniques	7
3.3 Adiabatic scanning calorimetry principle	8
3.4 The classical adiabatic scanning calorimeter implementation	8
3.5 pASC implementation	10
3.6 On the choice of the calorimetry technique	10
3.6.1 Why ASC?	10
3.6.2 Why not DSC?	11
4 The experimental set-up	13
4.1 The pASC set-up	13
4.2 The Peltier element	15
4.3 The calibration of the Peltier element	17
4.3.1 Principle of the calibration of the Peltier element	17
4.3.2 Determination of the calibration coefficient	18
4.3.3 Conclusion	19
4.4 The modes of operation of the calorimeter	19
4.5 Sample preparation	21
4.6 Detecting a phase transition, based on C27 alkane	22
4.6.1 Direct data and calculations	24
4.6.2 Discussion of the heat capacity and the enthalpy	27

5	Lipid-membrane phases	31
5.1	Lipids in biology	31
5.2	Lipids in chemical terms	33
5.3	Lipids from the physics point of view	35
5.3.1	The self-assembly process	35
5.3.2	Phases of lipids in bilayers	39
5.3.3	Phase transitions of lipids	42
5.4	Phase transitions of lipids detected by ASC	42
5.4.1	Pure lipids	44
5.4.2	Mixture lipids	48
5.4.3	The phase diagram	53
6	Effects of cholesterol on lipid membrane phases	59
6.1	Special behaviour of cholesterol	59
6.1.1	Composition of cholesterol	59
6.1.2	Physical states of membranes with cholesterol	60
6.2	Addition of cholesterol to a lipid bilayer	63
6.3	Phase transitions observed by ASC	64
6.3.1	Observations	64
6.3.2	Interpretation and comparison with the literature	68
7	Thermograms of blood plasma	69
7.1	Proteins and blood plasma in the human body	69
7.1.1	Proteins	69
7.1.2	Plasma	70
7.2	Blood plasma situated in literature	70
7.3	Blood plasma observed by ASC	73
7.4	Albumin	74
7.4.1	The influence of the environment based on the literature	74
7.4.2	The influence of the environment based on ASC experiments	75
7.5	Conclusion	77
8	Conclusion	78

Chapter 1

About this work

Phase transitions are occurring in many materials and they are a rewarding topic in soft matter physics. In this Master's thesis, biomolecular systems such as lipids, lipid bilayers, proteins and blood plasma are investigated by Peltier-based adiabatic scanning calorimetry.

In this first chapter more information about this work is shortly given and the content of the different chapters is briefly explained.

The second chapter of this work explains the theoretical part. First of all some thermodynamics concepts are explained. Each thermodynamic system is defined with typical quantities such as internal energy U , Helmholtz free energy F , Gibbs free energy G , entropy S , heat capacity C_p and enthalpy H . Next, some theoretical background on first-order phase transitions and second-order (or continuous) phase transitions are given.

Chapter 3 gives an introduction about the adiabatic scanning calorimetry (ASC) technique used to measure the concerning quantities. ASC is the most optimal calorimeter technique here to investigate the biomolecular system. The adiabatic scanning calorimeter principle is explained, together with classical ASC. The use of a pASC is introduced, which is the type of calorimeter used in the experimental part of this thesis.

Chapter 4 gives more details about the experimental set-up of pASC, the use of the Peltier element and its calibration, and the several modes of the calorimeter. This set-up is completed with more information about the samples used in the experiments. Finally, to illustrate the performance of this calorimetric technique, an elaboration of the data, resulting in the phase transitions, of a C27 alkane is given.

The experimental part of this work starts at chapter 5. The first biomolecular system investigated are the lipid molecules. These molecules, organised in a membrane, are explained in the biological, the chemical and the physical field, explaining both their structures and their functions. The physical field introduces details about the processes observed in the biomolecular systems such as the self-assembly process. Several physical phases occurring in both pure lipids and binary mixtures of lipids, are clarified. The transitions between the different phases are observed by pASC, compared with results from the literature and compared with a parallel experiment based on QCM at the University of Hasselt.

In chapter 6, the investigation on lipids is enlarged by detecting the influence of cholesterol on a pure lipid. When adding cholesterol to a lipid membrane, new physical phases are observed, which are explained in this chapter. Finally, the core effects and its influences of cholesterol on the medical field are shortly explained.

The last chapter deals with blood plasma, which is a composition of several lipids and proteins. Because of this complex composition, a more extensive thermogram, representing the phase

transitions, is observed. Both blood plasma with (PRP) and without (PPP) blood platelets are measured to check the interactions between the components and the influences of the environment. More insight of these dependencies are gained by some additional experiments based on the albumin protein.

Finally, the Master's thesis ends with a conclusion about the results obtained and the insights gained in this thesis.

Chapter 2

Theoretical background

In this chapter, some theoretic concepts are explained, which are used throughout the thesis. The overview is based on the doctoral thesis of Bert Van Roie [72] and the thermodynamic book ‘Thermal Physics’ by Daniel V. Schroeder [62].

2.1 Thermodynamic concepts

2.1.1 The thermodynamic variables

In thermodynamics, thermodynamic parameters are macroscopic variables, which describe the macrostate of the system. To describe such a system, state variables, such as mass m , pressure p and volume V are used. There are two kinds of state variables. The first variables are independent of the mass or size of the system and are called intensive. The pressure p , temperature T or the density ρ of for instance a brick does not change when dealing with one or two bricks. The other variables are known as the extensive variables, and are quantities which are proportional to the mass. Examples of extensive variables are volume V , enthalpy H and entropy S [34].

Quantities which are defined per unit of mass are expressed with ‘specific’. In the next chapters, the specific heat capacity c_p is measured, together with the specific enthalpy h . This specific heat capacity deals with the amount of heat required to raise the temperature of a gram of material by one Kelvin at a constant pressure [34].

The first law of thermodynamics states the law of conservation of energy. In a closed system the energy is conserved, resulting in a relation between the internal energy of the system dU , the heat supplied to the system by its surroundings δQ and the work done by the system δW :

$$dU = \delta Q - \delta W \quad (2.1)$$

Consider mechanical work done by expansion, this equation can be rewritten as

$$dU = TdS - pdV \quad (2.2)$$

The second law of thermodynamics states that a system strives to achieve a state of maximum entropy, so the entropy of an isolated system will never decrease. The entropy S is a physical quantity which represents the indication of disorder in a system and it is defined as

$$dS = \frac{\delta Q}{T} \quad (2.3)$$

2.1.2 The thermodynamic potentials

In a system four different thermodynamic potentials (U , H , F and G) are defined. Based on the book of Schroeder [62] these potentials are explained for a system with an internal energy U . This energy is the first thermodynamic potential and is defined as a function of both the entropy and the volume $U(S, V)$.

Another thermodynamic potential is the Helmholtz free energy, defined by

$$F(T, V) = U - TS \quad (2.4)$$

$$dF = -SdT - pdV \quad (2.5)$$

This is the total energy of a system (internal energy), minus the heat received for free from an environment at temperature T .

The next energy in a system is the Gibbs free energy defined by

$$G(T, p) = U - TS + PV = F + pV = H - TS \quad (2.6)$$

$$dG = -SdT - Vdp \quad (2.7)$$

If a system is in an environment with constant pressure P and constant temperature T , the work obtainable from the system is given by this energy. So the Gibbs free energy is the system's energy, minus the heat that is contained in the Helmholtz free energy, plus the atmospheric work term of H , which is the last thermodynamic potential.

The fourth one is the enthalpy H , given by

$$H(S, p) = U + pV \quad (2.8)$$

$$dH = TdS + Vdp \quad (2.9)$$

This energy is the total energy composed in a system and will be extracted when annihilating a system. The enthalpy is the addition of the internal energy U and the work (pV) done by the atmosphere as the system collapses to fill the vacuum left behind.

The type of calorimetry used in this thesis is the constant pressure calorimetry. Here, the enthalpy is an important quantity, remark that $(dH)_p = (\delta Q)_p$. So the heat capacity can be defined as follows

$$C_p = \left(\frac{\delta Q}{dT} \right)_p = \left(\frac{dH}{dT} \right)_p \quad (2.10)$$

The heat capacity C_p is the amount of heat needed to raise the temperature of a system by one Kelvin. A more fundamental quantity is the specific heat capacity c_p , defined as the heat capacity per unit mass. Linked to this thermal property, the specific enthalpy h is defined as the enthalpy per unit mass [72, 62].

2.2 Phase transitions

In this Master's thesis, phase transitions in biological material such as lipids are investigated. In the neighbourhood of a phase transition, it is important to perform a high-resolution study to extract a maximum amount of information about the sample.

A phase transition occurs when matter changes state, the matter changes from one phase to the other. Assume for instance spherical molecules without any internal degrees of freedom. The known phases are solid, liquid and gas. As presented in the introduction, an everyday example is water: the three phases are ice, water and water vapour. The three states consist of the same molecules but are different in view and properties. Phase transitions take place between them at a particular temperature (dependent on the pressure and the volume) and are caused by the interaction of the molecules.

In Figure 2.1, phase transitions are presented graphically in a three-dimensional phase diagram, in which pressure versus temperature versus volume curves are plotted. This phase diagram shows the phase transitions when changing the temperature, the pressure or the volume. A phase transition is represented by the black lines, called coexistence lines or phase lines. The coexistence lines represent a phase boundary and give the conditions when two phases may stably coexist, independent of the relative proportion of the two phases. When acting on such a line, the Gibbs free energy is the same for both phases. By changing the temperature, the pressure or the volume, such a line is crossed. The constant-pressure and the constant-temperature line are represented in the Figure. When following these lines, an abrupt change in phase takes place, the system goes from one state to the other. Even when energy (or heat) is added to the system, the applied energy is used to go through the phase transition while not changing the temperature, the pressure or the volume.

As indicated in the Figure, both single phases and two phases are present in the phase diagram. Between those phases, a saturation state is observed. For instance, the line between the liquid phase and the liquid-vapour phase is called the liquid-saturation phase. Or, another example, a point on the border of the vapour and the liquid-vapour phase, is at a saturated-vapour state. Both states meet each other at a critical point, observed at (p_c, V_c, T_c) . Here the properties of both phases are indistinguishable from each other.

Finally, the three single phases meet at the triple state, here the three phases stably coexist and all have the same amount of Gibbs free energy [55].

Paul Ehrenfest, an Austrian physicist, classified the different phase transitions based on the behaviour of the thermodynamic free energy as a function of other thermodynamic variables. A first-order transition is thermodynamically characterised by finite discontinuities in the first derivative of the thermodynamic potential G . This leads to a jump in the volume, since $V = (\frac{\partial G}{\partial p})_T$ and in the entropy $S = -(\frac{\partial G}{\partial T})_p$. Furthermore, $dH = T_0 dS$, so a transition goes along with a discontinuous jump in the enthalpy, called the latent heat. Here T_0 is the temperature at the phase transition.

At a second-order transition, also called a continuous transition, the entropy S and the volume V are continuous, but at the second derivative of the Gibbs free energy, a discontinuity is presented. Such thermodynamic quantities are the heat capacity $C_p = T(\frac{\partial S}{\partial T})_p$ and the compressibility $\kappa_T = -\frac{1}{V}(\frac{\partial V}{\partial p})_T$.

In theory also higher order phase transitions are possible, but in experiments, they have never been observed [69].

In summary, when a step is observed in the enthalpy (which is the first derivative), a first-order transition is taking place. If no step is visible, the phase transition is second order. Furthermore, the heat capacity, which is the second derivative, shows a discontinuity when dealing with a first-order transition. If a divergence or another anomaly is observed in the heat capacity, the phase transition is second order [72].

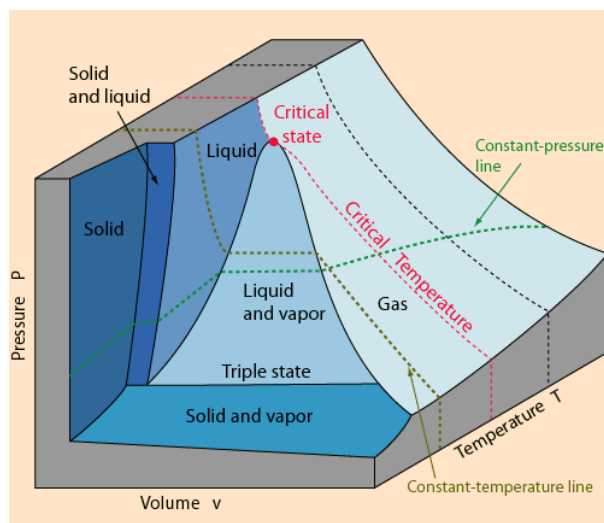


Figure 2.1: The three-dimensional phase diagram of a normal, pure material as a function of temperature, pressure and volume. Several phase transitions are distinguished by the coexistence lines (the black lines) [55].

Chapter 3

Adiabatic scanning calorimetry

3.1 Why calorimetry?

Phase transitions of biomolecular systems can be efficiently studied by measuring the heat capacity C_p with a calorimeter. The heat capacity reflects the quantity of heat needed to change the temperature of a system with one Kelvin. At a phase transition, a peak in the heat capacity occurs, because an important part of the supplied energy is now used to turn the system into a new phase. The temperature dependence of the specific heat capacity is thus a sensitive marker for phase transitions, especially when the amounts of active material are small.

3.2 Possible techniques

The goal of calorimetry is to determine the heat capacity and the enthalpy of a sample. Calorimetric techniques are based on the equalities:

$$C_p(T) = \frac{\Delta Q}{\Delta T} = \frac{\Delta Q/\Delta t}{\Delta T/\Delta t} \approx \frac{P}{\dot{T}} \quad (3.1)$$

The heat capacity $C_p(T)$ is related to the heat Q on the temperature T . By dividing both terms by a time interval, the heat capacity is written as a function of the power P and the evolution of the temperature in time $\dot{T} = \frac{dT}{dt}$.

Step Calorimetry In (heat-) step calorimetries, the heat capacity is determined by the change of temperature ΔT that results from a finite supply of heat ΔQ . After this pulse, the evolution of the temperature is measured, followed by the evolution of the heat capacity of the sample. The enthalpy is calculated by converting the heat capacity obtained from the discrete points.

Ac-Calorimetry Here heat is periodically supplied to the sample and the resulting temperature oscillation is being measured. The amplitude of the temperature oscillations is inversely proportional to the specific heat of the sample. By integrating this heat capacity, the enthalpy can be calculated, except when a first-order transition occurs [66].

Differential Scanning Calorimetry The differential scanning calorimeter is recognised by the use of two cells. The first cell is a reference cell, the second contains the sample. The reference cell is used to directly measure the heat capacity of the sample, by the difference in heat capacity

observed from the reference and the sample cell. This calorimeter technique, also called a heat exchange calorimeter, measures the heat flux between the two cells with a high precision due to the difference. Both cells are heated at a constant temperature rate and the power is measured, resulting in the heat capacity and by integrating this results, the enthalpy is observed [52].

Adiabatic Scanning Calorimetry In adiabatic scanning calorimetry (ASC), a constant power is applied to the sample. This sample is placed in an adiabatic environment. The temporal evolution of the temperature is being measured, from which the heat capacity is calculated. Also the enthalpy is immediately calculated from the power and the temperature evolution [69].

3.3 Adiabatic scanning calorimetry principle

In the late 1970's, the adiabatic scanning calorimeter was developed at the Katholieke Universiteit Leuven. Passing the years, many insights are gained into phase transitions of liquid crystals, binary and ternary liquid mixtures, fullerene and other systems. A lot of high resolution experiments are published because of the impressive results [3, 68, 70, 67, 43, 19].

The temperature dependence of the heat capacity $C_p(T)$ and the enthalpy $H(T)$ is derived by measuring the temperature of the cell T , the applied power P and the time evolution t while applying a constant heating or cooling power to the sample, placed in a cell. The basic set-up of the adiabatic scanning calorimeter is presented in Figure 3.1. The sample is surrounded by an adiabatic shield which is kept at the same temperature of the sample, in order to eliminate all heat leaks between the sample and the shield.

The technique behind adiabatic scanning calorimetry, assuming a constant pressure, is fully presented by two formula:

$$C_p = \left(\frac{dQ}{dT} \right)_p = \left(\frac{P}{T} \right)_p \quad (3.2)$$

$$H(T) - H(T_s) = P[t(T) - t(T_s)] \quad (3.3)$$

Measuring the constant power P , the evolution of the temperature in time $T(t)$ and the time evolution t , results into the determination of the heat capacity and the enthalpy, as a function of temperature. The temperature of the scanning run starts at temperature T_s at time t_s . The heat capacity obtained is the total heat capacity, containing the sample, the cell, the thermal paste and other addenda.

An example of a heating run with a constant power is schematically illustrated in Figure 3.2, where a first-order phase transition is observed. A constant power P is applied to the cell at time t_s , so the temperature of the cell $T(t)$ increases as a function of time. Near a transition temperature, the scanning rate is slowing down, expressing the onset of a first-order phase transition and the channeling of the supplied power to latent heat [69].

3.4 The classical adiabatic scanning calorimeter implementation

The classical calorimeter is based on equation (3.1) and was the first calorimeter that deals with a constant electrical power. The classical ASC device is an adiabatic device due to the construction. The cell, (containing the sample) and the adiabatic shield are hardly in contact. Further, large samples were needed. Still, over the years the samples masses were decreased from the initial 50 g to the order of 0.5 g. Second, low scanning rates were used in the classical

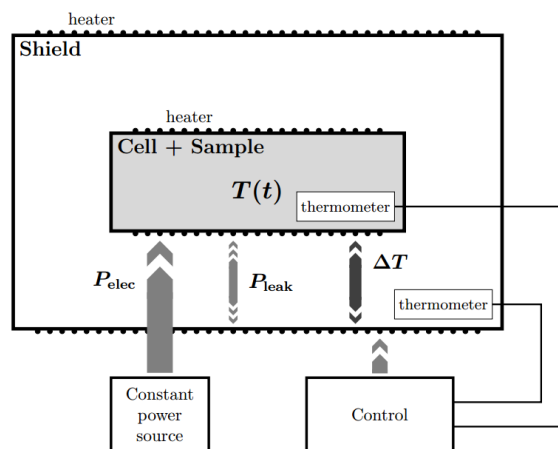


Figure 3.1: The basic set-up of an adiabatic scanning calorimeter. The configuration consists of a sample surrounded by an adiabatic shield to manage the heat leakage P_{leak} when applying a constant power P_{elec} to the sample.

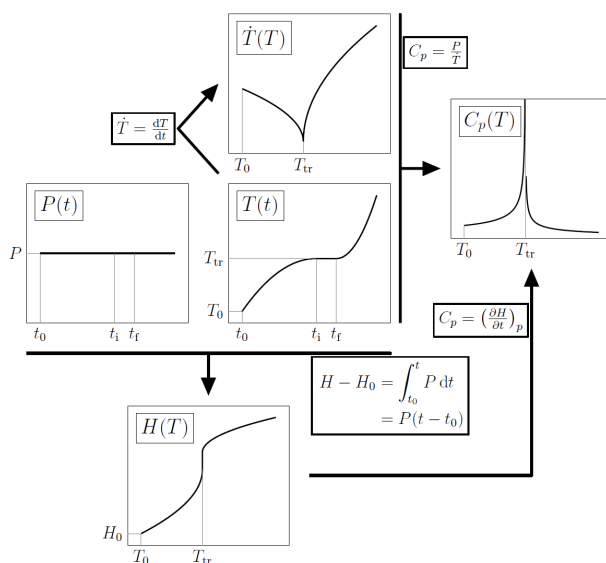


Figure 3.2: An illustration of a heating run, measured with ASC. A first-order phase transition is visible [69].

ASC. Typical rates are mK/min or lower, which result in a very high resolution. Further, the operation of the instrument required skilled and trained personnel, especially the mounting of the sample cell, which is mounted by some thin wires. Mounting the sample is a difficult and specialised process. Finally, the correct operation relied heavily on the close matching between different thermistors for the calculation of the temperature difference between cell and adiabatic shield. These thermistors are resistance thermometers with a high resolution but with a low long-term stability, and require frequent and tedious calibrations, hindering operations over wide temperature ranges.

3.5 pASC implementation

In 2010, research at ATF led to a solution of the problems of the classical ASC. Instead of relying on thermistors to calculate the temperature difference between the sample cell and the adiabatic shield, a Peltier element used as a differential temperature sensor was used. Thus the repeated tedious thermistor recalibrations were eliminated. In this calorimeter, it is more easy to place the cell into the calorimeter on the Peltier element. The cell does not have to be suspended to thin wires anymore as done in the classical adiabatic scanning calorimeter. Furthermore, because of the use of the Peltier element, the temperature difference can be measured directly (this compared to the subtraction of nearly the same numbers as in the classical ASC), and secondly the heat leakage can be calculated in a straightforward way. All the advantages of the classical ASC still remain, or, even more, are improved. Furthermore, a decrease in the amount of sample took place. A reduction of the order of two occurs, while the resolution in temperature does not change. Because of the smaller amount of sample, the whole set-up could be made smaller.

3.6 On the choice of the calorimetry technique

3.6.1 Why ASC?

Three different scanning techniques are available, nevertheless the strengths of ASC extol the pASC technique, compared to DSC and classical ASC. Because of the constant supplied power, the sample is free to evolve and not forced to follow a constant temperature rate. This power can be tuned to achieve a certain overall heating rate. Using ASC results into a good resolution (sub-mK): the lower the rates, the better the resolution and the better the thermal equilibrium. Further, the thermodynamic equilibrium is reached because of the low scanning rates. The constant power keeps the sample closer to thermodynamic equilibrium when a certain temperature is reached. With pASC, compared to other techniques, a good mK temperature resolution is possible.

To investigate biomolecular systems and their phase transitions, different calorimetric techniques are available. Nevertheless, also here, the advantages of ASC show a particular potential for biophysical research. In this research, an experiment with high temperature and high sensitivities units to changes in heat capacity is needed to observe the small peaks representing the phase transitions. Due to slow heating rate and high temperature resolution, very sharp peaks are not smeared out (contrary DSC results). Because of the thermodynamic equilibrium, the observation in the neighbourhood of a phase transition is reliable. The correct phase transition temperature is measured, together with the correct absolute value of the heat capacity and the enthalpy. The last quantity is directly determined, without any integration needed [68].

3.6.2 Why not DSC?

The most common calorimetric technique is the differential scanning calorimetry. However, DSC is not optimal to detect phase transitions in biomolecular systems.

The most important reason why DSC is not suitable to investigate biomolecular systems is the low temperature resolution, about the order of 0.1 K. A measurement with DSC is faster compared to ASC, but due to that, thermodynamic and thermal equilibrium are not reached. Equilibrium is extremely important in the neighbourhood of the phase transitions. That way, DSC is not a favourable technique to investigate biomolecular systems. The small amounts of enthalpy involved in phase transitions in systems such as lipids, are not always visible with DSC. The peaks are broadened and suffer from a bad resolution.

The Privalov calorimeter is a DSC calorimeter solving the problem of the bad resolution of the normal DSC. This calorimeter works in an opposite way compared to DSC, but still a constant rate is achieved. A constant power is applied to the reference, while a not-constant power is applied to the sample because of the change in heat capacity. Despite the higher resolution (the best resolution reachable with a Privalov calorimeter is equal to the worse resolution reachable with ASC), transition peaks are still sharper and more symmetric in pASC runs.

Finally, Figure 3.3 shows differences in the evolution of the specific heat capacity of a linear alkane, measured by ASC (left) and by DSC (right). Upon heating this alkane, several physical phases (crystal phase, rotator phases and liquid phase) occur. By cooling this sample, some additional rotator phases were observed. The differences in temperature resolution between ASC and DSC are clearly observed. The ASC data are measured by the pASC prototype, a sample of 59 mg with an averaged rate of 0.36 K/h has been measured [76]. The results of DSC are obtained by measuring an unknown mass with an average rate of 120 K/h [60]. The DSC runs show substantial rounding, and nearly an elimination of the second rotator phase occurred in the cooling run.

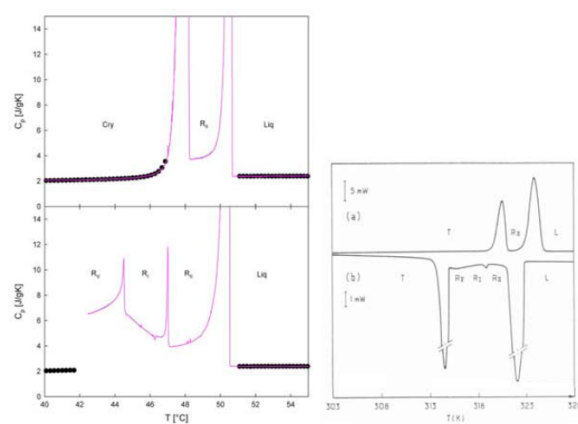


Figure 3.3: Comparison of the temperature dependence of the specific heat capacity of a linear alkane tetracosane ($C_{24}H_{50}$). Several phase transitions were obtained by heating the sample: crystal phase, rotator phase. By cooling some additional rotator phases are observed. Left: Results obtained by a heating run (top) and a cooling run (bottom) by pASC [76]. Right: Results obtained by a heating run (top) and a cooling run (bottom) by DSC [60]. A clearly broadening of the peak is observed and a difference in temperature resolution occurs.

Chapter 4

The experimental set-up

4.1 The pASC set-up

The Peltier-element-based adiabatic scanning calorimeter set-up is given in Figure 4.1. This pASC contains (from the inside to the outside) a sample (1), a first (adiabatic) shield (8 and 9), a second shield (14 and 18) and an outer can (vacuum jacket) (21 and 24) which is placed in a heat bath. The more on the outside, the lower the temperature. The sample is placed in a cell. The first shield is kept at the same temperature as the sample, which satisfies the adiabatic principle. The second shield is kept at a constant ΔT below the first shield. Eventually, also the heat bath is kept at a constant ΔT below the second shield. The exact values of the ΔT are varied with the type of run performed. The difference in temperature between the first and the second shield, during a heating run, are around 0.2 °C, during a cooling run 5 °C, during a pulse run 0.2 °C and during a stabilisation run 1 °C. The difference in temperature between the second shield and the heat bath is 3 °C during a heating run, 10 °C during a cooling run, 3 °C during a pulse run and 5 °C during a stabilisation run. To obtain a precise heating, the temperature differences between the first and the second shield, and between shield 2 and the bath are kept small.

The whole set-up is placed in high-vacuum (about 10^{-4} - 10^{-5} mbar) by a vacuum pump. The vacuum set-up limits the thermal contact between the different shields. The good isolation makes the heat leakage small, so small powers are permitted, and on his turn small temperature rates are achieved. In a medium, there are three principles to transport heat: convection, conduction and radiation. Working in vacuum, convection and conduction are roughly zero. Due to the Stefan–Boltzmann law (also called Stefan’s law), $P = \sigma T^4$ or $dP = \sigma(T_{\text{cell}}^4 - T_{\text{shield1}}^4) \approx 4\sigma T_{\text{cell}}^3(T_{\text{cell}} - T_{\text{shield1}})$, the power of the radiation goes up with the temperature difference between the cell and the first shield. The temperature of the cell, to the third power, is seen as background. So, the heat leak due to the radiation is proportional to the difference in temperature. Because this difference is very small, also the radiation in vacuum is neglected.

At the cell, containing the sample, six wires are attached. The first two are linked to the thermistor that measures the temperature of the cell. A thermistor is an electrical component (resistor) of which electrical resistance is dependent on his temperature. When raising the temperature, the electric resistance decreases. This kind of resistance is called a NTC-resistance because of the negative temperature coefficient. The second two wires are used to measure the voltage of the Peltier element (and so the difference in temperature). The last two wires are two filaments connected to a heater, in this case a miniature strain gauge, providing power to the sample. The

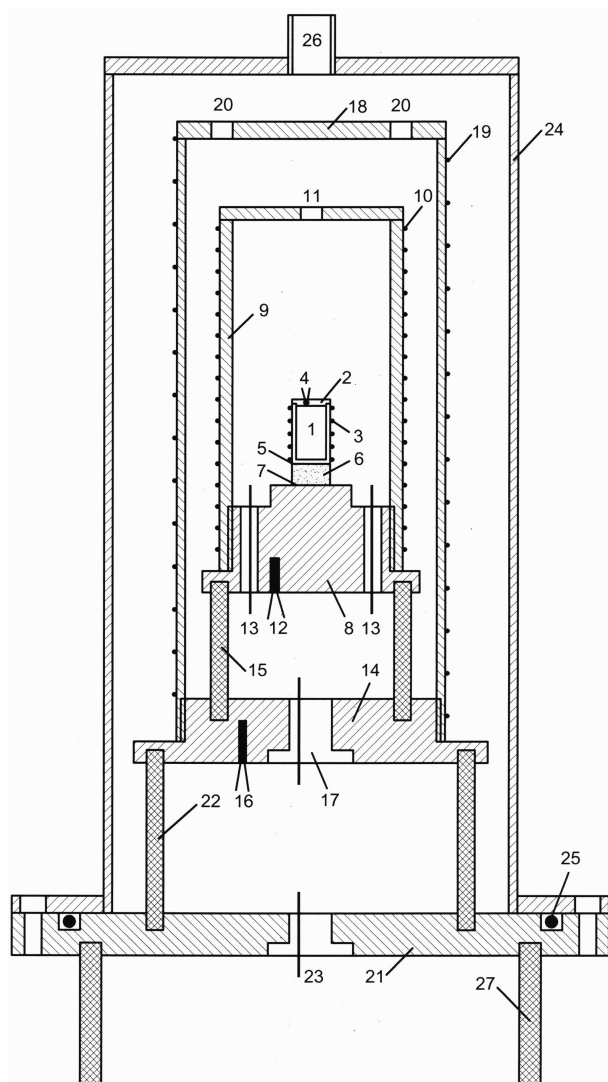


Figure 4.1: The pASC set-up containing the sample (1), a first or an adiabatic shield (8+9), a second shield (14+18) and a bath (21+24). The cell is placed on a Peltier element to measure the temperature difference.

longer these wires are, the smaller the heat leak is. In the current set-up, the wires are about 7 to 8 cm.

Power measurement To measure the power, maintained by a current source, the voltage of the cell is measured with a multimeter. Due to the series circuit, the current is known and the power can be measured very precisely.

The sample is heated by applying a constant electric power to the sample cell. This heating is measured by using a reference resistor, placed in a series circuit as drawn in Figure 4.2. The power of the cell can be expressed in function of the voltage and the current I_{cell} . This current is the sample current as the current going through the reference (because the series circuit). The following relations are known:

$$\begin{aligned} P_{\text{cell}} &= V_{\text{cell}} \cdot I_{\text{cell}} \\ I_{\text{ref}} &= \frac{V_{\text{ref}}}{R_{\text{ref}}} \end{aligned} \quad (4.1)$$

From this, the power to the cell can be calculated

$$P_{\text{cell}} = I_{\text{cell}} \cdot V_{\text{cell}} = I_{\text{ref}} \cdot V_{\text{cell}} = \frac{V_{\text{ref}}}{R_{\text{ref}}} \cdot V_{\text{cell}} \quad (4.2)$$

Temperature measurement The temperature of the cell, the first and the second shield, and the resistance of the cell and the reference, are measured with a multimeter. This multimeter reads the resistance of the thermistor. By using the known temperature dependence on the thermistor, the temperature of the cell can be measured precisely.

PV measurement A second multimeter measures voltage generated by the Peltier element. This voltage is dependent on the difference in temperature between the cell and the first shield. To maintain the adiabatic environment in a heating run, this voltage needs to be zero.

4.2 The Peltier element

To eliminate the calibrations of the thermistors, the difference in temperature is measured by a differential temperature sensor. In pASC, a Peltier element is integrated to measure the difference in temperature between the sample and the cell in a very accurate way. This device uses the Peltier effect and the Seebeck effect. Still some calibration is needed before using the device. This is an easy job which is described below.

The Peltier element principle A Peltier element can be used to generate several thermo-electric effects. This device exists of two different kinds of metals, pictured in Figure 4.3 (a), each with an energy Fermi level E_1 and E_2 . When a direct current (DC) goes through those metals, the difference in energy need to be passed from E_1 tot E_2 with E_1 smaller than E_2 . This is done by transporting heat contracted from the environment, leaving the environment at a lower temperature. This effect is known as the Peltier effect. The more current flows, the more heat is transported and the larger the temperature difference will be. The other way around, a current is created when electrons are pushed due to some heat between the Fermi levels. Due to the difference in temperature (T_2 smaller than T_1), a current is generated which is known as the Seebeck effect.

The Peltier element, as seen in Figure 4.3 (b), is characterised by both thermo-electric effects.

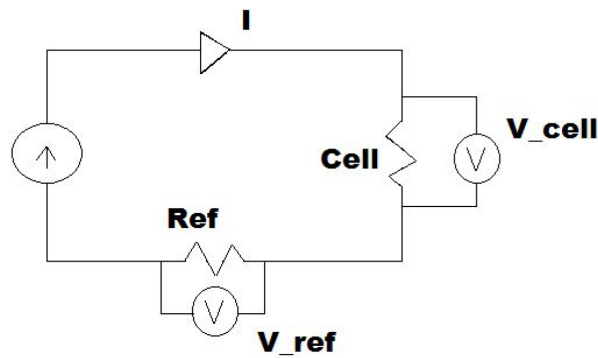


Figure 4.2: The circuit used to apply and measure the electric power of the cell. An additional reference resistor is placed in a series circuit, so the current through the cell and the reference resistor are the same.

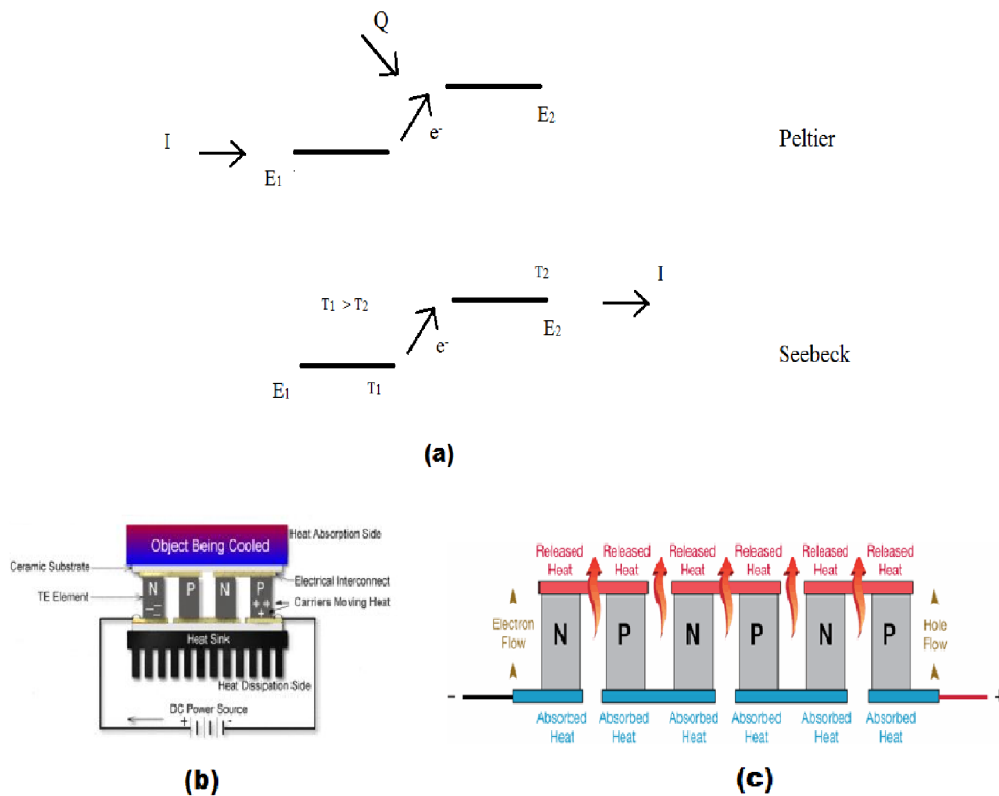


Figure 4.3: (a) The Peltier element principle, consisting of two different metals with a Fermi level E_1 and E_2 . (b) The Peltier element in practise, containing a thermoelectric element. (c) The thermoelectric element, consisting of P and N junctions, which pumps the heat to the metals when a current is created (the Peltier effect) [71].

The device consists of two different metals, compared with a thermoelectric element (see Figure 4.3 (c)). This element consists of several P and N junctions. They make sure the heat is pumped between the metals to create a current [71]. In our experimental set-up, the PE consists of a semiconductor (not a metal) with junctions of Bi_2Te_3 .

In pASC, the Peltier element measures the differences in temperature between the sample and the first shield. This difference generates a current which is measured. So the Peltier element produces a voltage proportional to the temperature difference. This, the Seebeck effect, is based on $\Delta V = S\Delta T$ with S the Seebeck coefficient. Since the experiments are carried out in an adiabatic environment, ΔT has to be kept zero by keeping ΔV zero. The potential difference over the Peltier needs to be kept zero.

4.3 The calibration of the Peltier element

When operating the Peltier-element-based calorimeter, a heat leakage is observed through the Peltier element. This leakage is desired when doing a cooling run, dealing with an induced heat leak from the cell to the shield. During a heating run, the Peltier voltage is kept at zero. By calibrating the Peltier element, two coefficients, the Seebeck coefficient S and the thermal conductance K are determined, both are used to analyse the different heating and cooling runs. The ratio of both coefficient K/S gives the relation between the applied power and the difference in voltage on the PE.

4.3.1 Principle of the calibration of the Peltier element

Principle of calibration To calibrate a Peltier element (PE), the temperature of the bottom is heated by applying an electric power. The bottom of the Peltier element is kept at a constant temperature by connecting the PE to a heat sink. When applying a power P_{elec} on the top of the Peltier element, the temperature of the cell increases. This increase causes a difference in temperature between the cell and the first shield. Because of the Peltier effect, this difference results into a difference in voltage ΔV through the Peltier element. After some time, the temperature difference between the cell and the first shield no longer increases. The applied power yields into a heat leakage through the Peltier element.

By determining this heat leakage, both coefficients can be calculated. First of all, the difference in temperature, due to the power applied, causes a difference in potential, which is called the Seebeck effect.

$$\Delta V = S\Delta T \quad (4.3)$$

Reaching a steady state, the temperature difference between cell and first shield is stabilised, so the applied power all leaks away through

$$P_{\text{leak}} = K\Delta T \quad (4.4)$$

Combing both equations

$$P_{\text{leak}} = \frac{K}{S}\Delta V \quad (4.5)$$

results into the ratio of the Seebeck coefficient and the thermal conductance.

The data collected The Peltier element is placed on copper matter which keeps the bottom of the Peltier element at a constant temperature. The other side, the top, is heated by applying an

electric power, resulting in a heat transport. This is repeated several time with different powers. The first step of the calibration is to stabilize Shield 1, this is done by obtaining a stabilisation run. In Labview ‘stab T=25 man’ is used. This shield, at the bottom of the PE, is kept at this temperature due to the connection with a big coper matter. Next a particular power is applied to the top of the PE. This electric power is selected by the user. When a steady state regime is obtained after a few minutes, the power is put back to zero. This procedure is repeated several times.

During the stabilisation run, the temperature of the first shield stays constant and the temperature of the cell changes due to the power applied on it. The temperatures of both the cell and the first shield are measured, together with the differences between both components. To determine the Seebeck coefficient, the potential difference, due to the difference is temperature, is measured. Finally, to determine the thermal conductance, the electric power applied has to be known.

The errors collected During the experiment, two kind of errors, resulting in offsets, need to be taken into account. The first error is caused by measuring the temperatures of both the cell and the first shield. These temperatures are measured by two thermistors which are calibrated. This calibration causes an error, which can be calculated when reaching a stabilisation state. When a long stabilisation occurs, the temperature of the cell and the first shield have the same temperature because of the thermal contact. Nevertheless, because of the calibration, a small deviation occurs.

The second error occurs when measuring the voltage through the Peltier element. Several thermovoltages are generated, both due to the Peltier element, and due to other components. On every electrical contact, a voltage is created, which has to be taken into.

4.3.2 Determination of the calibration coefficient

As plotted in Figure 4.4, five different powers were applied to the top plate of the Peltier element, alternating with a power of zero. The heat delivered by this power is transported through the Peltier element, where a potential difference $\Delta V(t)$ takes place due to the difference in temperature ΔT observed. The temperature T as a function of time t for both the cell and the first shield is plotted in Figure 4.5, the voltage ΔV of the Peltier element as a function of time t is plotted in Figure 4.6 and the difference in temperature ΔT as a function of time t is plotted in Figure 4.7.

Both the thermal conductance and the Seebeck coefficient are calculated for all five powers, taking into account the offset. All data are presented in Table 4.1. The thermal conductance is calculated by using equation (4.4). The Seebeck coefficient is calculated by using equation (4.3). Finally, the calibration coefficient $\frac{K}{S}$ is obtained by dividing the conductance coefficient K by the

Table 4.1: Data from the calibration of the Peltier element. The Seebeck coefficient and the thermal conductance are calculated for five different powers.

	$P(mW)$	$\Delta T(K)$	$\Delta V(mV)$	$K (W/K)$	$S(V/K)$	$K/S (W/V)$
First power	0.1	0.0145	0.1090	0.0069	0.0075	0.9195
Second power	0.2	0.0294	0.2228	0.0068	0.0076	0.8951
Third power	1	0.1488	1.1365	0.0067	0.0076	0.8843
Fourth power	2	0.3016	2.2959	0.0066	0.0076	0.8725
Fifth power	1	0.1513	1.1585	0.0066	0.0077	0.8584

Seebeck coefficient S . This determines the relation between the power going through the Peltier element and the potential difference on the Peltier element.

The results of the calibration are in line with the coefficients used in the current analysis of the heating- and cooling runs ($K = 4.87 \cdot 10^{-3} \text{ W/K}$ and $S = 7.6 \cdot 10^{-3} \text{ V/K}$). Further, the calibration coefficient is nearly one, meaning that a reading of 1 V for the Peltier voltage corresponds to a heat leak of nearly 1 W.

4.3.3 Conclusion

The Seebeck coefficient S has not changed remarkable compared to other calibrations. Nevertheless, the conductance coefficient K has been multiplied by two, still no remarkable difference in order takes place. By using both coefficients, the calibration coefficient K/S is calculated which shows that a power of about 0.9 W is needed to create one volt over the Peltier element.

4.4 The modes of operation of the calorimeter

There are four different jobs possible for the calorimeter to perform. Three runs generate data from the sample: a heating run, a cooling run and a pulsing run. Further, a stabilisation run is possible, which is a technical mode, needed before starting a measurement.

A heating run The first mode of pASC is the heating run. A constant power is imposed on the sample, while the voltage of the Peltier element is kept zero during the heating run. The temperature of the outer can is controlled in such a way that a fixed temperature difference is maintained between the temperature of the first and the second shield (about 0.2 °C), and between the second shield and the oven (about 3 °C). The power and the temperature evolution in time, are measured. This results into a direct calculation of the heat capacity $c_p(T)$ and the enthalpy $h(T)$.

A cooling run In a cooling run, a negative power needs to be applied to the cell. This is done by controlling the temperature of the first shield to force a constant non-zero Peltier voltage, and therefore a constant temperature difference (and heat leakage) between the cell and that shield. This because of $P_{\text{Peltier}} = \frac{K}{S} \Delta V$. Furthermore the temperature difference between shield 1 and 2, and between shield 2 and the bath is kept constant, around the same temperature difference as in the heating runs. The further outside, the lower the temperature. The temperature differences are generally larger than in a heating scan.

A pulse run This type of run is used to measure the absolute values in heat capacity with high accuracy by applying a large amount of heat in a short time. This is done by reaching first a stabilization, sample and first shield are kept at the same temperature, and the second shield and the oven are following at a constant temperature difference. Second, during a relatively short time, a power is delivered to the sample. Because of this heating pulse, a temperature change is induced and the temperature of the sample, first shield, second shield and the oven, are raised. After the heat pulse, the temperature of the sample is recorded until a steady-state is reached. From the temperature difference of the sample before and after the pulse, together with the pulse duration and the applied power, the heat capacity can be calculated.

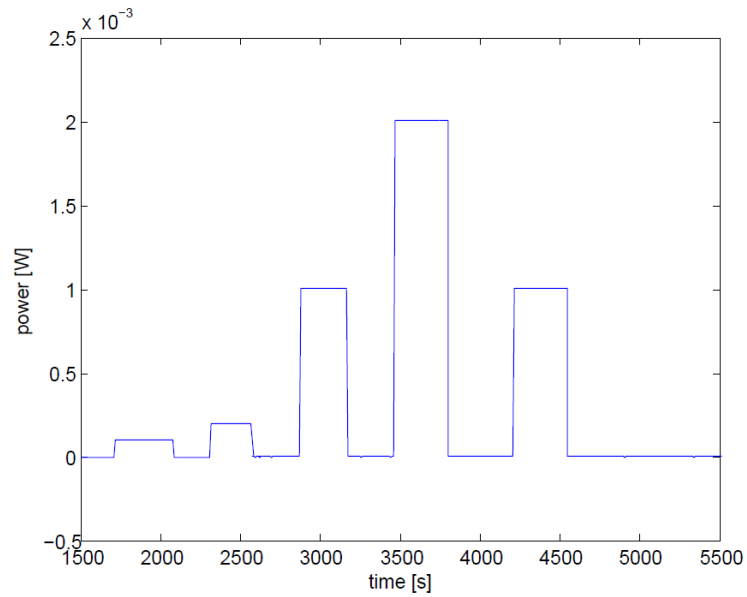


Figure 4.4: Power to the cell as a function of time. Five different powers are applied, alternated with a power of zero till a steady state is obtained.

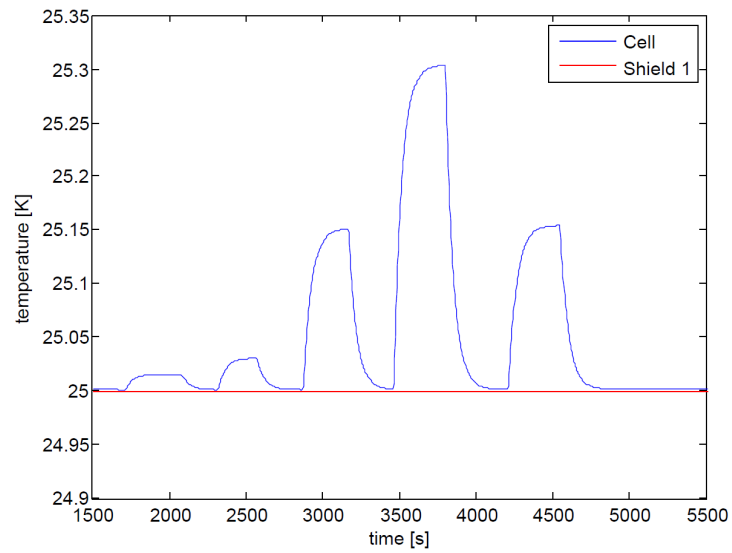


Figure 4.5: Temperature of the cell (red line) and temperature of Shield 1 (blue curve) as a function of time due to the applied power.

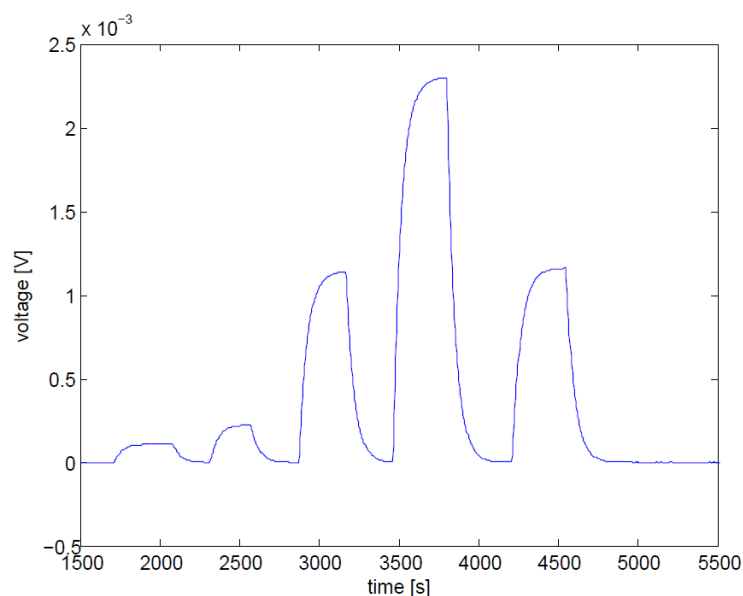


Figure 4.6: Voltage of the Peltier element as a function of time when applying an alternating power.

A stabilisation run When a typical measurement is started, first of all the stabilisation of the first shield at a given value is went through. The set-up has a certain time to achieve this stabilisation process. Depending on the run following the stabilisation run, different ΔT 's are used. Typical examples are large ΔT 's (several K) to cool the calorimeter fast to a low temperature starting point, or differences identical to those of the following run. Once the set-up is considered to be stable, a specific run (heating, cooling or pulsed) can be initiated.

4.5 Sample preparation

A lot of experiments in the calorimeter lab have been done as part of this Master's thesis. Measurements on single lipids (Chapter 5), lipid mixtures (Chapter 5), lipid membrane with cholesterol (Chapter 6) and on blood plasma (Chapter 7) took place.

The lipid samples used in the experimental part of this thesis, are prepared at the University of Hasselt [42]. The samples are based on three kinds of pure lipids: 1,2-dimyristoyl-sn-glycero-3-phosphocholine (DMPC), 1,2-dipalmitoyl-sn-glycero-3-phosphocholine (DPPC) and 1,2-distearoyl-sn-glycero-3-phosphocholine (DSPC), acquired from Avanti Polar Lipids (Alabaster, AL). From these pure lipids, several lipid mixtures are prepared. Depending on the mixture, different mole fractions of DMPC with DPPC (0.2, 0.4, 0.6 and 0.78) and different mole fractions of DMPC with DSPC (0.11, 0.2, 0.3, 0.4, 0.5, 0.6, 0.7, 0.8 and 0.9) are produced.

From the lipids, weighted in a flask, some multilamellar vesicles are produced by a conventional extrusion method. First of all, the lipid samples are dissolved in spectroscopic grade chloroform from Analar Normapur (assay 99.3 % and stabilised with 0.6 % ethanol). This solution (depending on the desired mixture) is stirred for a short time (about a minute). Next, the solvent is placed in a water bath at 60 °C and evaporated under a mild flow of nitrogen to dry the solution. After this process, when the solution contains a lipid film, this is stored in a vacuum environment

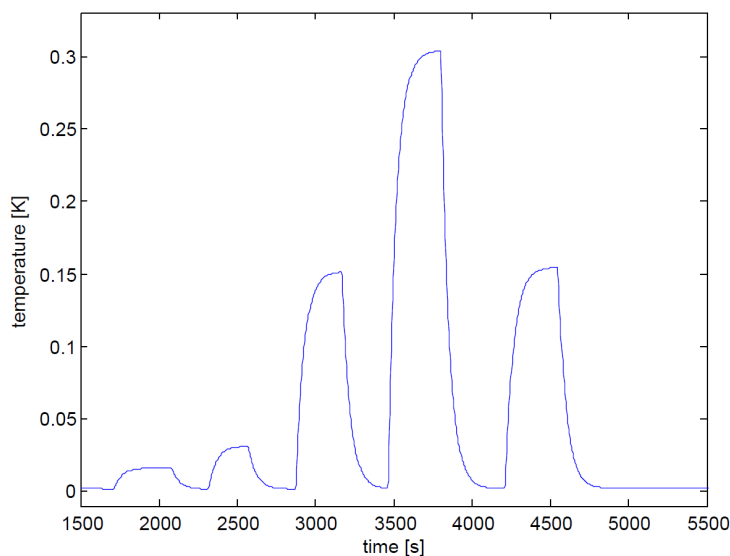


Figure 4.7: Difference in temperature of the cell and of Shield 1 as a function of time due to the applied power.

during one night. That way all the remaining residual solvents are eliminated. The next day, the lipid is hydrated with the 4-(2-Hydroxyethyl)-1-piperazineethanesulfonic acid (HEPES) till a concentration of 10 mg/ml is reached. HEPES is a buffer with a pH of 7.4 and consisting of 10 mM HEPES from Fisher Scientific (assay 99 %) and 150 mM NaCl from Sigma-Aldrich (assay ≥ 99.5 %). Finally, the solution is mixed for about one hour inside a water bath at 60 °C, and then placed in the fridge until the samples are measured by pASC. More information about the details of the lipid samples, both the pures and the mixtures, are listed in Table 4.2 for the DMPC with DPPC mixture and in Table 4.3 for the DMPC with DSPC mixture. The concentration of these lipid samples is 10 mg/ml.

Next to the pure lipids and the lipid mixtures, the addition of cholesterol to DPPC is measured with pASC. The same method as described above was used to prepare the samples. Three different mole ratios of cholesterol are prepared (0.13, 0.24 and 0.35). The data of the cholesterol samples are listed in Table 4.4.

Finally samples of blood plasma have been investigated by pASC. These samples, both platelets poor plasma (PPP) and platelets rich plasma (PRP), are prepared at the Katholieke Universiteit Leuven by Tristan Putzeys. More information about the preparation is explained in Chapter 7. Some general information about the samples measured by pASC is listed in Table 4.5.

4.6 Detecting a phase transition, based on C27 alkane

In order to illustrate the performance of pASC, a typical run with an alkane C27 is analysed. The analysis of this sample gives a clear view of the analysis of the data, which leads to the understanding of the phase transitions. The measurement is done with pASC, because a PI-controller was not tuned optimally for this run, considerable noise is visible in the Peltier signal. Due to the characteristics of the calorimeter and the run, this noise largely cancels out, and the final c_p and h are not influenced too much. For the purpose of illustrating the working of a pASC, this

Table 4.2: More details about the masses of the lipid mixtures of DMPC with DPPC, measured with pASC. The mass of the total sample (water+lipid mixture), the mass of the lipid mixture and the mass of the empty cell are listed.

	Mass sample (mg)	Mass lipid (mg)	Mass cell (mg)
1 · DMPC + 0 · DPPC	106.8	10.7	259.5
0.8 · DMPC + 0.2 · DPPC	106.7	10.7	250.8
0.6 · DMPC + 0.4 · DPPC	109.9	11.0	247.9
0.4 · DMPC + 0.6 · DPPC	107.9	10.8	251.2
0.22 · DMPC + 0.78 · DPPC	107.7	10.8	248.7
0 · DMPC + 1 · DPPC	104.0	10.4	250.4

Table 4.3: More details about the masses of the lipid mixtures of DMPC with DSPC, measured with pASC. The mass of the total sample (water+lipid mixture), the mass of the lipid mixture and the mass of the empty cell are listed.

	Mass sample (mg)	Mass lipid (mg)	Mass cell (mg)
1 · DMPC + 0 · DSPC	106.8	10.7	259.5
0.89 · DMPC + 0.11 · DSPC	112.3	11.2	258.4
0.8 · DMPC + 0.2 · DSPC	103.9	10.4	252.1
0.7 · DMPC + 0.3 · DSPC	77.1	7.8	252.8
0.6 · DMPC + 0.4 · DSPC	103.7	10.4	247.1
0.5 · DMPC + 0.5 · DSPC	101.5	10.2	248.8
0.4 · DMPC + 0.6 · DSPC	102.0	10.2	249.6
0.3 · DMPC + 0.7 · DSPC	101.1	10.1	251.6
0.2 · DMPC + 0.8 · DSPC	102.0	10.2	248.9
0.1 · DMPC + 0.9 · DSPC	117.1	11.7	248.0
0 · DMPC + 1 · DSPC	116.2	11.6	248.6

Table 4.4: More details about the masses of the lipid with cholesterol samples measured with pASC. The mass of the total sample (water+lipid+cholesterol) and the mass of the empty cell are listed.

	Mass sample (mg)	Mass cell (mg)
1 · DPPC + 0 · cholesterol	104.0	250.4
0.87 · DPPC + 0.13 · cholesterol	101.3	248.6
0.76 · DPPC + 0.24 · cholesterol	111.0	251.3
0.65 · DPPC + 0.35 · cholesterol	105.6	307.8

Table 4.5: More details about the masses of blood plasma measured with pASC. The mass of the total sample and the mass of the empty cell are listed for both the platelets poor plasma and platelets rich plasma.

	Mass sample (mg)	Mass cell (mg)
Platelets poor plasma	100.9	308.1
Platelets rich plasma	106.6	307.9

run is perfectly usable.

C27 is an alkane existing of 27 atoms of carbon and 56 atoms of hydrogen. This alkane is interesting because several phase transitions occur, and because the chemical simulants with the alkane tail of lipids. By heating C27 [64, 65] from a crystal phase, first another (second) crystal phase is observed, followed by three rotator phases. At lower temperatures the R_V phase occurs, where the molecules are tilted with respect to the layers which are packed in a monoclinic lattice. The next rotator phase is the R_{III} phase, here the molecules are tilted in a triclinic lattice. Further heating leads to the last observed rotator phase R_{IV} , the molecules are still tilted in a hexatic lattice. Finally, heating to higher temperatures gives rise to a liquid phase [64, 65]. The alkane is heated from 25 °C till 65 °C with an averaged rate of 1.29 K/h. The mass of the cell is 248.2 mg, containing 56.3 mg of the alkane.

4.6.1 Direct data and calculations

Evolution of the sample temperature Figure 4.8 shows the temperature of the cell, the first shield, the second shield and the oven as a function of time. Because of working in an adiabatic environment, the temperature of the cell and the first shield coincide. The second shield was kept at a fixed temperature difference of 0.2 °C below the temperature of the first shield. The temperature of the oven follows the temperature of the second shield at a constant temperature difference of 3 °C. All temperatures increase monotonically with time. There is a constant plateau when the phase transition takes place, because the power is no longer used to heat the cell, but to undergo the phase transition. Clearly, in C27, three phase transitions are observed.

Evolution of the power to the cell The second plot (Figure 4.9) shows the power to the cell as a function of time. The power P_{elec} is measured from the source. This power is supposed to be constant, nevertheless, the graph is rising very slowly. This is because the constant current of the source, makes the temperature of the set-up rise, resulting in a higher resistance, and therefore higher power, since $P = I^2 \cdot R$. Further, the phase transitions are visible in this power due to the plateaus in the temperature evolution representing the phase transitions.

Due to small temperature fluctuations, the Peltier element measures small differences in voltage, expressing heat leaks. The corresponding fluctuations of the power are of the order of $\pm 40 \mu\text{W}$, which is to be low compared to the electric power of 400 μW .

Time evolution of the voltage of the Peltier element Figure 4.10 shows the voltage of the Peltier element as a function of time. The temperature of the first shield is controlled with respect to the Peltier voltage. Due to the adiabatic condition, temperature of the cell and the first shield are maintained equal, the Peltier voltage has to be zero. Still, due to the heat leakage, a small Peltier voltage is measured. The voltage fluctuations are observed around -40 μV and 40 μV , which leads to an average close to zero.

Time evolution of the time derivative of the temperature The fourth plot (Figure 4.11) shows \dot{T} as a function of time. The temperature increases linearly, except at the phase transitions where it remains constant. Looking to the derivative, \dot{T} as a function of time, during the phase transition a peak, going to zero, in the derivative is observed. Beyond these phase transitions the derivative is rather constant. The peak observed corresponds to the plateau observed in the Figure 4.8. Finally, remark that this graph is inverse proportional to the heat capacity because $C_p = \frac{P}{\dot{T}}$ with P quasi constant. The derivative was calculated based on 51 points in a temperature region of 40 °C.

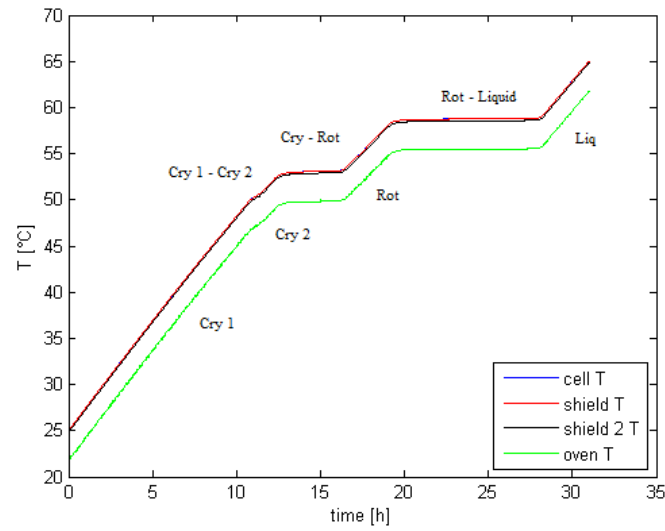


Figure 4.8: Temperature of the cell, the first shield, the second shield, and the oven, as a function of time. The temperature increases constantly, at the phase transition a constant plateau is observed. The power on C27 is then supplying the latent heat.

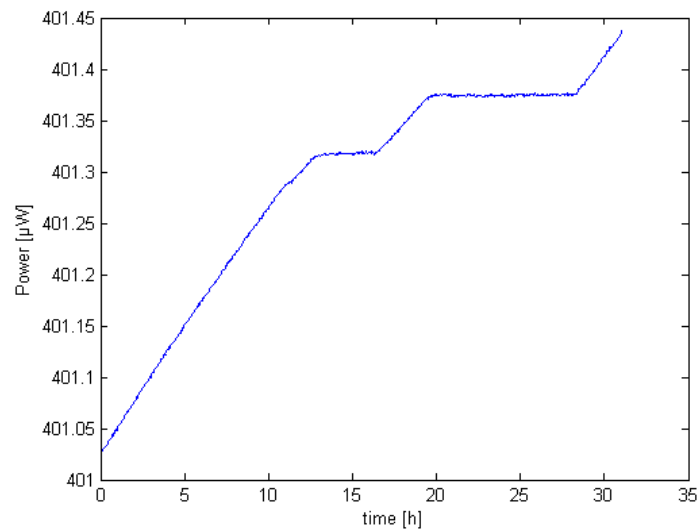


Figure 4.9: Power to the cell delivered by the source as a function of time for a heating run. The power is slightly increasing due to the increasing resistance of the heating element.

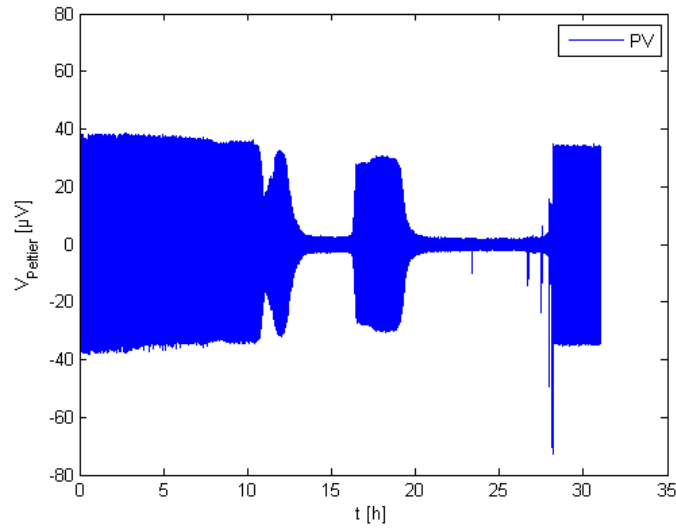


Figure 4.10: Voltage of the Peltier element as a function of time for a heating run on C27. The averaged fluctuations of the voltage are close to zero.

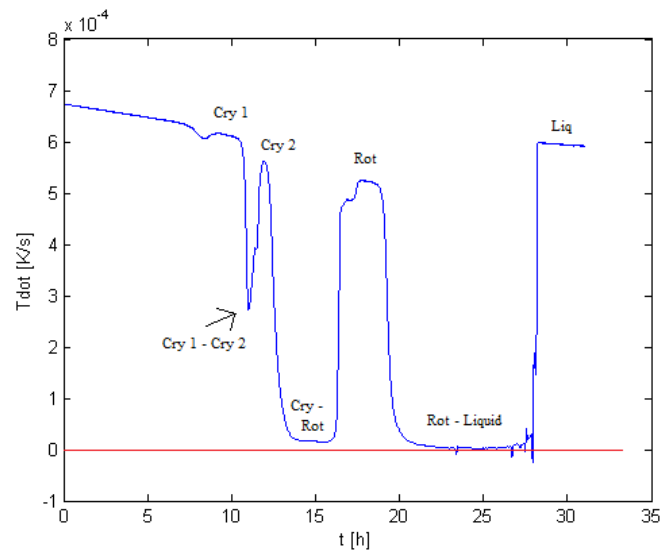


Figure 4.11: The time evolution of the time derivative of the temperature for a heating run. The red line (plotted on zero) illustrates that the peaks going to zero when a phase transition occurs. Beyond the phase transition, the derivative of the temperature (the blue line) is constant.

Temperature dependence of the specific heat capacity Figure 4.12 plots the temperature dependence of the specific heat capacity, which is the inverse of the latter figure. The peak observed in the heat capacity indicates a phase transition. For an ideal sample, the heat capacity would go to infinity. This heat capacity is the specific heat capacity which contains the heat capacity of the sample without the cell, thermal paste and addenda (platform, Peltier element, wires, etc).

A high temperature resolution (mK) near a phase transition is observed. Due to the constant power, the temperature rate near the phase transition will decrease because of the increasing heat capacity. A slow measurement takes place which results in a high temperature resolution. Beyond the phase transition, a temperature rate of 2.47 K/h is observed.

Temperature dependence of the specific enthalpy as a function of the temperature

Figure 4.13 shows the specific enthalpy as a function of the temperature. Being able to determine this quantity directly, by integrating the heat capacity, is an important advantage of pASC. Another way to calculate the enthalpy is by using the relation between the enthalpy and the power: $H = \int P dt$. From this, the specific enthalpy can be calculated, which is plotted in the figure. The enthalpy jumps at a first-order phase transition, reflecting the latent heat.

4.6.2 Discussion of the heat capacity and the enthalpy

The specific heat capacity of the alkane is presented in Figure 4.12. Three phase transitions (corresponding to the peaks) are observed. The first peak, at about 53 °C, represents the phase transition between a first crystal phase and a second crystal phase. The second phase transition takes place at about 55 °C. This is the transition from the crystal phase to the rotator phase. Finally, a peak is observed at 59 °C, coming from the transition between the rotator phase and the liquid phase.

When focussing on the rotator phase, several rotator phases are detected. The temperature region between 53 °C and 58 °C is zoomed in at Figure 4.14. In this figure three rotator phases are visible: the R_V phase, the R_{III} phase and the R_{IV} phase [64, 65].

Each phase transition is accompanied by an amount of energy which is released. The transition is readable from the step in the enthalpy. The enthalpy from the main transition was presented above, this amount of energy h has been calculated by using two different ways:

$$\Delta h(h) = h(T_{\text{end}}) - h(T_{\text{onset}}) \quad (4.6)$$

$$\Delta h(c_p) = \int_{T_{\text{onset}}}^{T_{\text{end}}} (c_p(T) - c_{p,\text{bg}}) dT \quad (4.7)$$

with $c_{p,\text{bg}}$ representing the baseline of the c_p behaviour, representing the heat capacity if no transition is observed. T_{onset} (T_{end}) represents the beginning (ending) temperature of the phase transition. The constructions used for the determination of the second crystal phase to the Rotator V transition are presented in Figure 4.15. The results are summarised in Table 4.6, together with the errorbars. The error on the determination of the transition enthalpies consists of two contributions: the accuracy of the measurements (thus, how well c_p and h have been measured), and the influence of the choice of the relevant temperatures and extrapolation lines. The first contribution is about 2 %, as discussed in [37]. Multiple evaluations with different temperatures and extrapolation lines were made in order to establish the second contribution.

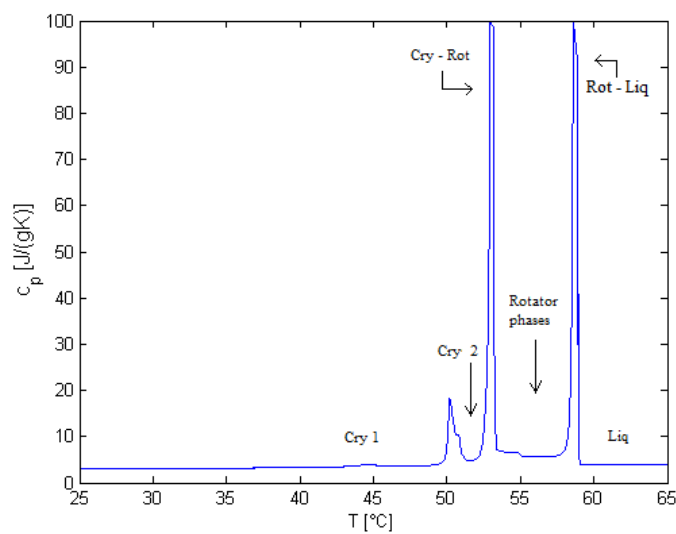


Figure 4.12: The temperature evolution of the specific heat capacity of C27 for a heating run. The transitions between the rotator phases are hardly visible on this scale, a detail of this region is given in Figure 4.14.

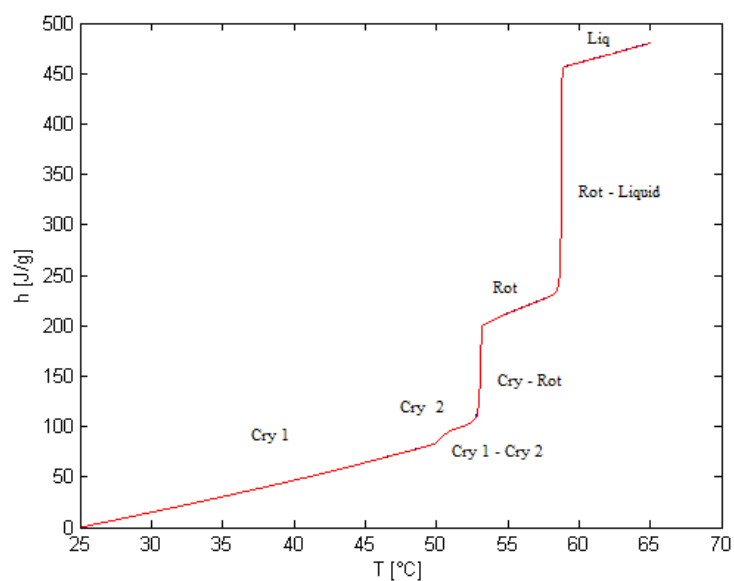


Figure 4.13: Specific enthalpy as a function of the temperature for a heating run on C27. Several heat steps are clearly visible, representing the heat contained in the phase transition.

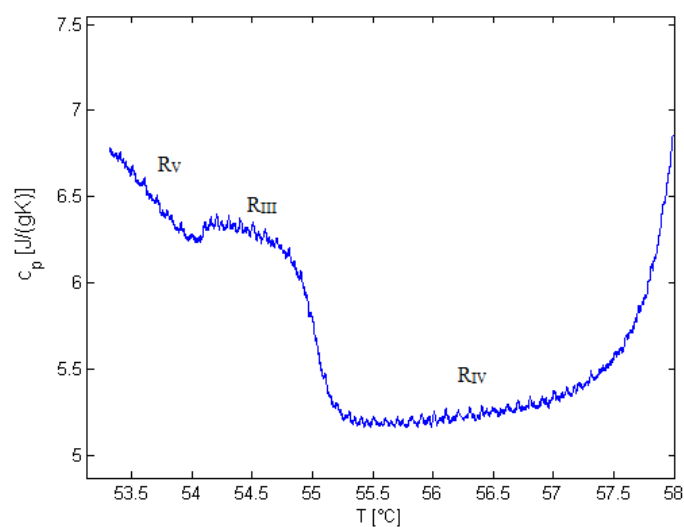


Figure 4.14: The specific heat capacity of C27, zoomed in on the different rotator phases. Three rotator phases are detected: the R_V phase, the R_{III} phase and the R_{IV} phase.

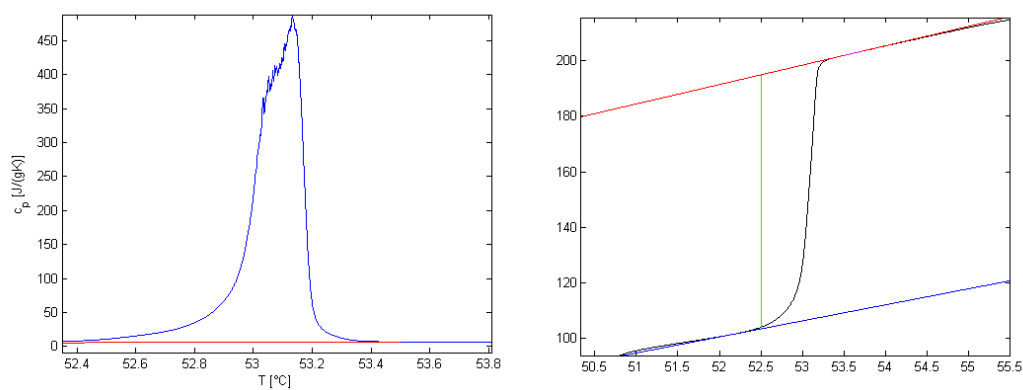


Figure 4.15: Determination of the amount of energy contained in the second crystal phase to the rotator V transition. Left: The specific heat capacity is plotted in blue. The red line represents the baseline, this is the specific heat capacity when no phase transition occurs. Right: The determination of the amount of energy contained in the phase transition. The melting heat is determined by the step in the enthalpy (the black curve). The red and the blue curves are determined based on the onset and the ending of the phase transition.

Table 4.6: The enthalpy of the phase transitions calculated based on two different methods. Values for the rotator transitions cannot be reported because the transition heats are too small to detect. It is not possible to give a reliable value of the energies of these transitions by pASC.

	$\Delta h(h)$ (J/g)	$\Delta h(c_p)$ (J/g)
Crystal 1 \rightarrow Crystal 2	8.39 ± 0.186	7.72 ± 0.515
Crystal 2 \rightarrow Rotator V	91.70 ± 0.8902	91.55 ± 1.495
Rotator V \rightarrow Rotator III	/	/
Rotator III \rightarrow Rotator VI	/	/
Rotator \rightarrow Liquid	265.17 ± 0.26575	223.52 ± 0.22091

Chapter 5

Lipid-membrane phases

As one of the most important building blocks of the biological membranes, lipids are interesting to investigate. A lipid bilayer in an aqueous environment is characterised by several physical phases. These phases influence the structure, resulting in a change of the biological function.

5.1 Lipids in biology

The cells in the body are built from small organic molecules that are based on the chemistry of carbon [54]. Four classes of small molecules can be distinguished: sugars, amino acids, nucleotides and fatty acids. These building blocks are represented in Figure 5.1. By combining these different small molecules, larger entities are formed. These entities are called macromolecules, or macromolecular assemblies. Four classifications of macromolecules are known: polysaccharides, proteins, nucleic acids and fats. Several fats can be combined again forming lipids, which can be put together into membranes. An example of a cell membrane, containing some lipids (in this case a lipid bilayer), saccharides and proteins, is present in Figure 5.2.

Sugars, amino acids and nucleotides are chemically bound to form polymers, i.e. sequences determine the properties of the macromolecules. In contrast, lipids (several fats together) do not link chemically to form polymers but instead, lipids form a macromolecular assembly in a solution. The most common is the lipid bilayer membrane, which could be seen in Figure 5.2.

The concept of the biological membrane [21], consisting of two layers (a bilayer) of lipids putted opposite together, is already known since 1925 and is found out by Gorter et al. Ten years later, Danielli et al completed the membrane by adding proteins. In 1972, Singer et al. proposed a model to these additional proteins. This model is known as the fluid mosaic model, characterising each leaflet of the bilayer as a homogeneous environment of lipids in a fluid state, completed with proteins. Almost thirty years later, in 1997, Simon et al. and Brown et al, proved the opposite: the biological membranes are not formed by homogeneous environments, but instead the membranes are organised by phase-separated domains at the microscale, called lipid rafts. This new concept increased the amount of investigations based on the biology of the membranes, as based on detecting the heterogeneities. Nowadays, the idea of the lipid rafts is still present, expanded with the presence of cholesterol and sphingolipids in the lipid rafts. The latter model expansion results in good physical and biological results, used to investigate a lot of biological processes [21].

Interactions between lipids and sugar, and between lipids and proteins, take place, indicating that the lipid bilayer is at the core of all biological membranes. A membrane possibly contains billions of lipid molecules and more than hundreds of different kinds of lipids. The plasma mem-

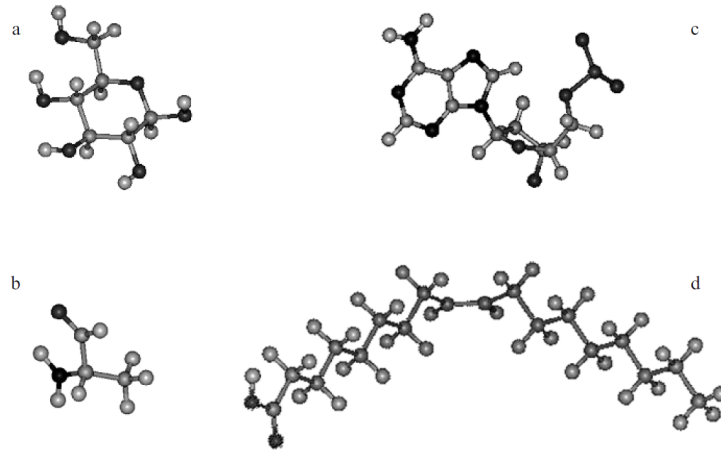


Figure 5.1: Four classes of small molecules: (a) sugar, (b) amino acid, (c) nucleotide and (d) fatty acid. These small molecules are combined to make larger entities. The dark atoms present oxygen atoms, the other atoms are hydrogen and carbon atoms [54].

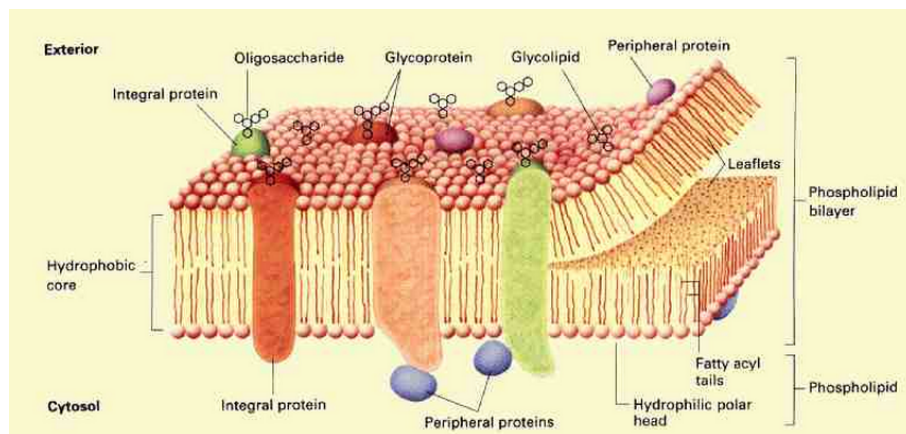


Figure 5.2: A cell membrane containing some macromolecules: saccharides, proteins and fats (combined until a lipid bilayer is formed) [5].

brane is an example of one of the most famous membranes in the body, containing a lipid bilayer as central element. This bilayer is extremely thin compared to the size of the cell which is encapsulated by the membrane. Another important membrane is the endoplasmatic reticulum (ER) membrane. This is connected to the porous double membrane of the cell nucleus and is the major site of synthesis of lipids. In general, many important biological processes in the cell take place in membranes or are mediated by membranes. The lipid bilayer, for instance, is a passive permeable barrier for ions and other molecular substances [54].

Compared to proteins and DNA, lipid molecules do not have function-related structural elements with a single molecule. Usually, their function is performed through the formation of supramolecular assemblies, often contained of many kinds of lipids. As such, it is not easy to link some structural order to the biological function. Nevertheless, both prokaryotic and eukaryotes cells contain a few hundred of different types of lipids, which makes the lipids the most diverse class of molecules in cells [54].

In modern biology, the stress of investigations falls on the relationship between the biological function and the macromolecular structure. Despite this increasing amount, the gain of understanding of the lipid membrane structure is rather slow. This is because one investigates the well-defined structures, based on several models, which are not traceable in the real lipid membranes due to the less ordered structures. This state of substantial disorder arises because of the self-assembled aggregation of the membranes which is an entropy-driven theory. The total entropy of the surrounding water increases, without the need of an outside energy source. Modern biology investigations are still going on, dealing with the challenge trying to make progress to identify the hidden elements of order [54].

Many lipids are naturally produced in the body and contain a group of naturally occurring molecules who are important in the biochemistry field. Other important lipids are not made by the body itself, but need to be digested by food. The main biological function of lipids is the storage of energy. Furthermore, they act as structural components of cell membranes and they act as signaling molecules. Lipids also take care of enzyme activation in the body, molecular transportation and metabolism. Finally, lipids (lipid bilayers) manage the incoming and the outgoing molecules in and to the cell. More exotic, the lipids occur as a shock absorber, in case of a shock, they will protect the vital organs [38].

5.2 Lipids in chemical terms

Based on the chemical composition, lipids can be divided into two groups: the simple lipids and the complex lipids [16]. The chemical composition of the lipids is explained based on the book of Mouritsen [54].

To form a lipid, some hydrocarbons are needed. These hydrocarbons (typically a long-chain) are composed of carbon (C) and hydrogen (H). The structure can be both saturated or unsaturated, dependent on the binding between the different carbon atoms. As seen in Figure 5.3 (a), if only single bonds are presented in the structure, it is called a saturated structure, as can be seen on the left. If the structure contains one or more double bonds, as presented in the right one, the structure is called unsaturated. Hydrocarbons are not easily dissolved in water, even more they will repel water because of their hydrophobic nature.

When adding a carboxyl (-COOH) group to the hydrocarbon chain, the hydrocarbon chain turns into a fatty acid. These structures are made of a combination of several carbon (C), hydrogen (H) and oxygen (O) atoms and are called simple lipids. The carboxyl group can be dissolved in

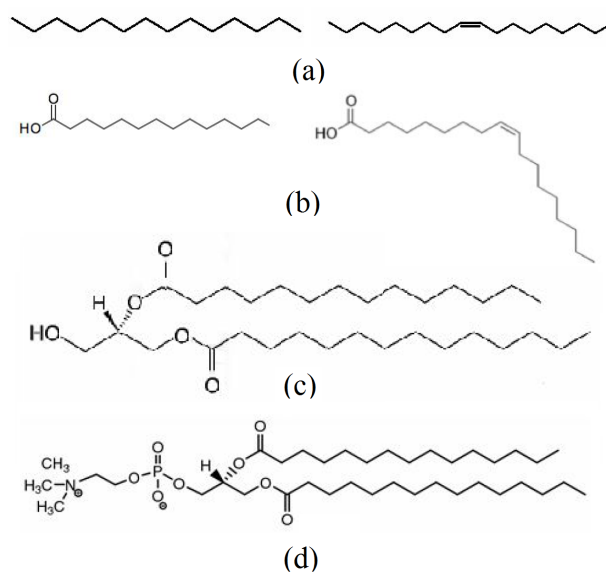


Figure 5.3: Four structures to illustrate the construction of a lipid. The basic construction (a) contains a hydrocarbon chain. The left one only contains single bonds (called saturated), the right one contains an additional double bonds (called unsaturated). By adding an additional group, such as a carboxyl group, a more complex lipid occurs, such as a fatty acid pictured in (b). A more complex lipid is observed by adding other elements. Two examples, both an apolar lipid (the myristic acid (c)) and a polar lipid molecule (1,2-Dimyristoyl-sn-glycero-3-phosphocholine, also called DMPC, pictured in (d)) are shown [54].

water in contrast the hydrocarbons, because of the hydrophilic character. A representation of a fatty acid, corresponding to the hydrocarbon described above, is given in Figure 5.3 (b).

A simple way to sort different fatty acid is by writing first the amount of carbon atoms, followed by the amount of double bounds. The myristic acid, presented in the figure, is given by 14:0, while the oleic acid can be written as 18:1.

In a cell, fatty acids are not frequently found as a free system. More frequently they are linked to a hydrophilic group, as for instance glycerol. The latter is an alcohol that can become an ester, so the lipid becomes more complex due to several additional elements as for instance phosphorus (P), nitrogen (N) or sulfur (S). Because of these additional atoms, these lipids are called complex lipids. Figure 5.3 (c) represents the lipid molecule of the myristic acid. This acid is an example of a non-polar lipid. For comparison, a polar lipid molecule (DMPC) is presented in Figure 5.3 (d). This lipid will be used in the experimental part of this chapter.

5.3 Lipids from the physics point of view

One field within condensed matter physics is soft matter physics [44], studying systems that react sensitively upon external mechanic perturbations. Most biomolecular systems are classified under soft materials. Compared to hard condensed materials [4], which deals with materials with structural rigidity (crystalline solids, glasses, metals, insulators and semiconductors), soft condensed materials have some unusual properties which are very different from hard condensed matter. Hard matter is commonly used to refer to matter governed by atomic or molecular forces and quantum mechanics. Because dealing with biomolecular systems, as part of the soft condensed matter, it is a challenge to determine all these soft condensed properties.

Lipid membranes are classified as soft matter. These membranes can be considered as structured liquids. Nevertheless, lipid bilayers are durable and tough, compared to ordinary liquids, due to the self-assembly principle. In general, the softness is a requirement of the various functions containing the membrane.

To create an idea of softness of biomolecular systems, membranes and lipid bilayers could be compared to the softness of a simple soft plastic. Talking about bending, a DMPC lipid bilayer is about five times softer than a red blood cell membrane, which is 50000 times softer than a film of plastic of the same thickness. In terms of area compressibility, a DMPC bilayer is about ten times softer than a red blood cell membrane, which is about five times softer than a film of plastic, again of the same thickness [54].

A lot of factors influence the softness. Cholesterol tends to make membranes less soft, both in terms of bending stiffness and area compressibility. In that way, new phases are observed, as explained more into detail in Chapter 7. Further, the fatty-acid chain length plays a role in the softness. The shorter the chain length, the greater the softness. Also the degree of saturation offers a contribution, a more unsaturated chain provides a greater softness. At last, various solutes influence the softness remarkably [54].

5.3.1 The self-assembly process

Soft matter systems are interesting to investigate because of the range of spectacular properties, such as self-assembly [54]. Molecules arrange themselves in supramolecular assemblies, which pack in structures that can be highly ordered. This process occurs when mixing water with amphiphilic molecules, such as lipids.

Amphiphilic structures have a hydrophobic (nonpolar, water-avoiding) part and a hydrophilic

(polar, water-seeking) part. Putting these amphiphilic molecules into an aqueous solution results into several remarkable structures, due to the self-assembly process. A whole family of supramolecular aggregates are formed spontaneously, as illustrated in Figure 5.4. The hydrophilic end of the lipid faces toward the water-filled environments, both inside and outside the cell. While the hydrophobic end stays between the inside- and outside-facing layers, as far as possible from the aqueous solution. The process is caused by the hydrophobic effect where the lipid molecules are oriented as far as possible of water. Many lipid molecules act together in this process (the many-molecule effect) so a family of several lipid aggregates are formed. The first structure possibly formed is a simple lipid monolayer, shown in Figure 5.4 (a), this is a monomolecular film of lipids which is formed on the separation of water and a hydrophobic substance. In a pure aqueous solution, this monolayer is never found. When combining two lipid monolayers back to back, a lipid bilayer is formed, as presented in (b). This bilayer is never constructed when there is a lack of water. When several bilayers are combined, a multi-lamellar structure (c) arises. This structure is stabilised due to a colloidal force. This is a thermodynamic force, defined as the spacial derivative of a free energy G .

$$F = - \left(\frac{\partial G}{\partial r} \right) = - \left(\frac{\partial H}{\partial r} \right) + T \left(\frac{\partial S}{\partial r} \right) \quad (5.1)$$

Further, the three structures explained first (a-c) contain an open end, which is not acceptable in the aqueous solution. These structures will re-organise until the formation of a micelle (d), a unilamellar vesicle (e), a multi-lamellar vesicle or liposome (f). Because this self-assembly process is a spontaneous process resulting in a stable assembly, those lipid aggregates heal themselves if needed.

Aggregation of amphiphilic molecule A lot of different structures can be formed due to the self-assembly process. The behaviour of all these structures is explained by a simple model, explained by [8]. This model is dependent on a few parameters to characterise the geometry of the molecules. For all structures, the driving force of the self-assembly is the minimalisation of the free energy, keeping into account that the hydrophilic head needs to be kept in contact with the water, and the hydrophobic tail has to be kept away from the water. The minimalisation of the free energy is dependent on the energy ϵ_N needed to bring a molecule from a bulk into an aggregate containing N molecules. This energy minimalisation is kept in balance because of the presence of the hydrophilic head and the hydrophobic tail. This condition leads into a thermodynamically arrested phase separation where aggregates are formed, rather than forming two separated and isolated microscopic phases.

This simple model considers a solute that has the possibility to aggregate. In the equilibrium state, the solute can both form isolated molecules and aggregate into an aggregation containing N molecules. The overall volume fraction of the solute is called ϕ , the volume fraction of the aggregate is defined as X_N . Working in a system in equilibrium, the volume fraction of a solute in the aggregate with a size N as a function of the fraction of the isolated (free) solute molecules X_1 is given by

$$X_N = N \left(X_1 \exp \left(\frac{(\epsilon_1 - \epsilon_N)}{k_B T} \right) \right)^N \quad (5.2)$$

Assuming $\epsilon_N \geq \epsilon_1$, most of the molecules will prefer to be isolated because of the lower energy needed. The other case, when $\epsilon_N < \epsilon_1$, the solute prefers to form an aggregate. Dealing with simple fluids, the energy needed to aggregate ϵ_N is monotonically decreasing as a function of N . Because of the decrease, a critical volume fraction ϕ_c is present, observing the size of the aggregate going to infinity. Nevertheless, in more complex fluids, such as amphiphiles, at a finite

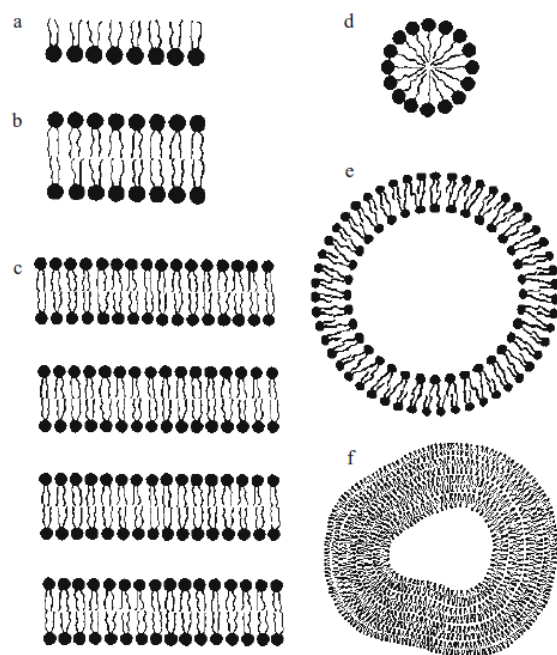


Figure 5.4: The self-assembly of supramolecular aggregates. (a) a lipid monolayer, (b) a lipid bilayer, (c) a multi-lamellar structure, (d) a micelle, (e) closed lipid layer (vesicle or liposome), (f) a multi-lamellar vesicle or liposome [54].

value N , the energy has a minimum. This minimum is observed because of the balance between the hydrophobic tail, that needs to be kept away from water, and the hydrophilic head that needs to be kept in contact with water. Reaching the critical volume fraction ϕ_c , the aggregate does not become infinite in size. This finite aggregate is called a micelle, and the corresponding concentration is called the critical micelle concentration CMC.

Spherical micelles The most common aggregate is the spherical micelle. The geometry is dependent on the critical chain length l_c , the hydrocarbon volume v and the optimum head-group area a_0 . The critical length chain l_c is the length of the hydrocarbon chain when it is fully extended. The hydrocarbon volume v is related to the volume of that hydrocarbon chain. Finally, the optimum head-group area a_0 is the optimum area between several head-groups. This is dependent, as illustrated in Figure 5.5, on the repulsion between head-groups coming too close to each other due to the electrostatic interaction, and the elimination of the tail coming in contact with water when the head-groups are too far away from each other. The optimum head-group area a_0 is found when balancing both contributions. Imagine a micelle as a sphere with radius r and containing M molecules. Together they present a volume of $4\pi r^3/3$ and a surface area of $4\pi r^2 = Ma_0$. This leads into a micelle with a radius of $3v/a_0$. Because dealing with a spherical micelle, the radius needs to be less than the critical chain length l_c . This fact gives the condition of dealing with spherical micelle, resulting in $\frac{v}{l_c a_0} \leq \frac{1}{3}$.

Cylindrical micelles Another geometric aggregate is the cylindrical micelle. This micelle is also presented by the same three parameter as the spherical micelle: the critical chain length l_c , the hydrocarbon volume v and the optimum head-group a_0 . Assume a cylindrical micelle, containing M molecules, a length l and a radius r . The volume of this micelle is $\pi r^2 l = Mv$, while the surface area is equal to $2\pi r l = Ma_0$. This leads into a cylindrical micelle with a radius of $2v/a_0$. Dealing with a cylindrical micelle is possible when the radius is larger compared to the chain length. This leads into the condition $\frac{1}{3} < \frac{v}{l_c a_0} \leq \frac{1}{2}$. Passing this limit on the upperside gives a preference to the formation of a bilayer.

Bilayers and vesicles The condition to deal with bilayers and vesicles is given by $\frac{1}{2} < \frac{v}{l_c a_0}$. Satisfying this condition favorites the formation of a bilayer or a vesicle. These are the structures used in the experimental part of this thesis. This bilayer structure is the most likely structure when dealing with amphiphiles with a large hydrocarbon volume and a rather small value of critical chain length. The optimum head-group area tends to self-assemble in a bilayer. Materials with two hydrocarbons, such as our phospholipids, achieve these properties easily, resulting in the formation of a bilayer, which are indeed the lipids used in the experiments. The free energy change ϵ_N when an amphiphile is put into a micelle, is independent of the area (at a certain distance from the boundaries). From this energy, the volume fraction of the molecules in the aggregate with N molecules is determined [8], depending exponential on \sqrt{N} . This shows that, above the CMC, adding an amphiphile results in an infinite, two-dimensional aggregate with the shape of a sheet.

All cases described above are summarised in Figure 5.6. This figure presents the three main aggregations of the lipids (the spherical micelle, the cylindrical micelle and the bilayer/vesicle), depending on the critical parameter. As can be seen in the last row, bilayers are indeed observed in double-chained lipids, which is indeed observed in phospholipids [13].

A few remarks have to be made to end the explanation of the self-assembly process. The ideas explained above deal with structures formed in a polar solution. On the other hand, placing the amphiphilic molecules in a non polar solvent, an inverse micelle is formed. The hydrocarbon tail

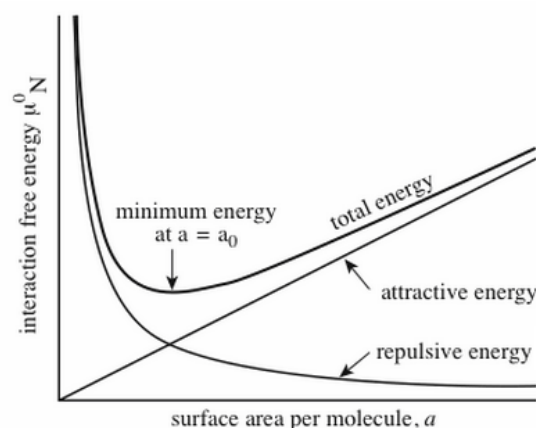


Figure 5.5: The optimum head-group area of a micelle. When head-groups are too close, the electrostatic interaction pulls them away. When head-groups are too far away from each other, the hydrophobic tails come in contact with water [8].

is exposed to the solvent at the outside of the inverse micelle, while the polar heads are pointed to each other, based on the repulsion between the hydrophilic head and the polar solvent at the outside. A second remark deals with the packing of the lipid molecules. The aggregates explained above are examples of lamellar phases, next to these phases also tubular arrangements can occur. The lipid membranes form hexagonal phases, also called nonlamellar phases, depending on the environment of the lipid.

5.3.2 Phases of lipids in bilayers

The discussion of the phases is focussed on the lipid molecules, organised in a lipid bilayer. Several physical phases are observed when heating a lipid bilayer. A lipid bilayer is formed because of the hydrophobic interaction. In a biological membrane, both the van der Waals interaction (holding the hydrophobic tails together) and the hydrogen bonding (holding the hydrophilic heads at the water interface) keep the lipid phase in equilibrium. Changing the composition of the solution, temperature regions will be shifted and the stability of a particular phase of the lipid bilayer changes. Next to the hydrophobic interaction also the general electrostatic forces are present.

Lipids are biomolecular systems containing several physical-phase states [36]. Next to the most obvious phases (the gel, also called the solid-ordered phase, and the isotropic liquid phase), other mesomorphic phases are present. Phases such as gel phases occur, in a pure lipid for instance, a subgel phase is observed, which is called a mesophase. In a mesophase, the molecules are separated in parallel layers of quasi-crystalline order. The lipids are capable of forming highly ordered structures (the gel phases) or by melting (raising the temperature) a liquid phase is formed. Cooling the samples down, the same transitions will occur, so the melting process is reversible (compared for instance to the DNA denaturation which is not reversible). The driving forces of the physical phases are based on the hydrophobic force, because of dealing with amphiphilic biomolecular systems.

Lipids present in water are characterised by a large variety of phases, each with their own structure and morphology. Lipids can form various ordered, crystalline, gel or liquid (also called liquid-

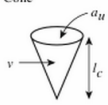
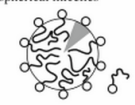

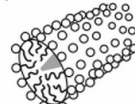


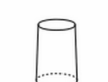

Lipid	Critical packing parameter $v/a_l l_c$	Critical packing shape	Structures formed
Single-chained lipids (surfactants) with large head-group areas	$< 1/3$	Cone 	spherical micelles 
Single-chained lipids with small head-group areas	$1/3 - 1/2$	Truncated cone 	cylindrical micelles 
Double-chained lipids with large head-group areas, fluid chains	$1/2 - 1$	truncated cone 	flexible bilayers, vesicles 
Double-chained lipids with small head-group areas	> 1	inverted truncated cone or wedge 	inverted micelles 

Figure 5.6: An overview of the different aggregates of lipids, depending on the critical parameter. The lipids measured with pASC are assembled to lipid bilayers, which is indeed confirmed by the double chain which is present in the phospholipids [13].

crystalline) phases, depending on the amount of water, the temperature and the lipid structure. Figure 5.7 shows several conformations of lipid membranes. The figure represents different lamellar phases: a subgel phase L_c (a), a gel phase with untilted chains L_β (b), a gel phase with tilted chain $L_{\beta'}$ (c), a rippled gel $P_{\beta'}$ (d), a fully interdigitated gel L_β (e), a partially interdigitated gel (f), a mixed interdigitated gel (g) and a liquid crystal L_a (h). In this nomenclature, determined by Luzzati [36], the lattice periodicity is characterized by L for a one-dimensional lamellar lattice and a P for a two dimensional oblique or rectangular lattice. A hexagonal lattice is indicated by H and is not found in these lipid phases. The subscript describes the chain conformation: α for a disordered chain (a liquid crystal), a β for an ordered chain (gel) and a β' for an ordered tilted chain.

The nature of the pure and the binary lipid determine whether a particular phase is observed in the aqueous solution. For the phospholipids that are studied in this work, the typical sequence is: the subgel, gel, ripple-gel and the liquid phase. In addition, the visibility of the phase transitions for the calorimeter may be limited by the energy involved ('small peaks') and by the temperature at which they occur, for example the subgel to gel transition takes place near 0 °C in DMPC.

Another phase is the so-called liquid-ordered phase, occurring between the liquid crystalline phase and the gel phase in lipid mixtures containing cholesterol. This phase has the ordering of the liquid, and generally, the chains are extended, resulting in this intermediate state. This behaviour will be discussed in more detail in Chapter 6.

Before discussing the different phase transitions, a short explanation, based on an article of Hirst [30], about the structure of the different lipid phases observed in the lipids bilayer is given. When heating a lipid bilayer, the first phase observed is the subgel phase. This phase is not observed in the biological membrane in the human body. Nevertheless, a crystalline structure, characterised by an oblique lattice is observed. The lipids are tilted with respect to the lipid bilayer normal. This phase has a long-range order, without any freedom for rotation or diffusion. Heating the lipid bilayer results into a phase transition between this subgel and the gel phase, recognised by an orthorhombic ordering. Still, the lipids are tilted and a long-range order is observed. Nevertheless, in this phase an (extreme) low diffusion rate is detected. Raising the temperature results into a second phase transition, from the gel phase to the ripple-gel phase. This phase has the same properties of the gel phase (the lipids are still tilted), but in this phase some ripples (some clear undulations) are observed. Finally, at the main transition, the last phase transition takes place from the ripple-gel phase to the liquid phase. In this liquid phase, the lipid molecules have a free motion, so a free rotation and diffusion are both observed. Because of

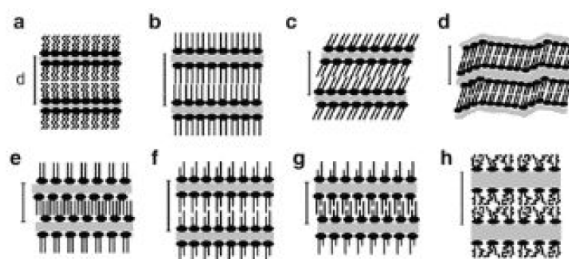


Figure 5.7: Different lamellar phases of lipids: a subgel phase L_c (a), a gel phase with untilted chains L_β (b), a gel phase with tilted chain $L_{\beta'}$ (c), a rippled gel $P_{\beta'}$ (d), a fully interdigitated gel L_β (e), a partially interdigitated gel (f), a mixed interdigitated gel (g) and a liquid crystal L_a (h) [36].

these motions, the area occupied by the heads increases and the bilayer is characterised by a short-range ordering.

5.3.3 Phase transitions of lipids

Dealing with a single lipid structure, the most important transition is the (chain)melting transition, also called the order-disorder or the solid-fluid transition. This transition is associated with the transition of the hydrocarbon chains from a less disordered state to a fully disordered state. It is the major energetic event in the lipid bilayers, with a large amount of enthalpy released, accompanied by volume expansion and increased hydrophobic exposure at the polar-apolar interface to increase the bilayer area. This energy is used to fight against the attractive van der Waals interactions. In calorimetric measurements, this results in a sharp, narrow heat capacity peak. Another transition, the transition from a gel phase into an intermediate equilibrium state, is observed and is called the ripple-gel phase. At last, a third transition is observed, presenting the transformation between the subgel and the gel phase. By heating the lipid, the more ordered gel phase with orthorhombic hydrocarbon chain packing (the subgel) transforms into a less ordered gel phase [54].

Mixing lipids results into a lipid bilayer consisting of more than one type of lipid molecules and is presented by a more complex phase transition behaviour. Lipid molecules of the same type have a stronger attractive interaction compared to lipids of different types. This results in a different phase diagram, the temperature of the transition is changed and a coexistence region is observed. The more both lipids are different, the more complex phase behaviour occurs and the broader the two-phase state because the different molecules do not interact easily.

One of the possible differences between two lipids is the difference in head, which is not dealt with in this thesis. Another variation is the chain length, the more closely they match, the larger the preference for being together and the more easily they interact [54]. Some examples of the phase diagrams of different lipid mixtures are given in Figure 5.8. The first mixture, between DPPC and DSPC, has the smallest phase separation region of all mixtures presented. The minimum difference between lipids with a chain with an even amount of carbons is indeed two. In this mixture, a two-phase region in the lipid mixture bilayer appears. The type of lipid with the lowest phase transition temperature (in this case DSPC) is developed in the liquid-disordered phase. The other kind of lipid is developed in the solid-ordered phase. The second mixture, DMPC with DSPC shows a more striking phase-separation due to the larger difference in chain lengths. The last mixture, between DLPC (chain length of 12) and DSPC (chain length of 18) is much more complicated because of the large chain length difference, here an extra phase separation, the solid-solid phase separation, arises. The second mixture, presented here, will be verified in the experimental part of this chapter, where also the DMPC with DPPC mixture will be handled.

A three dimensional plot of the specific heat capacity of a lipid mixture DMPC with DSPC, as a function of both the temperature and the ratio of the mixture, is shown in Figure 5.9. Compared to a pure lipid where one peak is observed, two peaks are visible in the specific heat capacity of the mixture. This two-phase system is dependent on the composition of the mixture and the temperature. This three-dimensional graph will be verified by one of the mixtures measured with pASC.

5.4 Phase transitions of lipids detected by ASC

In this work, the thermal properties of both three pure lipids and two types of binary mixtures of phospholipids are measured with pASC. The aim of this research is to establish the influence of

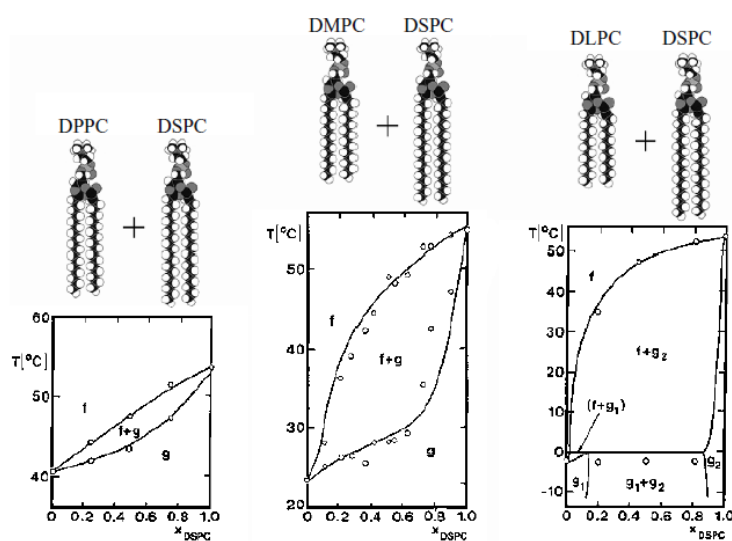


Figure 5.8: Three phase diagrams of mixtures of lipids. The more different both lipids are, the more complex phase diagram is observed. The liquid-disordered phase is indicated by f , the solid-ordered phase by g [54].

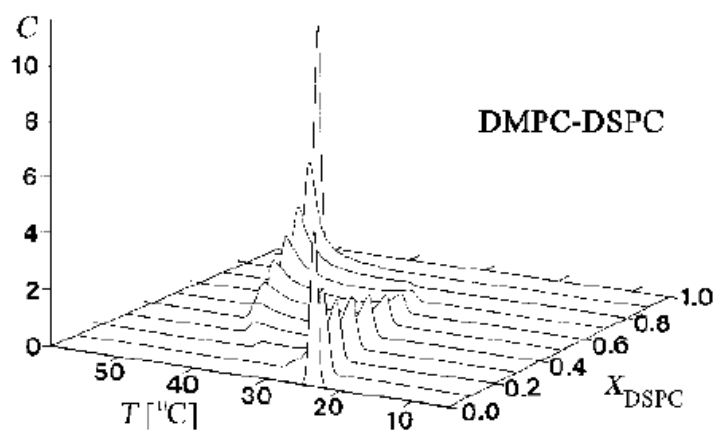


Figure 5.9: Specific heat capacity of a bilayer mixture composed of DMPC and DSPC, dependent on the temperature and the composition. Compared to a pure lipid, no longer a single transition peak take place in a lipid mixture. A two-phase region, where both the gel and the liquid phase are observed, is detected [54].

mixing a second lipid bilayer into a single lipid. The changes in the thermal properties (the phase transition temperature and the enthalpy) are investigated. Both lipids in the mixture have the same polar head but differ in length (14, 16 and 18 respectively) of the alkyl chain. A mixture of 1,2-dimyristoyl-sn-glycero-3-phosphocholine (DMPC, with a melting temperature around 24 °C) with 1,2-dipalmitoyl-sn-glycero-3-phosphocholine (DPPC with a melting temperature around 41 °C) and with 1,2-distearoyl-sn-glycero-3-phosphocholine (DSPC, with a melting temperature around 55 °C) are measured. The structure of the three pure lipids is presented in Figure 5.10. Both mixtures are isomorphous, so they are totally miscible in both the liquid and the gel phase. Because of the smaller difference in chain length between DMPC and DPPC, this mixture tends more to the ideal mixture behavior compared to the DMPC with DSPC mixture. Several mole fractions were prepared in steps of 0.1 for the DMPC + DSPC mixture and 0.2 for the DMPC + DPPC mixture. The most attention is put on the main transition, nevertheless the low-temperature transitions are not ignored. Other investigations on lipid transitions can be found in [41] where several techniques (pASC and QCM-D) are compared to each other, this comparison is also made in this thesis.

5.4.1 Pure lipids

The thermal properties of three pure phospholipids with different chain lengths were measured with ASC. For each pure lipid a heating run was obtained with an averaged scanning rate between 1.67 K/h and 2.65 K/h. The results are plotted in Figure 5.11 and more values about the thermal properties can be found in Table 5.2. The data in the plot were shifted vertically to obtain a better display, the absolute values of the specific heat capacity of the lipids can be found in the table. In each pure lipid, three different first-order phase transitions are clearly observed, which can be verified by the step observed in the enthalpy as seen in Figure 5.12. Comparing the different lipids, the phase transition temperatures shift to higher temperatures, by an increasing chain length. This because of the specific heat capacity is dependent on the composition of the lipid (both head group and chain length). In these measurements, the head group stays unchanged, while the chain length increases. The amount of methyl groups present in the lipid tail influences the amount of heat needed to melt the lipid. In the following, the results are discussed in terms of contributions of hydrophobic hydration of the lipid tails to the specific heat capacity. Based on our measurements and a book about thermal biophysics of membranes [29], the different phases and phase transitions are explained.

The main transition The most important and the most notable phase transition is the main transition, occurring at 297.5 K, 314.5 K and 328.1 K respectively, corresponding with the melting from a system in gel phase to the liquid phase. More information about the samples is given in Chapter 4. In the gel phase, lipids are ordered on a triangular lattice, compared to the liquid phase where the lipids are no longer present on a lateral order but are randomly organised. Because of the more tight packing in the gel phase, an increase in membrane thickness takes place. Typically, there is a reduction of about 20 à 25 % of the surface area, combined with a decrease in volume of more or less 3 % [58]. Both the polar heads and the apolar chains lose order by melting. The crystalline order of the polar heads is lost, changing to a liquid structure. Also the tail loses its ordered structure, i.e. an all-trans configuration, but by melting, other less ordered configurations (trans and gauche) are emerging. This transformation is also called the order-disorder transition. Both lost of ordering can take place at the same temperature, even though this is not necessary. If not, other phases occur, such as the liquid-ordered and the solid-disordered phases. The first one is for instance exploring as a result of adding cholesterol to a pure lipid, because of the mixture of molecules with too different sizes, by which the formation of a lateral lattice is

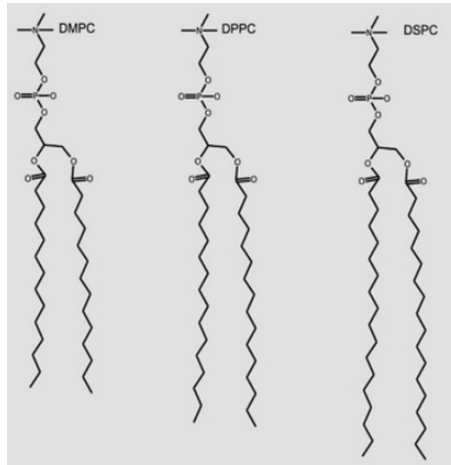


Figure 5.10: The structure of the three pure lipids used in the experiments. All three are phospholipids (PC), so they have the same head, but differ in length of chain. From left to right, DMPC, DPPC and DSPC are shown, with an increasing length of the chain [53].

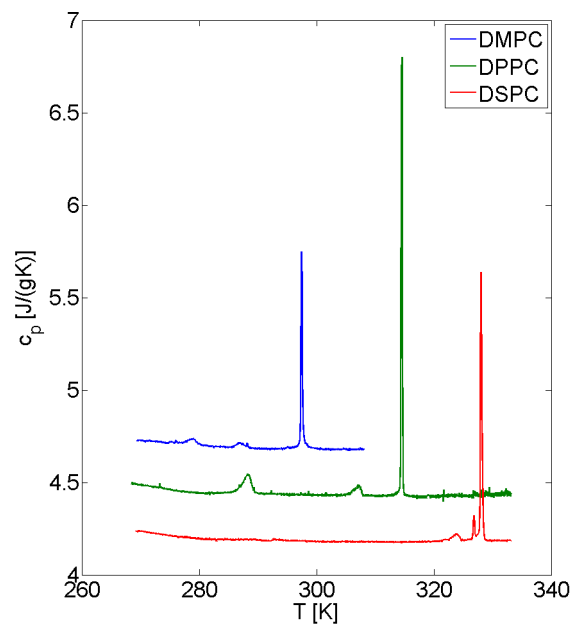


Figure 5.11: The specific heat capacity of pure lipids with different chain length. The transition temperatures increase with an increasing chain length. Four phases, subgel-gel-ripple-liquid, are characterised by the three phase transitions observed. In DSPC, a fourth phase transition at 326.90 K is observed. Its nature is still unknown [35].

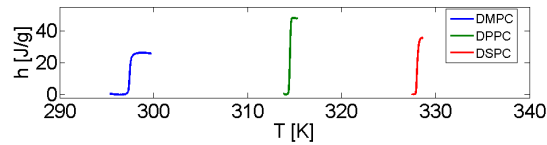


Figure 5.12: The specific enthalpy of pure lipids with different chain length. An increasing enthalpy step is observed with an increasing chain length. The step of DSPC is smaller compared to the step of DPPC because the additional peak observed at DSPC (which nature has not yet clarified) is not included in this step, nevertheless, in the calculations this peak does contribute to the enthalpy [35].

not possible. This phase can be seen as a gel phase without a lateral packing order. More details about the influences of cholesterol on a lipid bilayer are explained in Chapter 6.

The specific enthalpy of the melting curves of the pure lipids can be determined right away, representing the heat contained in the phase transition. Calculating this enthalpy in practice is depending on the phase transition and the baseline determination. Both thermodynamic properties are calculated on a systematic way, nevertheless this can be a significant source of error. The melting enthalpies of our measurements are presented in Table 5.2 and compared to some literature in Table 5.1. The literature experiments are done with DSC and the enthalpy has been calculated by the area under the transition peak. These values can be used to cross-check our experimental values. As observed in both data, the melting enthalpy increases with an increasing chain length. This has also been verified in Figure 5.12, keeping in mind that the step of DSPC is only caused by the main transition. Eventhough, in the calculations, the additional transition observed does contribute to the enthalpy value, indeed resulting in an increasing enthalpy. This behavior has also been observed in other investigations [35]. An extrapolation of this linear dependence shows that the straight line does not cross the origin (see [69]). Lipids with less than 10 carbons would have a negative enthalpy value and will not undergo a phase transition. At this moment the lipid chain is too short and the negative contribution of the lipid head dominates the positive contribution of the lipid chain to the enthalpy. The increase of the specific enthalpy as a function of chain length is linked to the chain isomerizations between the trans and the gauche configurations. At high temperatures, most of the states are in the gauche configurations. More information can be found in the article of Marcalja [48], assuming that the melting is caused by the dispersion forces between adjacent lipids and all possible configurations (all-trans, trans and gauche) occur in the lipid.

The peak observed in the specific heat capacity is very sharp. The phase transitions of the pure lipids occur at a small temperature region. The width of the peak is reflected by the half-width of the peak, which can be linked to the cooperative unit CU, i.e. clusters of lipids melting together, CU expressing the size of these clusters. The larger this cooperative unit size, the narrower the transition peak, ultimately resulting in an ideal first-order transition where all lipids undergo the phase transition together (so all molecules are totally correlated). In practice experiments were done on a finite system with boundaries resulting in a non-zero bandwidth and a finite cooperative system. Nevertheless, still a first-order transition is observed, which implies that the properties of the system change abruptly. The melting transitions of the pure lipids are sharp so it deals with a highly cooperative transition. A way of presenting the amount of lipids interacting can be calculated using the van 't Hoff relation [49]

$$\Delta H_{\text{VH}} = 4RT_m^2 / \Delta T_{1/2} \quad (5.3)$$

In this equation ΔH_{HV} is the van 't Hoff enthalpy, R is the gas constant ($R = 8.3144 \text{ J}/(\text{mol K})$), T_m is the temperature of the maximum specific heat capacity value and $\Delta T_{1/2}$ is the half-width value of the specific heat capacity peak. From this equation, the cooperative unit can be calculated by

$$CU = \Delta H_{\text{VH}}/\Delta H_{\text{cal}} \quad (5.4)$$

with ΔH_{cal} the enthalpy of the transition as listed in Table 5.2, together with the results of the CU calculations for both the gel-ripple and the main transition. The shorter the lipid chain, the higher the degree of cooperativity. During the melting of a lipid with longer chain, less molecules will cooperate together in the phospholipid bilayer. This is indeed observed in the main transitions of the pure lipids. Nevertheless, the behaviour of the cooperative unit of the lower-temperature transition does not reflect this trend. Probably this is caused because of the small transition at the lower temperatures, which are less easily to observe. Comparing the CU with the DSC literature, visualised in Table 5.1, a difference in size is observed. This difference is no anomaly because of a broadened peak in the DSC results is observed. Because of this broadening, the half-width value increases, resulting in lower values of CU.

An evolution of the state of the transition is contained in the relation between the calorimetric enthalpy ΔH_{cal} and the Van 't Hoff enthalpy ΔH_{HV} . If these values are the same, the transition occurs in a two-state mode, occurring both totally independent of each other. A higher van 't Hoff enthalpy compared to the calorimetric enthalpy is observed in a system with intermolecular cooperations. This is indeed observed in our measurements, the CU calculated are different from unity [27].

The low-temperature transitions This main transition explained is a transition observed in a two-dimensional membrane. Taking into account the medium around the lipids, a third dimension is relevant, resulting in a possibility to form other phases, which is indeed observed in the specific heat capacity. In the pure lipids DMPC, DPPC and DSPC, a transition between the gel and the ripple phase occurs at 287.5 K, 306.8 K and 323.7 K respectively. Following the trend of the main transition, the transition temperatures of these phases also shift to higher temperatures with an increasing chain length. The ripple-gel phase characterises the curvature change of the lipid bilayer and displays some periodical undulations (linked to the name 'ripple'). The chain can be both tilted or not tilted compared to the normal of the lipid membrane. The gel-ripple transition is much more broadened compared to the main transition, so the cooperativity is much lower. This is indeed verified by DMPC and DPPC, but because of the contribution of the melting temperature T_m and the enthalpy ΔH_{cal} , this behaviour is not observed in DSPC. Further, the distance between this transition and the main transition decreases with an increasing chain length. Zooming in on this region shows that the specific heat capacity values do not return exactly to the same baseline as observed before and after the transition. This proves that the gel-ripple and the main transition should be considered together as a total melting process.

The last transition observed by ASC is the transition between the subgel and the gel phase. The subgel is a crystalline, stable phase, characterised by more order and by orthorhombic hydrocarbon chain packing. The lipid molecules experience long-range order resulting in a two-dimensional crystalline order. This transition was not observed in DSPC by our measurements. Based on DMPC and DPPC, the phase transition also shifts to higher temperatures with an increasing chain length. A quick look to Figure 5.11 shows that the enthalpy possibly increases with an increasing chain length. So based on the area under the peak transition, the same behaviour as in the main transition and the gel to ripple-gel most likely occurs. This cannot be checked based on our normal procedure (as done for the other transitions) because the step in the enthalpy is too small to detect without making errors. Nevertheless, observing these low phase transitions is a progressive evolution, hardly investigated until now. The fact that pASC

Table 5.1: The enthalpy and the cooperative unit of the pASC measurements, compared to the literature values of Mabrey et al. [69]. The size of the units is particularly affected due to the way of calculating the enthalpy and due to impurities and other unrecognizable influences. Left: the low-temperature transition. Right: the main transition.

	Δh_{pASC} (J/g)	Δh_{Lit} (J/g)	CU _{pASC}	CU _{Lit}
Gel-ripple transition				
DMPC	5.7	6.2	458	280
DPPC	5.1	10.3	505	290
DSPC	6.1	9.5	656	160
Ripple-liquid transition				
DMPC	28.1	33.3	775	330
DPPC	41.7	49.6	597	260
DSPC	42.5	56.1	508	130

observes these transitions shows the great possibilities of this technique and proves the power of the adiabatic scanning calorimetry technique. As far as we know, these observations have not yet been made in other researches. To obtain a better insight in the evolution of the low-temperature transitions, the difference in transition temperature of the main transition and the low-temperature transitions are plotted in Figure 5.13. This phase diagram shows the increasing distance between the subgel-gel transition and the main transition for an increasing chain length, and analogous a decreasing distance between the gel-ripple transition and the ripple-liquid transition.

Finally, an additional peak is visible in the specific heat capacity of DSPC, this peak has been verified in other experiments [35] even though no explanation has been found yet about the nature of this transition.

5.4.2 Mixture lipids

Biological membranes in the human body consist of a complex mixture of lipids. The different lipid species do not melt independently but rather influence each other in the melting process. To get an idea of the influence, the melting of two lipid mixtures, DMPC with DPPC and DMPC with DSPC were measured by pASC. The thermal properties of these sample materials are listed in Table 5.3 and in Table 5.4. The first mixture approaches more to the ideal mixing because of the smaller difference in chain length (14 carbon atoms vs 16 carbon atoms). The second mixture observed, DMPC with DSPC, is characterised by a larger variation in chain length (14 carbon

Table 5.2: Transition temperature, enthalpy and the cooperative unit of both the gel to ripple transition (left) and the ripple to liquid-disordered transition (right) of the pure lipid bilayers. The enthalpy has been calculated based on a systematic method, the CU is calculated via the van't Hoff relation and the specific heat capacity is obtained by the maximum of the graphs.

	T(K)	Δh (J/g)	CU	c_p (J/(gK))	T(K)	Δh (J/g)	CU	c_{ps} (J/(gK))
DMPC	287.5	5.7	458	4.18	297.5	28.1	775	5.25
DPPC	306.8	5.1	505	4.30	314.5	41.7	597	6.55
DSPC	323.7	6.1	656	4.22	328.1	42.5	508	5.64

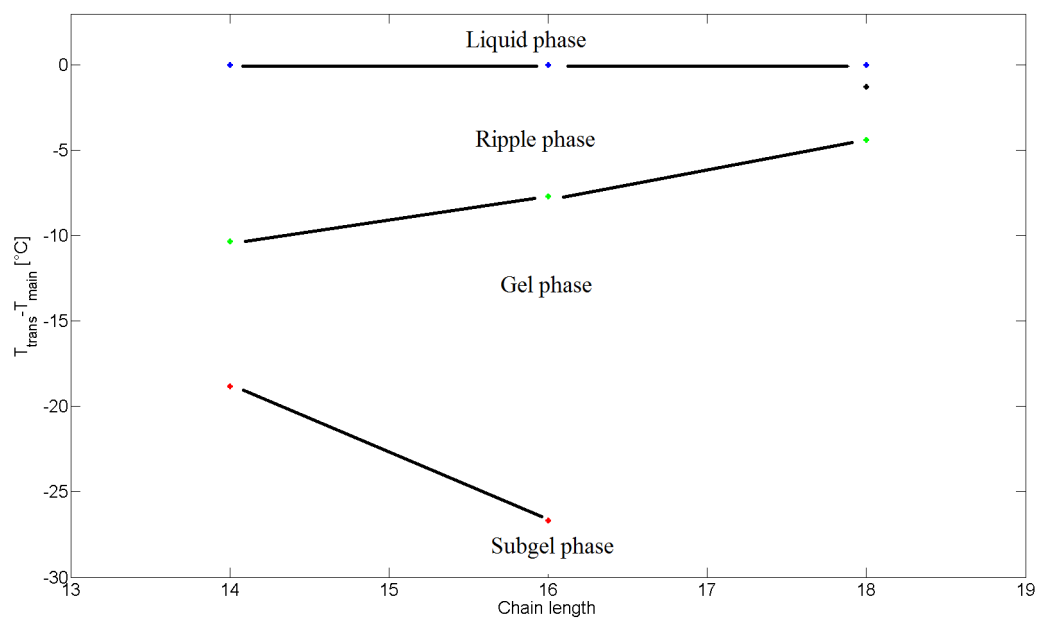


Figure 5.13: Difference in transition temperature of the observed phases between the main transition and respectively the main transition (blue), the gel-ripple transition (green) and the subgel transition (red). The black point shows the addition peak observed in DSPC.

atoms vs 18 carbon atoms).

From main transition to coexistence region Lipid mixtures no longer undergo a clear main-melting transition. Instead, this transition is replaced by a phase coexistence region, which appears because of the difference in melting temperature of both lipids separately. When heating the mixture, the lipid with the lowest melting transition starts to melt before the other one, so both molecules in a gel phase and in a liquid phase are present in the bilayer. Reaching the melting temperature of the lipid with the highest melting temperature, the mixture acts normal again because all molecules are situated in the liquid phase.

Results from the first mixture, DMPC with DPPC, are presented in Figure 5.14. This mixture tends the most to ideal mixing because of the small difference in chain length between both lipids. In general, the single peak observed in the pure lipid is broadened and shifted to higher temperatures. The more DPPC is added (an increasing mole ratio), the higher the transition temperature and the broader the peak. The peak observed at the lowest temperature is called the solidus line, while the highest temperature of the coexistence region is linked to the liquidus line. As soon as the second lipid, DPPC, has the upper hand, the apparent heat capacity at the liquidus line becomes the highest. This line shifts more to the main transition temperature of the pure lipid with the highest melting temperature. Along with the broadening of the peak, the cooperative unit decreases, which is the result of adding some strange (other length) molecules to the lipid bilayer. Reaching the equimolar state, the heights of the solidus and the liquidus side are equal and the cooperative unit achieves its minimum. Adding even more DPPC, the peak of the coexistence region becomes smaller again, and evidently the cooperative unit increases.

The same influence is observed when mixing DMPC (chain length of 14) with DSPC (chain length of 18). The results of the heating runs are presented in Figure 5.15. The difference in chain length of both lipids is larger, so this mixture deviates more from ideal mixing than the previous one. Also here a phase coexistence region is observed, clearly defined by two peaks. The more DSPC is added, the higher becomes the second peak and the lower becomes the first peak. Furthermore, the peak is broadened again till reaching the equimolar system. At this state, the cooperative unit reaches its minimum size (so less molecules are interacting with each other). The maximum half-width value is larger in this mixture compared to the DMPC with DPPC mixture and the melting temperatures of the current mixture deviate more from each other because of the larger difference in chain length.

The melting enthalpy of the mixtures, listed in Table 5.3 and in practice presented by the area under the peak of the transition, has been measured by pASC. For the DMPC with DPPC mixture, the specific enthalpy caused by the transition of the lipids, are shown in Figure 5.16. The temperature evolution of the enthalpy, within the estimated uncertainty, is characterised by an increasing jump upon the addition of the second lipid. Further, the slope of the enthalpy jump decreases as the mixtures approach equimolarity, because of the increasing temperature domain of the coexistence region in the specific heat capacity. The melting enthalpies of the less ideal mixture, DMPC with DSPC has not been included in this thesis. Nevertheless, a decreasing slope was observed by approaching equimolarity. The values of the enthalpy of the different mole fraction are listed in Table 5.4.

The lower-temperature transitions Next to the main transition, also the low temperature transitions observed in the pure lipid are influenced by adding a second lipid. The subgel-gel transition of the most ideal mixture, DMPC with DPPC, is still observed when adding the second lipid. So both the subgel and the gel phase remain, even when adding lipids with a different chain length. An increasing transition temperature is observed by an increasing amount of DPPC. So

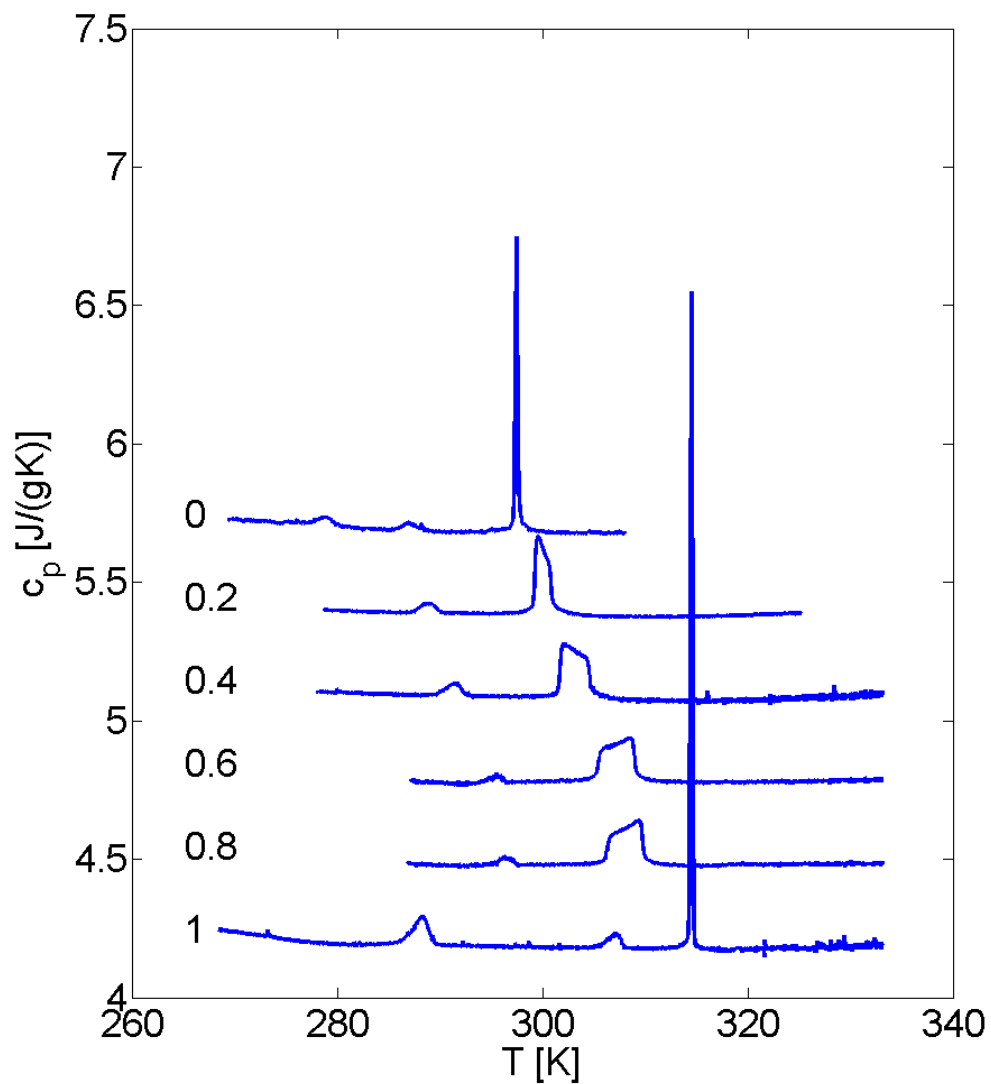


Figure 5.14: Temperature dependence of the specific heat capacity of a binary lipid mixtures, DMPC (chain length 14) with DPPC (chain length 16). The data are vertically shifted to get a better display. From top to bottom more DPPC was added to the pure DMPC. Adding a second lipid influences the phase transitions of the pure lipid: the subgel-gel transition shifts to higher temperatures, the gel-ripple transition disappears and a two-phase region appears.

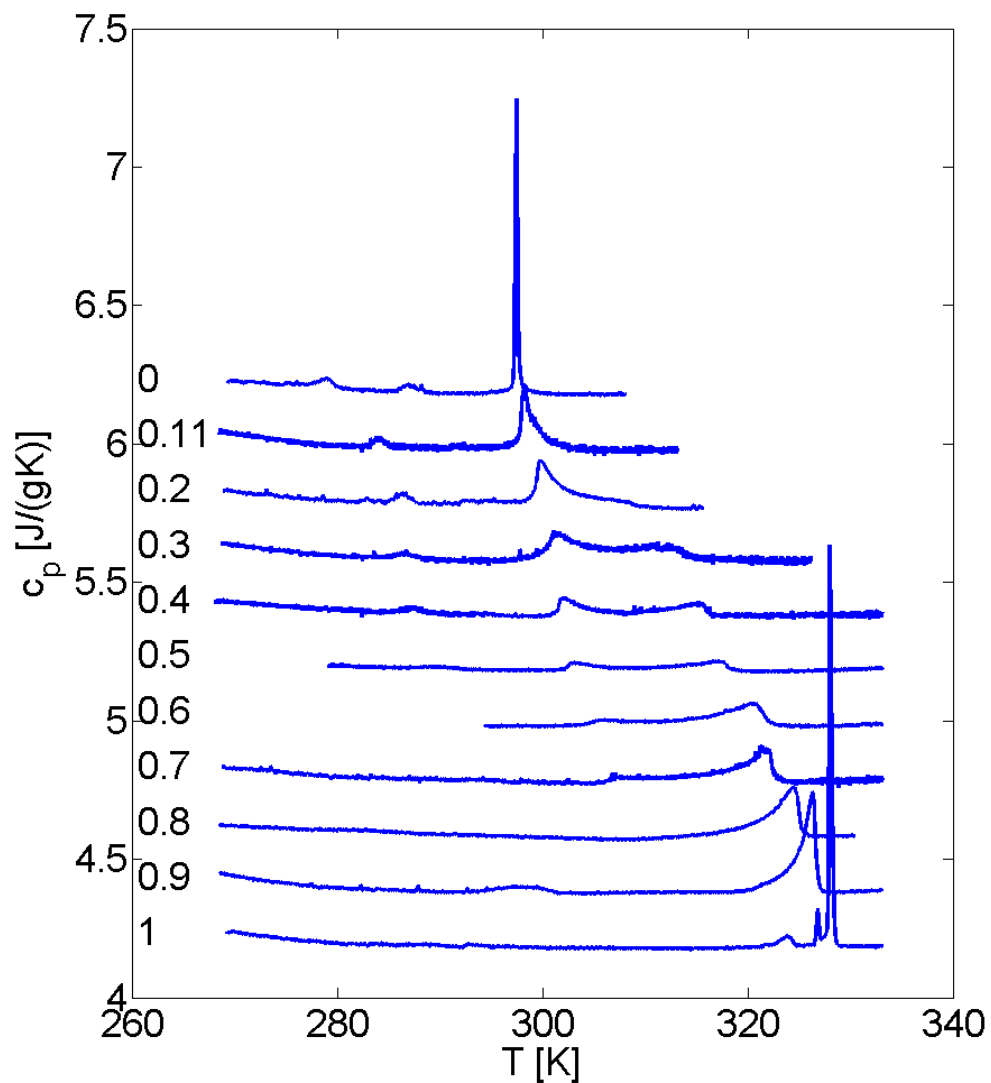


Figure 5.15: Temperature dependence of the specific heat capacity of two binary lipid mixtures, DMPC (chain length 14) with DSPC (chain length 18). The data are vertically shifted to get a better display. From top to bottom more DSPC (an increasing mole ratio) was added to the pure DMPC. Adding a second lipid influences the phase transitions of the pure lipid: the subgel-gel transition shifts to higher temperatures, the gel-ripple transition disappears and a two-phase region appears.

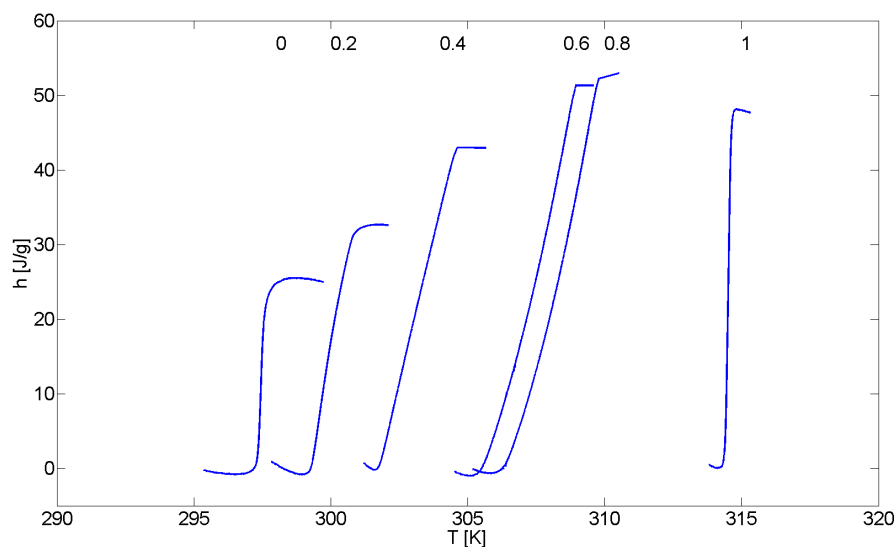


Figure 5.16: The jump in the specific enthalpy for the DMPC with DPPC mixture. An increasing jump is observed upon adding the second lipid. The slope of the jump decreases when approaching equimolarity.

thanks to the interaction between both lipids, the phase transition occurs at higher temperatures. This trend has been verified in the less ideal mixture. The increase in transition temperature changes parallel to the increasing main-transition temperature: the distance between both phase transitions remains more or less the same by adding the second lipid.

The ripple phase observed in the pure state is no longer observed in the lipid mixtures. Apparently, the difference in length of the alkyl chain between both components prevent the formation of the ripple phase. Because of the gel phase, the lipid layer has to stay flat, which is not possible due to the difference in length. The disappearance of the transition between the gel and the ripple-gel phase is observed in both mixtures.

To gain more insight into the behaviour of these lower-temperature transitions, additional phase diagrams for both the mixtures are present in Figure 5.17. The subgel-gel transition has not been observed in every measurement for the DMPC with DSPC mixture. Nevertheless, a clearly difference between both diagrams is observed. As discussed before, the coexistence region is indeed smaller in the more ideal mixture (left) compared to the less-ideal mixture (right). For both mixtures, the behaviour of the subgel-gel and the gel-ripple transitions are more or less the same. Increasing the amount of the second lipid, shifts the low-transition temperatures to higher temperatures, as observed in Figure 5.18. This figure pictures the phase diagram obtained by our pASC measurements, more information about this diagram will be given in the next section.

5.4.3 The phase diagram

Collecting all the data together results into a phase diagram as presented in Figure 5.19. This presents the different phases observed for the different ratios of the different mixtures. As explained before, the more ideal the mixing, the more the phase diagram approaches a lens-shaped

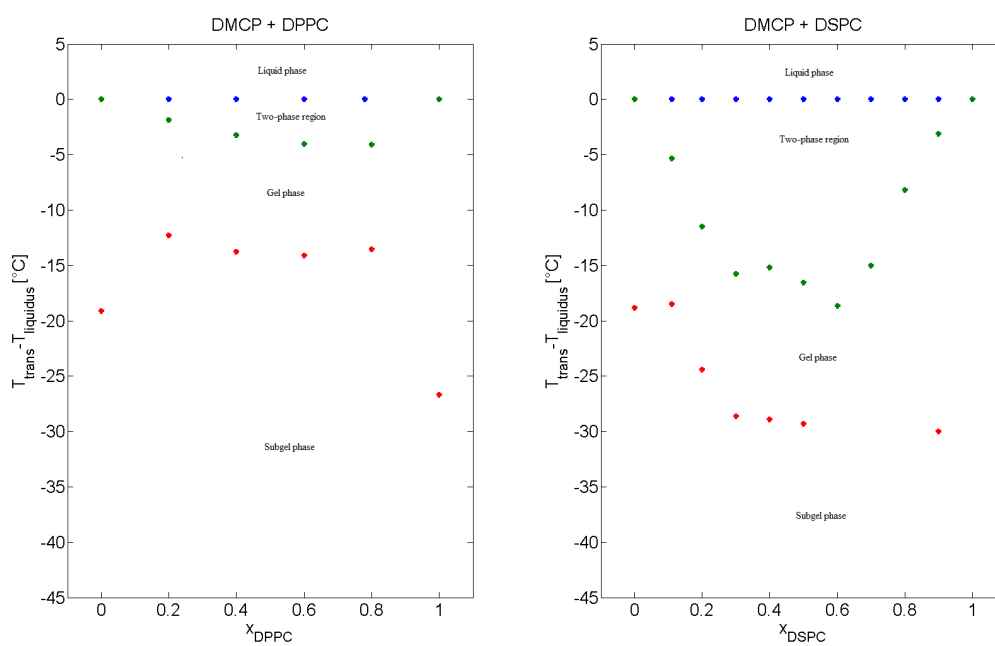


Figure 5.17: The phase diagram based on the difference in transition temperature between the liquidus-line transition and the other transition temperatures, of the DMPC with DPPC mixture (left) and the DMPC with DSPC mixture (right). The behaviour of the transitions changes by adding DPPC, respectively DSPC.

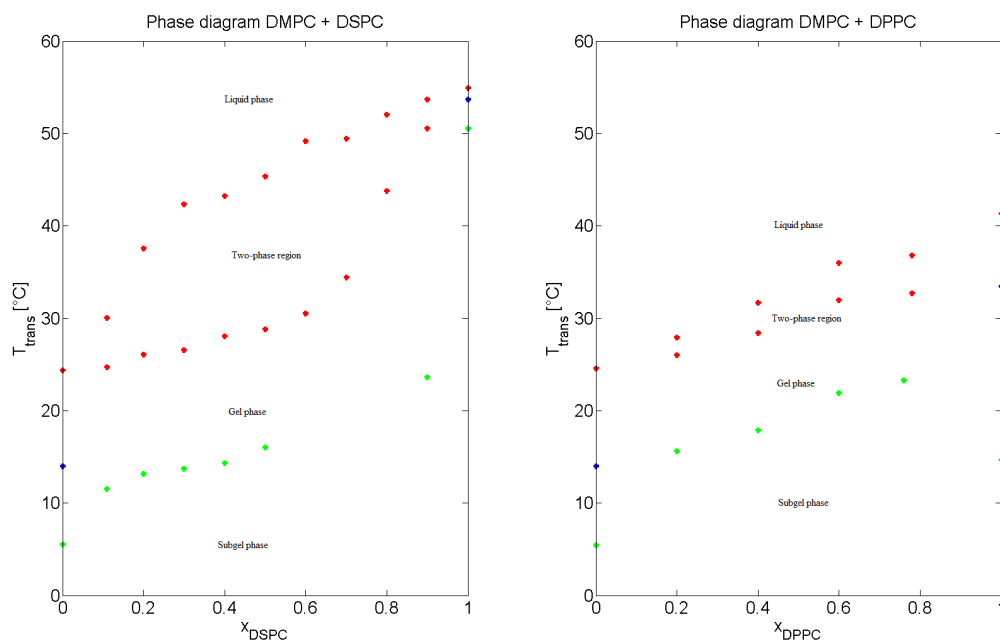


Figure 5.18: The phase diagram of two binary lipid mixtures. DMPC with DSPC (left) is a more ideal mixture, characterised by a larger two-phase region compared to the DMPC with DPPC (right) mixture. In the lipid mixtures, no longer a ripple phase is observed, nevertheless the subgel phase and the gel phase still occur. The more DSPC, respectively DPPC is added, the higher the transition temperature.

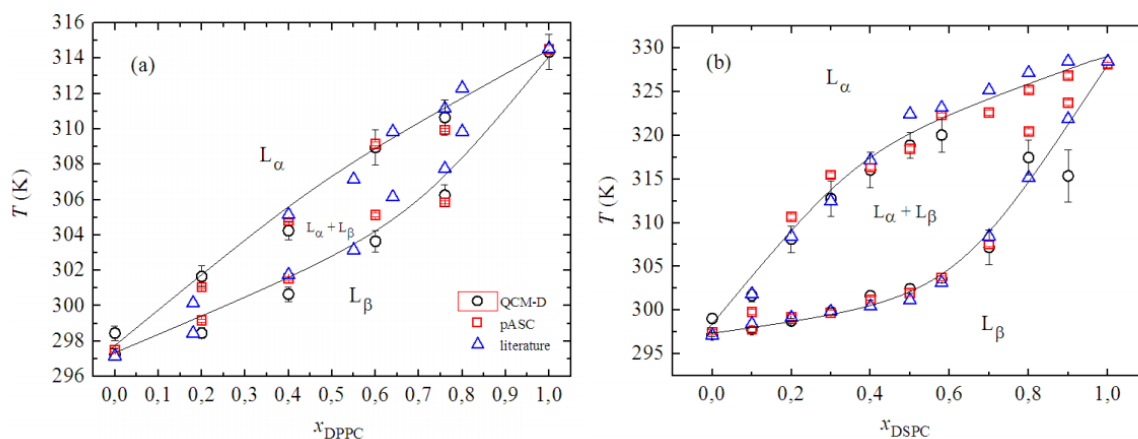


Figure 5.19: The phase diagram for a mixture of DMPC with DPPC (at the left side) and of DMPC with DSPC (right). The black circles were obtained by the QCM-D experiment, the red squared are values from the pASC measurements and the blue triangles are the literature values [42].

diagram. Our measurements based on Peltier-based adiabatic scanning calorimetry, are compared to both the literature [46], and to an experiment based on quartz crystal microbalance with dissipation (QCM-D). The latter took place at the University of Hasselt, with the same samples as used by pASC (ignoring the fact that the QCM-samples were diluted and filtered to get small unilamellar vesicles (SUV)). QCM-D is an acoustic surface-sensitive technique based on the inverse piezoelectric effect. By applying an AC voltage, transverse acoustic waves are sent through the crystal. This crystal oscillates at a resonance frequency. When the voltage source is switched off, an exponential decay of the oscillation is recorded. The frequency (f) and the energy dissipation factor (D) of this process are extracted. When absorbing the lipid to the oscillating quartz crystal, a coupling between the water and lipids occurs and a lipid vesicle is formed. This process changes the behavior of f and D . Heating and cooling scans were performed after this absorption, resulting in an increasing frequency and dissipation. This behavior changes at the phase transition, revealing the structural changes of the lipid bilayers [42]. The phase diagram clearly shows the two-phase region and the dependence on the composition of the mixture. The trend of the peak broadening till the equimolar composition is clearly visible for both mixtures. The difference between DMPC with DPPC and with DSPC is clearly observed, comparing both diagrams.

To conclude the discussion on the influence of a second lipid to a pure lipid bilayer, a three-dimensional plot of both binary mixtures is displayed in Figure 5.20 and Figure 5.21. This shows the specific heat capacity for both mixtures, as a function of temperature and as a function of the mole ratio of the second lipid added.

Table 5.3: Solidus and liquidus transition temperatures, total heats and cooperative units of the lipid mixture DMPC with DPPC.

x_{DPPC}	$T_{\text{solidus}}(\text{K})$	$T_{\text{liquidus}}(\text{K})$	Δh (J/g)	CU
0.20	299.2	301.1	38	74
0.40	301.6	304.8	43	37
0.60	305.1	309.2	26	29
0.76	305.9	310.0	42	51

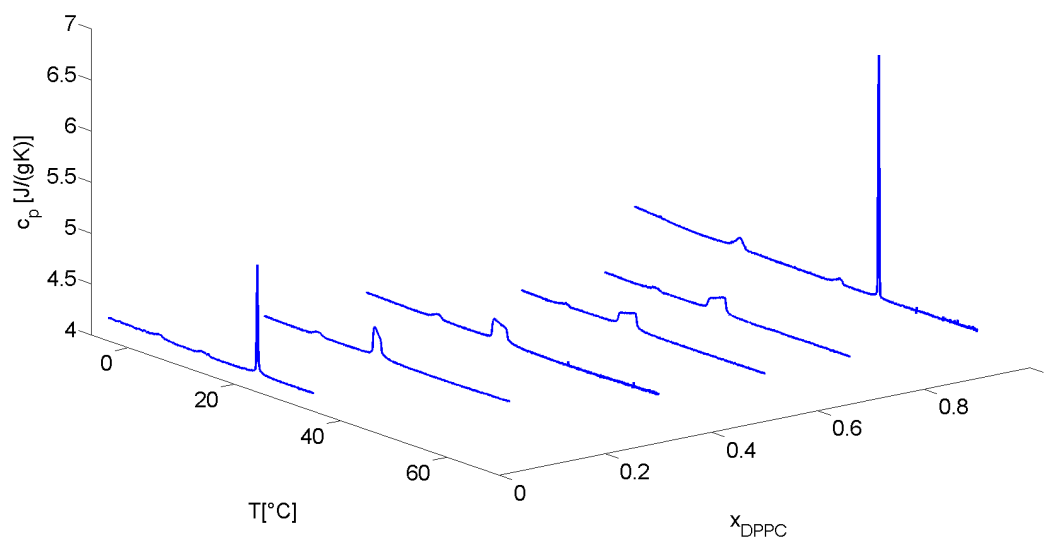


Figure 5.20: The specific heat capacity of DMPC+DPPC displayed in a three-dimensional plot, as a function of both the temperature and the ratio of the lipids.

Table 5.4: Both the solidus and the liquidus transition temperatures, the total heats, the latent heats and the cooperative units of the lipid mixture DMPC with DSPC.

x_{DSPC}	T_{solidus} (K)	T_{liquidus} (K)	Δh (J/g)	CU
0.1	297.82	299.82	41	88
0.2	299.19	310.68	29	93
0.3	299.69	315.47	38	30
0.4	301.20	316.40	24	69
0.5	301.94	318.47	40	19
0.6	303.65	322.30	26	32
0.7	307.57	322.57	21	72
0.8	320.42	325.16	27	66
0.9	323.71	326.80	31	132

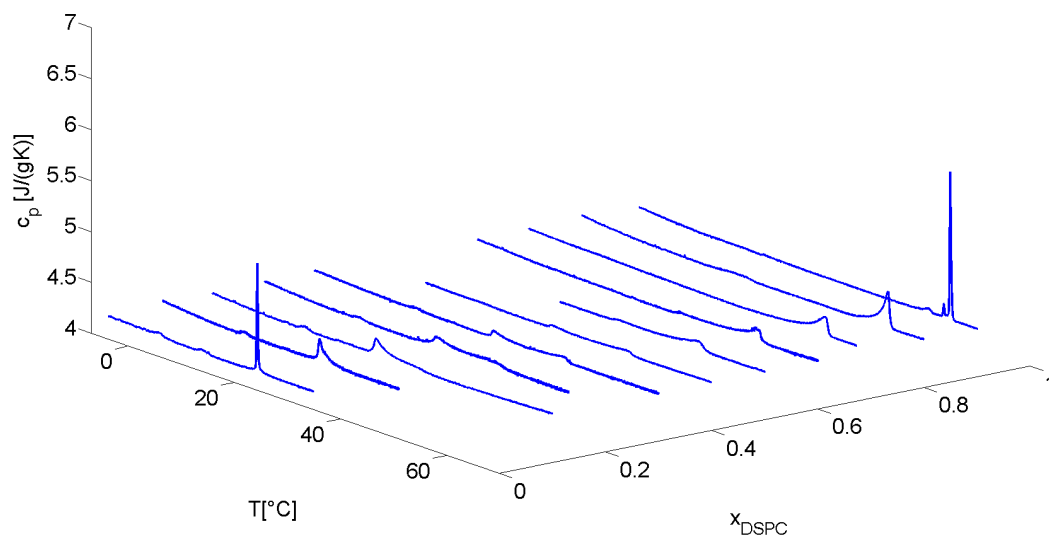


Figure 5.21: The specific heat capacity of two binary mixtures DMPC+DSPC displayed in a three-dimensional plot, as a function of both the temperature and the ratio of the lipids.

Chapter 6

Effects of cholesterol on lipid membrane phases

The investigation of the influence of cholesterol on the behaviour of lipid membranes is an interesting issue. Cholesterol contributes to several biological functions, even at low concentrations. Theoretical research [32, 20] has inferred the importance of cholesterol in biomolecular systems such as vesicles. Fluctuations of these vesicles, because of the phase separation of the lipid and cholesterol, were observed. These fluctuations lead to vesicular fission, even in the absence of proteins, leading to some new phase transitions such as the formation of the liquid-disordered phase. In view of this interesting phenomenologies, we have tackled the investigation of the complex interaction between lipids and cholesterol by ASC. Furthermore, the core effects of cholesterol are its influences on the mechanical properties of the membrane (bending, rigidity,...).

6.1 Special behaviour of cholesterol

6.1.1 Composition of cholesterol

Cholesterol, pictured in Figure 6.1, is a sterol lipid, containing a bulky, stiff structure, a non-polar tail and a small polar head. The hydrophobic part of cholesterol does not consist of a fatty-acid chain (as in most membrane lipids), but a steroid ring structure is present, with a small hydrocarbon chain at the end. The polar (hydrophilic) head consists of a simple hydroxyl group that together with the hydrophobic tail, makes cholesterol an amphiphilic lipid. Both the steroid ring structure and the hydroxyl group allow cholesterol to easily incorporate into a lipid bilayer. The hydrophilic hydroxyl head group incorporates at the bilayer-water interface, while the steroid skeleton incorporates inside the hydrophobic core. Such a structure (and in general all sterols) is found in plasma membranes, sub-cellular compartments in eukaryotes and in membranes of red blood cell (erythrocyte membranes).

As a lipid, cholesterol is not solved in the human body, containing a lot of water. Lipids are linked to proteins, together forming lipoproteins. Two types of these lipoproteins are the high-density lipoprotein (HDL) and the low-density lipoprotein (LDL). Cholesterol is attached to a high density (cholesterol represents half of the weight), respectively low density of proteins (where 20 % of the weight is cholesterol). Both the lipoproteins transport cholesterol through the body. The HDL transports cholesterol away from the body, from several organs to the liver.

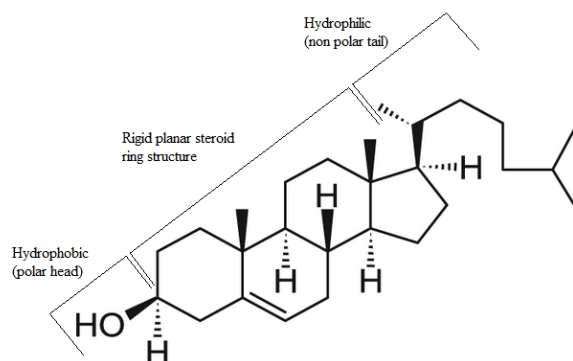


Figure 6.1: The structure of cholesterol, a special lipid based on a steroid structure, the polycyclic structure in the center of the molecule, a small hydrocarbon chain and a hydroxyl group as polar head [6].

The LDL, on the other hand, also carries the cholesterol through the body. Nevertheless, a buildup of molecules possibly occur, causing an arterial blockage and an increasing risk to get heart diseases [33].

When placing cholesterol (the free molecule) into a lipid bilayer, the molecules are not distributed in one of the two leaflets of the lipid bilayer. Cholesterol is present in both leaflets of the lipid bilayer, assuming an equal amount in each of the leaflets. So based on cholesterol, the composition of a biomolecular membrane is symmetric. Nevertheless, assuming the composition of the lipids in the leaflets, it is no longer symmetric. Lipids are likely more found in the inner- or the outer leaflet. This asymmetry results into a particular curvature of the membrane, which influences the biological functions of the body. In the leaflets, cholesterol has the possibility to flip-flop between the outer and the inner leaflet. This flip-flop dynamics, called transversal diffusion, is in general a slow process which is not energetically favourable. But dealing with cholesterol, this process happens faster than one second. This is a two-step process, first the lipid molecules of the cholesterol have to rotate in the plane of the bilayer, second a transition perpendicular to the plane of the bilayer takes place [21].

6.1.2 Physical states of membranes with cholesterol

Pure lipid As presented in Chapter 4, a lipid bilayer in an aqueous environment results into different physical states, dependent on the composition. In a pure lipid such as DPPC, four lamellar phases are observed: the subgel phase L_c , the gel phase $L_{\beta'}$, the ripple phase $P_{\beta'}$ and the liquid phase L_α . These phases are visible in the specific heat capacity of DPPC, plotted in Figure 6.2.

The first phase is the gel phase $L_{\beta'}$, also called the solid-ordered phase S_o , and is characterised by a two-dimensional triangular lattice in the plane of the lipid membrane. The hydrocarbon chains form a compact (rigid and ordered) network, with typical lipid chains that are elongated maximally. In the case of DPPC, these chains are tilted compared to the normal of the membrane, which is also mentioned in the name $L_{\beta'}$ by the accent mark. The structure of this phase is illustrated in Figure 6.3. The next gel phase is the subgel phase, containing ordered lipid

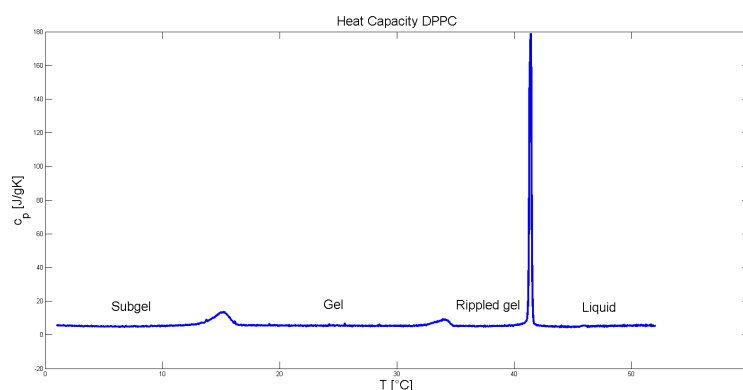


Figure 6.2: Temperature dependence of the specific heat capacity of DPPC as a function of temperature. Four physical states are observed: the subgel phase, the gel phase, the rippled-gel phase and the liquid phase.

chains. In the direction normal to the hydrocarbon chains, the chains are significantly closer together in the subgel phase as compared to the normal gel phase. Further, the chains are not fully extended in this phase. The last gel phase is the ripple phase and is observed after the subgel-ripple transition. This transition influences the lipid order and the membrane curvature. The rippled-gel phase $P_{\beta'}$ is characterised by a periodical change between ordered and disordered lipid domains and is visualised in Figure 6.3. The last phase transition is the main transition, leading to the liquid phase. In this fluid phase, also pictured in Figure 6.3, which is also called the liquid-disordered phase L_{α} or L_d , the triangular lattice is lost. Furthermore, the hydrocarbon chains are not stretched out compared to the gel phase. This phase is the favorite phase, characterised by a higher diffusion [21].

Pure lipid + cholesterol Compared to the phospholipids that were discussed so far, cholesterol is a relatively bulky lipid, with a large hydrophobic part and a small polar head. This geometrical shape influences the position of cholesterol in the bilayer membranes [21]. Since the hydrophobic part of cholesterol takes a substantial amount of space, it forces the surrounding alkyl chains into a configuration that takes up the least lateral space: their all-trans or fully extended configuration. However, even under such circumstances, cholesterol is still ‘too brood’, and also forces a reorganisation of the polar head groups. They take a more liquid-like order. Thus, the addition of cholesterol leads to a phase in which the alkyl chains are more extended, like in the low-temperature gel phases, but where the polar groups have liquid-order, like in the liquid-crystalline phase. This intermediate phase is the liquid-disordered phase L_o , depicted in Figure 6.3.

Adding cholesterol increases the thickness and the fluidity of the lipid bilayer. These membranes are mechanically stable and less leaky. Because of the lower permeability, the LDL particles in the lipid membranes no longer transport the water insoluble compounds (such as vitamins and hormones) through the membrane. This insolubility causes a buildup on the walls of the artery, increasing the chance to have a stroke or to suffer from cardiovascular diseases [54].

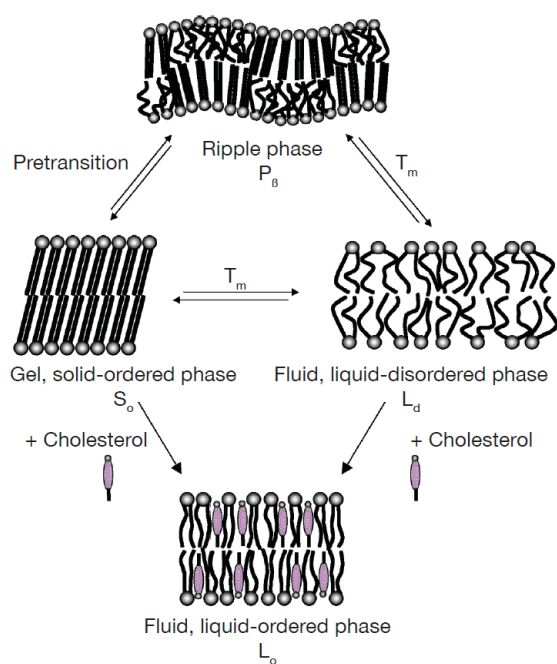


Figure 6.3: Four possible physical states of a lipid membrane. Without cholesterol, beyond the subgel phase, other phases are observed such as the gel phase (solid-ordered), the fluid phase (liquid-disordered) and the ripple phase (which is a mix between the gel and the fluid phase.) Adding cholesterol results into a new (fluid) phase, called the liquid-ordered phase. The ripple phase is no longer observed when adding cholesterol [21].

6.2 Addition of cholesterol to a lipid bilayer

Cholesterol is an essential and common component of the membrane, making it worthwhile to investigate the influence on a lipid bilayer. Investigations about the influence on phospholipid bilayers have already been done based on several techniques, such as differential scanning calorimetry [73], proton nuclear magnetic resonance (H-NMR) [73], electron paramagnetic resonance (EPR) [63, 59], freeze-fracture electron microscopy [18] and micromechanics (Needham, D. and Evans, E., unpublished data). That way, both the molecular and the thermodynamic level have been investigated. These investigations gave insight into the structures and the interactions due to the cholesterol in the phospholipid bilayers. Research is still going on to solve remaining questions.

Vist and Davis investigated the influence of cholesterol on the phase transitions of DPPC based on DSC and H-NMR [73]. The results of the measurements are pictured in Figure 6.4. Adding a small amount of cholesterol (less than 5 %) influences the low-temperature transitions, both the subgel-gel and the gel-ripple transition temperatures are changed. Both processes are linked to a decrease in enthalpy. The more cholesterol added, the lower the transition temperature of the gel-ripple transition. Reaching an amount of 5 % cholesterol, the latter transition no longer occurs, while the subgel-gel transition is still visible with a slight change in transition temperature. The additional cholesterol also influences the main transition, both the melting temperature and the enthalpy decrease with an increasing amount of cholesterol.

Increasing the cholesterol concentration, higher than 5 % and less than 20-25 %, the subgel-gel transition and the main transition are still observed. The low-temperature transition still changes in temperature, linked with a decrease in enthalpy. Reaching a high amount of cholesterol (20 %) this phase transition has totally disappeared. Besides this transition, the high-temperature transition shifts to lower melting temperatures and the main transition peak become more broadened. Vist and Davis [73] model the main transition as a superposition of a sharp and a broad peak. An example is given in Figure 6.5 for a mixture of DPPC with cholesterol in a concentration region between 2 % and 11 %. The same idea is continued at higher concentrations. As can be seen in this figure, the sharp peak is linked to the melting of the cholesterol-poor phospholipid domain, while the broad peak occurs because of the melting of the cholesterol-rich domain. In the region of the sharp peak, the transition temperature decreases slightly, as well as the enthalpy and the cooperativity. At the broad peak, by increasing the amount of cholesterol, the phase transition temperature and the enthalpy increase, while the cooperativity decreases.

At cholesterol concentrations above 20 - 25 %, the sharp peak further increases until it disappears. The broad peak is still observed, characterised by an increasing melting temperature and a decrease in both enthalpy and the cooperativity. When the concentration of cholesterol becomes too high, the broad peak disappears and no longer any phase transition will be observed.

Those observations are dependent on the hydrocarbon chain length, mainly the broad transition is dependent on this length. Lipids with a length of 16 or less atoms result into an increase of the transition temperature, while lipids with a longer chain (18 and more) are observed with a decrease of transition temperature. This because the hydrocarbon chains are too long compared to the hydrophobic part of the cholesterol molecule, which results into a mismatch. Because of this mismatch, the transition temperature of the cholesterol-rich domains no longer increase but decrease [51].

The phase diagram, worked out by Vist and Davis [73], is plotted (see Figure 6.6) as a function of temperature and as a function of the concentration of cholesterol. Several coexistence lines and

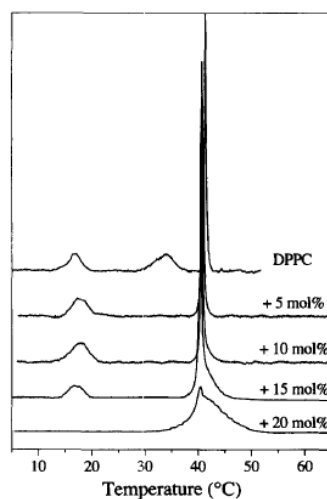


Figure 6.4: Some DSC scans of DPPC with cholesterol. The subgel-gel transition shifts to higher energies with the increasing cholesterol. The subgel-gel transition disappears when adding more than 15 %. The gel-ripple transition, observed in the pure lipid, is no longer observed. The gel and the ripple-gel phase transform into a new state, the solid-ordered phase. The main transition shifts to lower temperatures and at higher cholesterol concentrations the superposition of the sharp (lipid-rich domain) and broad peak (cholesterol-rich domain) is visible [31].

regions are observed. The first two-phase coexistence is observed between 0 and 7 % cholesterol (and between 40 and 41.25 °C) and contains both the rippled-gel phase and the liquid-disordered phase. Because of this two-phase region, cholesterol is soluble both in the solid-ordered phase and in the liquid-disordered phase. This proves the unusual behaviour of cholesterol, as normal a solid state is not a good solvent compared to a liquid phase. The second coexistence region is located between 7.5 and 22 % cholesterol and at the temperature region between 28 and 40 °C, here the rippled-gel (solid-ordered) and the liquid-ordered phase coexist. The last two-phase region is between 7.5 and 10 % cholesterol and occurs above 40 °C and is composed of the liquid-disordered and the liquid-ordered phase. Apparently cholesterol favours the liquid phase at higher concentrations, and no longer the solid phases as in the pure lipid. A triple point is observed by Vist and Davis [73] at 7.5 % cholesterol, nevertheless, this point has not been observed by other research teams [47, 22, 45, 26, 50], nor by our measurements.

6.3 Phase transitions observed by ASC

6.3.1 Observations

The specific heat capacity as a function of temperature has been measured in order to investigate the influence on the phase transitions of cholesterol on DPPC. Samples of DPPC with cholesterol are prepared as explained in Chapter 4, for three different cholesterol mole concentrations. Each sample measured with the calorimeter has been scanned while heating between 18 °C and 50 °C. The mol ratio of the amount of cholesterol has been increased each sample, the ratios 0, 0.13, 0.24 and 0.35 have been measured (with respectively rates of 1.67 K/h, 2.37 K/h, 2.25 K/h

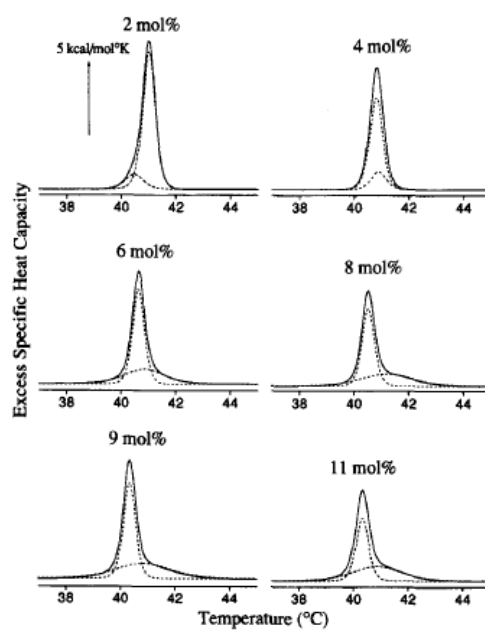


Figure 6.5: The evolution of the main transition peak by an increasing amount of cholesterol. In this model, the main transition is a superposition of a sharp (melting of the cholesterol-poor domains) and a broad (melting of the cholesterol-rich domains) peak. The melting temperature, the enthalpy and the cooperativity decrease in the sharp peak. In the broad peak, an increase in both melting temperature and enthalpy is observed, with a decrease in cooperativity [51].

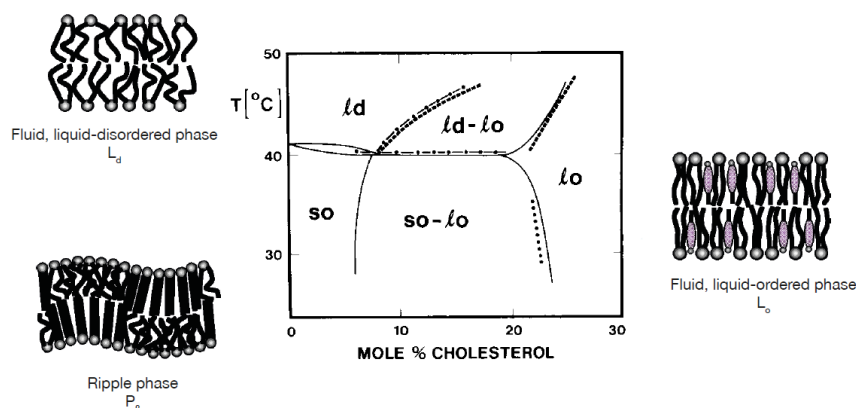


Figure 6.6: The phase diagram of DPPC as a function of the concentration of cholesterol and temperature. Three phases are observed: the liquid-disordered phase (L_d), the rippled-gel phase (P_{β}) and the liquid-ordered phase (L_o). The latter contains both cholesterol and phospholipid. Three coexistence region are observed: the ripple-gel phase and the liquid-disordered phase, the rippled-gel (solid-ordered) and the liquid-ordered phase, and the liquid-disordered and the liquid-ordered phase [21].

and 2.35 K/h). All heating runs measured the regions of the gel phase, the ripple phase and the liquid phase of the pure DPPC lipid. The subgel phase has not been measured. The results of the measurements are presented in Figure 6.7. The results are vertically shifted to make the changes in the phase transition even visible.

In the pure lipid DPPC three physical phases are observed. Two transitions peaks occur in the specific heat capacity, the first one at 33.44 $^{\circ}\text{C}$, the second one at 41.34 $^{\circ}\text{C}$. Also the enthalpy of both transitions was measured, together with the cooperativity. All data of the DPPC with cholesterol samples are listed in Table 6.1. Adding cholesterol (13 %) results into a single peak in the specific heat capacity. So two physical phases are still observed. The first peak observed in the pure lipid has disappeared and the main transition peak has shifted to lower temperatures. This main peak is broadened because of the contribution of the cholesterol-rich domains. When increasing the amount of cholesterol, 24 %, the peak is still broadened and the transition temperature has shifted to higher values. This transition peak is observed at about 41.92 $^{\circ}\text{C}$. Finally, adding 35 % of cholesterol to DPPC results in a specific heat capacity where no longer a transition peak is observed. The superposition of the peak, as done in the literature, is not possible with our pASC data because of the great temperature resolution. Our results are not smeared out enough to construct a clear difference in both the sharp and the broad peak. Nevertheless the evolution between a sharp peak (in the pure lipid) and a broad peak (when adding 13 % of cholesterol) is visible.

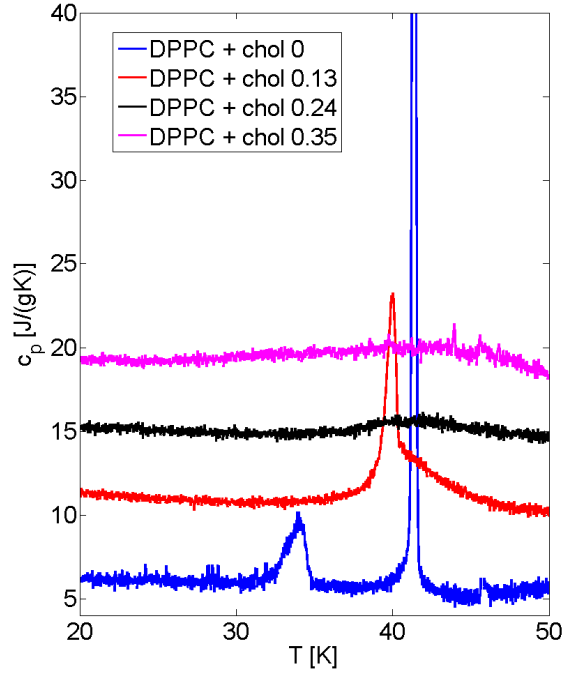


Figure 6.7: Temperature dependence of the specific heat capacity of DPPC with different mole ratios of cholesterol as a function of temperature. In pure DPPC, two phase transitions are observed: the rippled-gel to gel transition at 33.44 °C and ripple to liquid transition at 41.34 °C. Adding cholesterol (13 %) shifts the main peak to lower temperatures. The ripple phase is no longer observed when increasing the cholesterol concentration. Adding more cholesterol, a broad transition becomes visible. Increasing the cholesterol (35 %) results into a system without any phase transition.

Table 6.1: The data calculated by the measurements done with pASC.

x_{chol}	0	0.13	0.24	0.35
$T_{\text{gel} \rightarrow \text{ripple}} (^{\circ}\text{C})$	33.7	no transition	no transition	no transition
Δh (J/g)	5.70	no transition	no transition	no transition
CU	490	no transition	no transition	no transition
$T_{\text{ripple} \rightarrow \text{liq, DSC}} (^{\circ}\text{C})$	41.25	40.00	46.25	no transition
$T_{\text{ripple} \rightarrow \text{liq, ASC}} (^{\circ}\text{C})$	41.34	40.00	41.92	no transition
Δh (J/g)	40.00	12.42	1.06	0
CU	1019	397	1131	0

6.3.2 Interpretation and comparison with the literature

The data of our ASC measurements are compared with the literature [73, 31], see Table 6.1. The phase diagram of Vist and Davis (Figure 6.6) were obtained by several techniques: DSC [73], EPR spectroscopy [63, 59], freeze-fracture electron microscopy [18] and micromechanics (Needham, D. and Evans, E., unpublished data). The part of the diagram measured with DSC (the solid lines) can be compared to our ASC measurements.

Observations The main phase transition of DPPC was observed by Vist and Davis at 41.25 °C and presents the transition from a gel (ordered) phase to the liquid (disordered) phase. The main transition observed by ASC (at 41.34 °C) agrees very well with this transition temperature. Our measurements detected also the gel-ripple transition, presenting the phase transition between the gel and the rippled-gel phase, these phases are taken together by Vist and Davis and is called the solid ordered phase.

Addition of cholesterol (13 %) to the lipid bilayer, resulted in one phase transition peak at 40.00 °C. The phase diagram confirms this phase transition, also at 40.00 °C, and describes the transition between two two-phase regions : solid-ordered and liquid-ordered respectively the liquid-disordered and the liquid-ordered phase.

At high concentrations of cholesterol (24 %) still one, but broadened, transition peak is visible. The peak is observed at 41.92 °C and conforms more or less the liquid-ordered to the two-phase system (liquid-disordered and liquid-ordered) transition.

Finally a large amount cholesterol (50 %) has been added to the lipid bilayer, this ratio is no longer covered by the measurements done by Vist and Davis. Extrapolating the data results in a lack of transition so the sample is totally dominated by the cholesterol. Only the liquid-ordered phase occurs in the temperature range at this concentration.

Explanations In the pure DPPC lipid bilayer three gel phases (subgel, gel and ripple) and one liquid phase occur. Early investigations [50] showed that the subgel phase is still present at concentrations between 0 and 20 % cholesterol, as can be seen in Figure 6.4. The runs with ASC did not lower this temperature region, so the DSC data could not be cross validated by our data. Nevertheless, the fact that this subgel phase still occurs at high cholesterol concentrations proves the existence of a phase separated mixture containing domains with pure DPPC and domains with both DPPC and cholesterol. Increasing the amount of cholesterol decreases the enthalpy of the subgel-gel transition, further the transition temperature changes slightly to lower temperatures. Reaching 20 % cholesterol results into the suppression of the subgel-gel transition, the cholesterol domains have the upper hand.

As confirmed in our data, the gel-ripple transition, observed in the pure lipid, disappears by adding cholesterol. This disappearance is already observed at 5 %. The gel and rippled-gel phase fuse, only the gel phase is still observed and the chains are not tilted anymore.

Finally the phase diagram can be separated in two parts. The first part represents the lipid bilayer containing 20 % cholesterol or less. In this case the sample consists both pure lipid domains and lipid-cholesterol domains. The more cholesterol is added, the more the influence is visible: new phases occurring, change in transition temperature, enthalpy and cooperativity. The second part of the phase diagram, above 20 %, represents only lipid-cholesterol domains, the pure lipid domains are totally suppressed and the influence of the cholesterol dominates the system.

Chapter 7

Thermograms of blood plasma

7.1 Proteins and blood plasma in the human body

Proteins are, next to lipids, an important component in the human body with a range of functions. The investigation of these macromolecules is definitely worth the effort. A lot of proteins are found in the human plasma, which is another important component of the human body and which is investigated in this chapter.

7.1.1 Proteins

The human body contains about 45 % proteins which are essential for the body to repair, regulate and protect itself. For instance, when dealing with a high body temperature (having a fever), several processes in the body get disturbed. Reaching a body temperature of 42 °C, the proteins that control the temperature of the body extinguish themselves. The velocity of the increasing temperature increases which results in a deadly end. Therefore, investigations of the proteome are a matter of life and death.

Many functions in the human body are related to proteins. Proteins take care of the molecular transport, they are important in cellular signalling, and most important, they act as enzymes. Also less active proteins are present such as the structural proteins, although they are not less important. They offer strength and rigidity to biological membranes and they contribute to the functions of the muscles [40].

The function of proteins is dependent on the three-dimensional shape. When putting proteins into an aqueous environment, no self-assembly process occurs but they will be folded by enzymes. This process is determined by the linear, one-dimensional structure (called the primary structure) of the proteins and deals with biological interactions in the soft matter region. This assembled process, in contrast with the self-assembly process of the lipids, has only one well-defined structure, which is called the native state [24].

A characteristic denaturation is observed in a thermogram, which represents the specific heat capacity as a function of temperature, when heating a pure protein. Due to this heating, the protein loses its native state, the biological function is destroyed because of the change in structure which becomes more random and open. The primary structure is kept unchanged, while the secondary and tertiary structure is affected. Observing this denaturation process is done by calorimetry, resulting in thermal properties such as the melting temperature and the specific enthalpy which are characteristic for a particular protein. By cooling, in general, the denaturation process is not reversible because of the too complex behavior of a protein in its folded

state. Denatured proteins will interact more likely compared to a reversibility back to its original state. Nevertheless, some proteins are observed that will return to their origin configuration, this reversibility is depending on the kind of protein, on the concentration and on the environment. For some proteins, the native state will be observed again if the concentration of the protein is low enough, but in general it is not such as a cooked egg cannot bring back to his original structure [14].

7.1.2 Plasma

The human body contains about five liters of blood, which is an assembly of white blood cells (leukocytes), red blood cells (erythrocytes) and blood platelets (thrombocytes) all of this in an aqueous solution [2]. Putting non-clotable blood into a centrifuge separates the blood in several components. After the centrifugation plasma covers for about 55 % of the total volume, the other part contains the red cells, the white cells and the blood platelets. Extraction of the plasma gives the possibility to investigate this more into detail. This is important because plasma is a critical component in the treatment of many serious health problems. Several vital ingredients from plasma are isolated and used as treatments. These can potentially help save the lives of people suffering from burns, shock, trauma, and other medical emergencies [7]. This is the reason why people are frequently encouraged to donate blood plasma.

Blood plasma is green-yellow colored and consist of a mixture of mainly water, salts and enzymes, complemented by with fats, antibodies, clotting factors, proteins, sugars, . . . Plasma is an important part of the human body, dealing with the transportation of blood cells and minerals through the body. Further, plasma maintains the blood pressure and the proper pH in the body which are critical to cell function [1, 7].

The human plasma is a complex fluid, containing more than 3000 protein components, ranging in concentrations from picogram to milligram per milliliter. Next to the nucleid acids, the polysaccharides and the lipids, the proteins are one of the most important molecular components of life. In blood plasma, proteins are important when dealing with the clotting of blood and the defence against diseases.

Investigating thermal properties of human plasma is an important topic and yields important information about its components. Our samples measured are indeed irreversible so by cooling, the transition peaks are no longer observed. In the human plasma, a mixture of proteins are present, resulting into a more complex thermogram. This thermogram is a composition of several denaturations, each corresponding to a particular protein of the human plasma [57].

7.2 Blood plasma situated in literature

The heat capacity of blood plasma is measured based on calorimetry. This technique is useful to investigate the thermal properties of the plasma components. Other techniques, such as protein electrophoresis [56] and mass spectroscopy [39] are measured to gain information about the mass and the charge. During the years, the thermal properties of several blood plasmas are already observed using differential scanning calorimetry [25, 23, 24]. This way, calorimetry is a unique and new method to investigate the plasma proteome, resulting in a useful tool for disease diagnosis. A lot of investigations based on DSC, took already place to investigate the plasma proteome with the aim of detecting several diseases. A few of these diseases are cancer [23], diabetes [24], lupus [25], Lyme disease [25] and arthritis [25]. Cancer is the unregulated cell growth, resulting in a tumour, which can invade parts of the body. Diabetes is observed at persons with a high amount

of blood sugar, which causes symptoms such as increased thirst, increased urination, weight loss, fatigue and increased appetite [74]. These symptoms possibly result in many complications such as heart diseases. Lupus is an autoimmune disease characterised by the attack of a normal and healthy tissue. This affects body systems such as the skin, the kidneys, the lungs and the heart. Lyme disease is an infectious disease caused by three (or more) bacteria, resulting in a lot of symptoms in several body systems. Possibly rash can be observed, recognised by a small, red bump at the site of a bite [17]. Finally, arthritis is an inflammation of the joints, causing a rheumatic disease, which can cause a lot of pain.

Healthy individuals A general thermogram, based on 15 individuals (9 males and 6 females, aged between 22 and 50), is presented on the left side of Figure 7.1. The thermogram is dependent on the gender, the ethnicity and the age [23]. Both the transition temperature and the height of the peak change slightly. The shape of the thermogram of the human plasma has been verified by measuring the basic components of the plasma one by one and adding them together. Ten particular proteins have a contribution of 90 % to the mass of the plasma: albumin, immunoglobulin G (IgG), fibrinogen, transferrin, immunoglobulin A (IgA), α_2 -macroglobulin, α_1 -antitrypsin, complement C3, IgM and haptoglobin. Another 12 proteins represent 9 % of the plasma. Because of the big amount of proteins (more than 500), it is not easy to investigate the other 1 % mass of plasma by thermal techniques. The right figure of Figure 7.1 represents the different contributions of the most abundant proteins, presenting 90 % of the mass. Assuming there are no interactions among the different proteins, the sum of the components (dashed lines) has been measured. Depending on the protein, a simple two-state melting process (characterised by one peak) or a more complex denaturation pattern (characterised by more peaks) are observed. The weighted sum of these components has the same shape as the healthy plasma measured by DSC. Using the one by one plot, the peaks in the total plasma can be linked to a specific protein. The first small peak observed in healthy plasma, at 51 °C, can be assigned to a transition in the fibrinogen. The second peak, the main transition at 62.8 °C, is caused by the denaturation of human serum albumin (HSA) and the peak at 69.8 °C reflects the denaturation of IgG. The thermogram of the healthy sample is clearly dependent on the concentration of the proteins, presenting a particular profile of denaturation. Because of the concentration dependency, the thermograms of male persons is recognised by higher amplitudes because of the clinically accepted differences in the concentration of the plasma proteins between male and female, which proves the gender-dependency [23].

Sick individuals A lot of samples coming from several patients have been measured to investigate the influence of complications on the thermogram. Some results are presented in Figure 7.2. This represents the influence of three different diseases, the first one (A) represents the thermogram of individuals with lupus. The second one (B) comes from the plasma of people with a Lyme disease. Finally, the third one (C), deals with persons with rheumatoid arthritis. A change both in the transition temperature and in the amplitude is clearly visible in all the thermograms. One possible explanation of the distinction between both thermograms is the change in concentration. Although, researches of Anderson et al. based on electrophoresis [9, 10] proved that the concentration of a healthy plasma changes very slightly compared to the composition of diseased plasma, nor the size and the charge of the proteins change remarkable.

Another explanation is linked to the complex composition of the human plasma. A lot of binding interactions between the proteins themselves and between the proteins and the peptides take place. In this network of interactions, potential biomarkers are no longer free. They are bound to the most abundant proteins which results into a typical thermal stabilisation, which is present in the remarkable change in the thermogram. Depending on the disease, both the amplitude and

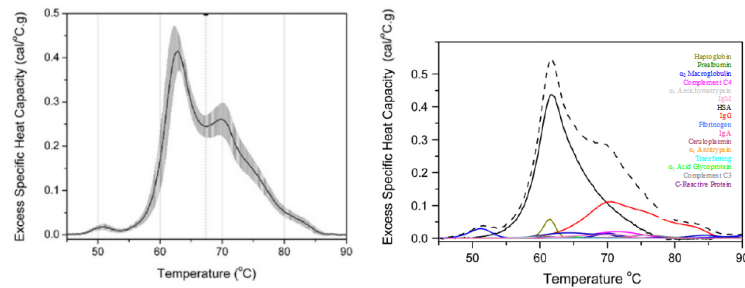


Figure 7.1: Left: Thermogram of blood plasma from 15 healthy individuals. Three peaks are visible, around 51 °C, 63 °C and 70 °C along with several smaller shoulders. Right: The most important proteins of the sample, measured one by one. The sum of these contributions is plotted in dashed lines. The sum of these proteins is a good approximation for the true plasma. The figure is taken from [23].

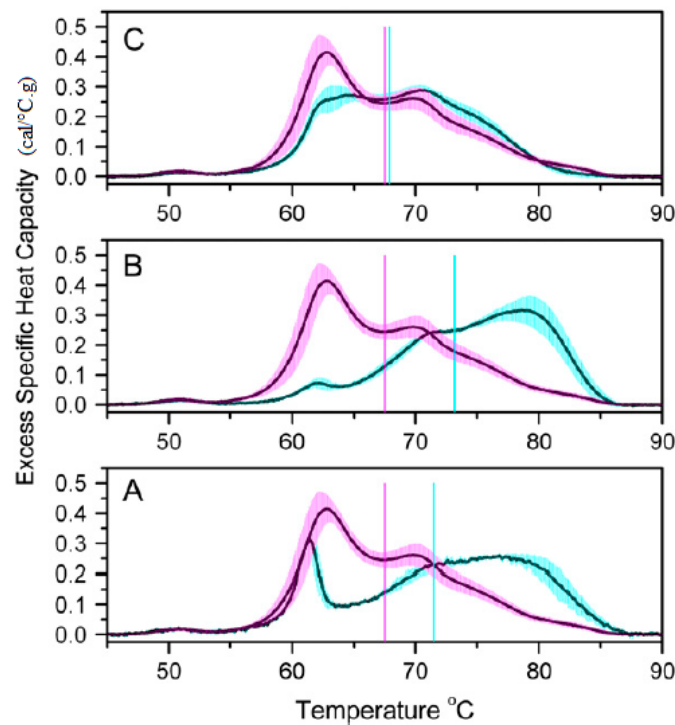


Figure 7.2: Thermogram of three different diseases, plotted together with the plasma from healthy persons. Both a change in transition temperature and amplitude is observed. The figure is taken from [25] and represents (A) the plasma from individuals with systemic lupus, (B) plasma from individuals with Lyme disease and (C) plasma from individuals with rheumatoid arthritis.

the location of the different peaks change. This concept of interactions in the human plasma is called ‘the interactome’ [25]. This explanation has been proved by using bromocresol green, more details are explained in [25]. This dye binds to human serum albumin (HSA) which is one of the most abundant proteins in the human plasma. This binding can be compared to the binding between a biomarker and the proteins. This experiment resulted in thermograms very close to the thermogram obtained by individuals carrying a disease. This proves the possibility of interactions, dependent on the proteins, which results in a particular change of the thermogram. Because of this significant difference, calorimetry is an interesting tool to screen rapidly and to observe particular diseases.

7.3 Blood plasma observed by ASC

Several samples of human plasma are measured by pASC. 100 ml blood has been collected from a healthy person, and mixed with 12 ml sodium citrate which bind with Ca^{2+} . One half of this mixture has been centrifuged at 1100 rpm for about 11 minutes, yielding in 8 ml of platelets rich plasma (PRP) of the 50 ml blood. The red blood cells are collected at the bottom. The other half has been centrifuged at 3700 rpm, during 12 minutes, resulting in both red blood cells and platelets at the bottom. Here a second (and faster) centrifugation took place, at 10000 rpm, resulting in 12 ml platelets poor plasma (PPP) of the 50 ml blood. Both plasma samples, with and without platelets, are scanned with the calorimeter. Both samples were heated from 30 °C to 80 °C with a temperature rate of 4.60 K/h and 4.55 K/h. Because of the irreversible process, this heating run could only take place once in a sample. The specific heat capacity of both samples is presented in Figure 7.3. The data of PRP have been shifted vertically to visualise the difference between the two samples. Two important properties are observed by our measurements.

First of all, the thermogram obtained by our measurements has the same shape as the healthy thermograms measured by Garbett et al. [25]. Three peaks are also observed, shifted slightly in transition temperatures compared to the healthy thermogram. Even with the shift in temperature, the first peak is still observed as caused by the denaturation of fibrinogen because this denaturation peak is the main peak in the thermogram, an investigation based on albumin took place (see next section). The second major peak is attributed to albumin and the last peak could arise from IgG. The shoulder, obtained by IgG, is not observed completely in the PPP measurement because the measurement ranged till 80 °C. To visualise the total shoulder, the run should have been continued till 90 °C. Nevertheless, the end of the thermogram is going in the right way. The transition temperatures of the three denaturation-components, listed in Table 7.1, do not fall between the standard deviations of the healthy plasma (the shaped area) observed by Garbet et al. The deviation is not that extreme keeping in mind that the plasma measured with ASC is obtained by measuring one individual, which is not enough to compare with a statistical average of 15 persons. Nevertheless, the shape is comparable with the healthy plasma shape of

Table 7.1: Phase transitions of the PPP and the PRP, obtained by our measurements (ASC) and taken from the literature (DSC) [25]. The ASC values deviates from the standard deviation of the DSC data, nevertheless because of the single ASC measurements, our results are comparable.

	Literature (°C) [25]	PPP (°C)	PRP (°C)
First transition	51.7	48.7	47.9
Second transition	63.8	61.6	59.4
Third transition	70.3	67.1	68.4

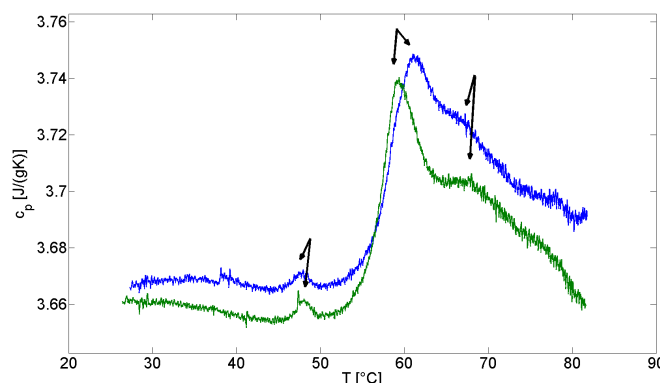


Figure 7.3: Thermogram of blood plasma without platelets (blue) and of blood plasma with platelets (green). The denaturation temperature shifts to lower temperatures because of the decrease in ions. The graphs are shifted vertically to visualise the shift in temperature.

the big experiment and an idea about the origin of the denaturation peak is given. Secondly, a slight shift between platelets rich (green) and platelets poor (blue) plasma is observed. Blood platelets are important in human plasma when dealing with coagulation. Together with several other clotting-factors, they make sure that when catching a wound, it will be staunched. Further, platelets are also used to handle several serious diseases such as cancer, disorders in the blood and so on. Having platelets in the body is clearly an important issue. As seen in the measurements, the loss of platelets does not suppress any peak: a denaturation still occurs. Nevertheless, a shift in temperature is observed but still lies between the normal deviation of the blood plasma composition.

7.4 Albumin

The main peak in the observed thermogram is linked to the denaturation of the albumin. Some additional experiments took place to investigate the origin of the shift observed in PPP compared to PRP.

7.4.1 The influence of the environment based on the literature

The shift in the main peak between PPP and PRP is possibly caused by the interaction between albumin and the proteins, as described in the 'interactome' process above. The denaturation temperature of a protein is dependent on the environment and their mutual interaction. The PPP has been produced by two centrifugations. Before the second (and fast) centrifugation, a foamy white film containing some lipids, has been removed. This results in a different environment for the proteins in the PPP and the PRP which may influence the denaturation temperature. The interactions between the ligands and the proteins in the plasma change the protein thermal stability, possible both in a negative and a positive way. For instance, investigations in the bovine serum albumin (BSA) and the anilinonaphtalene sulphonate (ANS) interactions took place [15]. The binding of ANS to BSA first increases the thermal stability and the thermostability increase as a function of the concentration. At higher proportions of ANS, the interaction results in a

decrease in protein stability because of the change in the protein conformation. The surface of the proteins is changed because of the hydrophobic interactions. Another experiment [28] deals with the interaction between human serum albumin (HSA) and several ligands. The change in structure observed is caused by crystal packing forces, resulting in a limit in the solvent accessibility. This interaction influences the protein before placing it in a solution. The ligand participates in a hydrophobic interaction, resulting in the change observed in the thermogram. Studies during the years proved the greater affinity of albumin to small, hydrophobic molecules. One group of these molecules are fatty acids, which can be found in the human plasma. So in general, the interaction between a ligand and a protein is different for each ligand and each protein and depends on the concentration and the environment. Similar to the main peak (caused by albumin), a shift in the denaturation temperature of the first peak is observed. This shift is linked to the interaction between the protein (fibrinogen) and their ligands. To obtain a platelet aggregation, fibrinogen needs to bind to its membrane receptor, called glycoprotein. This interaction is important to give the platelets the possibility to control the loss of blood. Finally, a third denaturation shift is observed in the peak assigned to the antibody immunoglobulin G (IgG). IgG is the main antibody isotype found in blood and controls infections in the body. This protein, contained in plasma, interacts with several ligands such as protein A and protein G [75].

7.4.2 The influence of the environment based on ASC experiments

The main transition observed around 60 °C and caused by the denaturation of albumin, is looked more in detail based on some additional experiments done with ASC. Albumin is measured in several environments to find out the motivation of the shift observed between the PRP and the PPP thermogram. The results of these measurements are presented in Figure 7.4. All samples contain bovine serum albumin (BSA). The first sample is a solution of BSA dissolved in water (pH=7). The second is an albumin-HEPES solution (pH=7.4), HEPES is the buffer which is also used in the production of the lipid membranes (as explained in Chapter 4). The pH of this solution is the same as the pH of plasma, which should give the best similarity, keeping in mind the difference occurring because of using BSA instead of HSA. The last solution is an albumin-saline solution, with a pH of 8. Data of the different solutions, together with the data of the blood plasma, are listed in Tabel 7.2. Besides the acidity, also the amount of ions (salts) of the solutions are listed.

Influence of the environment As explained before, the environment of proteins influences the denaturation. Shifting the pH from 7 to 7.4 results into a clearly increase in denaturation temperature. Increasing the pH even more, to pH=8, decreases the transition temperature. So no clear trend is visible in the pH-dependency. Looking to the amount of ions, an increase in denaturation temperature is observed by increasing the amount of ions. This trend is verified by all the albumin-solutions. The blood plasma, both PPP and PRP do not follow this trend, nevertheless, due to the change in ions, the transition temperature is changed. The change of the transition temperature as a function of ionic strength shows that electrostatic interactions influence the stability of the proteins. Early experiments by Ipsen et al. [12] verify this dependency. Furthermore, Ipsen et al. prove that the thermal stability of the proteins is dependent on the scanning rate. This kinetic influence is not explained more in detail in this thesis, more information can be found in papers of Ipsen et al. [12] and Sahini et al. [61]. Going back to the pH dependency, this experiment showed a pH-dependency with a minimum stabilisation at pH=7. It is possible that a maximum stability is also observed in our plasma samples (in the vicinity of 7.4), which could explain the trend of the pH-dependency.

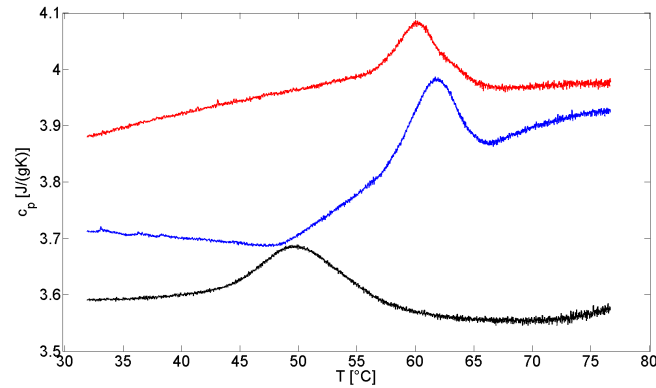


Figure 7.4: The temperature evolution of the specific heat capacity of three albumin-solutions: albumin solved in water (black) with pH=7, HEPES (blue) with pH=7.4, and saline (red) with pH=8. A shift in denaturation temperature is visible, depending on the environment. Both the influence of the pH and the ions are investigated. In the water-solution no ions are present, in the HEPES-solution more ions are observed compared to the saline-solution (see Table 7.2).

Table 7.2: Data of the albumin-solutions, compared to the blood plasma. The ions present in the blood plasma are the ions added during the preparation of the PPP and PRP plasmas. The seventh line, marked by 'other' presents the ions that are contained in the blood plasma by nature [11].

	water	HEPES	saline		blood plasma
pH	7	7.4	8		7.4
Tris/HEPES (mM)	–	10	50		0
Na ⁺ (mM)	–	150	138		3 · 110
K ⁺ (mM)	–	0	2.7		0
Cl [–] (mM)	–	150	140.7		0
(C ₆ H ₅ O ₇) ^{3–} (mM)	–	0	0		110
other (mM)	–	0	0		227.6
Total ions (mM)	–	300	281.4		687.6
Phase transition (°C)	50.0	61.9	60.0		59.1 - 60.7

Despite dealing with BSA instead of HSA, comparing the data of blood plasma and the albumin-solutions is worth the effort. Based on the acidity, blood plasma is on par with the HEPES solution. Nevertheless, the transition peaks of both samples are not equivalent in temperature. The denaturation temperature of the HEPES solution is higher compared to the blood plasma. This indicates that another parameter should influence the transition temperature. That reason, the influence of the amount of ions to the blood plasma is compared. The amount of ions of the HEPES and the saline solution are comparable and much higher compared to the ion-less water. The amount of ions in blood plasma are much higher than the buffer-solutions, this because of the contribution of the ions present in the blood plasma by nature. Although, the denaturation temperatures are clearly influenced by the addition of ions which proves the importance of the ions. Ignoring the blood plasma, an increase in denaturation temperature is observed with an increasing amount of ions. Leaving this blood plasma behind is meaningful because no extra information is known about the production of the blood plasma. The Ca^{2+} binding with the citrate can for instance change the concentration. Anyhow, a clear change in the denaturation temperature is visible, proving that the denaturation of proteins is depending on the ions, and in more general, on the environment.

In general, the shape of the peak and the transition temperature of the albumin-solutions in buffer (HEPES and saline), do not change remarkably compared to the human plasma. This confirms the fact that the main transition peak in the thermogram of the human plasma is coming from the albumin. The small deviation of the main peak observed in the plasma is linked to the environment dependency (the pH and the amount of ions) and the differences in HSA and BSA.

Denaturation of the protein By heating the blood plasma, denaturation (the destruction of the secondary structure and the reorientation of the side-chains) occurs, characterised by the peak in the thermogram as visible in Figure 7.4. The denaturation of the albumin-solutions are characterised by a simple two-state transition. All three solutions are dealing with a higher specific heat capacity after the transition. So the denatured protein has a higher heat capacity compared to the native state. This change in heat capacity is linked to the protein unfolding. Hydration of side-chains of the proteins are broken and added to the solvent in the denatured state. So more heat is required to raise the temperature of albumin in a solution with the unfolded protein, compared to the solution with a folded protein [15].

7.5 Conclusion

Blood plasma of both healthy and sick persons are investigated in this chapter. Human plasma contains a lot of different proteins that denature each at their particular temperature, which is present in the thermogram. The main peak seems to occur thanks to the denaturation of albumin. The shape of the thermogram and the denaturation temperatures of the different proteins change depending on some interactions and the environment. Some experiments on blood plasma, both PPP and PRP, took place by ASC and confirm the results of the literature, mostly based on DSC. ASC is then a useful and reliable technique to detect the denaturation of proteins. Although the investigation in the Master's thesis is rather short, in such a way a lot of possibility for further investigation is still present. Further investigation is possible to obtain more information about the influence of the environment, such as the ions present and the pH level of the solution. Also the influences of the interactions between the large amount of proteins are worth the investigation, as well as the kinetic influence on the thermal stability of the proteins.

Chapter 8

Conclusion

Several biomolecular systems are investigated by using Peltier-element based adiabatic scanning calorimetry. Due to the many advantages of this technique, a good analysis of the biomolecular system is possible. The temperature evolution of the specific heat capacity and the enthalpy is determined and analysed with success: a high temperature resolution is obtained. Because of this resolution, several phase transitions are determined, giving more insight in biomolecular systems. The first biomolecular system investigated is the lipid bilayer membrane. Based on pASC, a lot of measurements took place, observing several phase transitions. Based on these transitions, many insights are gained into the lipid structure, possibly linked to its biological function. Because of dealing with several types of lipid molecules in the body, the investigations are enlarged to lipid binary mixtures. The influence of an additional lipid is remarkable and indicates more complex phases, such as the two-phase regions observed. Investigations based on tertiary mixture give the possibility to further research and to expand the experiments done in this Master's thesis. Further the influence of cholesterol in the human body on the lipid bilayer is investigated. Cholesterol is a common and useful lipid, observed in the human body. Because of its rather special geometrical structure, the behaviour of the pure lipids is influenced. Because of dealing with a cholesterol-lipid system, the properties of the lipid membrane are changed, influencing the biological functions of the membrane. Changing these properties possibly results into serious health problems. To include several biomolecular systems together, human blood plasma, containing both lipids and proteins, is investigated. The pASC measurements on these samples result into a thermogram, providing a lot of information about human health. Because of the superposition of all components present, a detailed analysis occurs, revealing insight in both healthy and diseased plasma. These investigations can be used as a first observation of several diseases such as cancer.

Bibliography

- [1] Blood plasma http://en.wikipedia.org/wiki/Blood_plasma, April 2014.
- [2] Blood <http://en.wikipedia.org/wiki/Blood>, April 2014.
- [3] Calorimetry - publication list https://fys.kuleuven.be/atf/Research_themes/rt_calorimetry/rt_calorimetry_references, March 2014.
- [4] Hard condensed matter <http://www.physics.georgetown.edu/research/hard-condensed-matter>, March 2014.
- [5] Lipid bilayers and cell membranes <http://www.uic.edu/classes/phys/phys450/MARKO/N016.html>, May 2014.
- [6] Natural sterols, cholesterol http://avantilipids.com/index.php?option=com_content&view=article&id=4%01&Itemid=162&catnumber=700000, May 2014.
- [7] What is plasma? <http://www.urmc.rochester.edu/Encyclopedia/Content.aspx?ContentTypeID=160&ContentID=37>, March 2014.
- [8] R. A. L. Jones. *Soft condensed matter*. Oxford University Press, New York, seventh edition, 2003.
- [9] N. L. Anderson and N. G. Anderson. High resolution two-dimensional electrophoresis of human plasma proteins. *Proceedings of the National Academy of Sciences of the United States of America*, 74:5421–5425, 1977.
- [10] N. L. Anderson and N. G. Anderson. A two-dimensional gel database of human plasma proteins. *Electrophoresis*, 12:883–906, 1991.
- [11] R. J. Beckett. An aqueous metal bicarbonate solution and method of use <http://www.google.com/patents/W01998041218A1?cl=en>, May 2014.
- [12] A. Beldarraín, Y. Cruz, O. Cruz, M. Navarro, and M. Gil. Purification and conformational properties of a human interferon alpha2b produced in *Escherichia coli*. *Biotechnology and Applied Biochemistry*, 33(3):173–182, 2001.
- [13] P. F. Brevet and H. H. Girault. *Optical SHG measurements of amphiphiles at liquid/liquid interfaces*. Springer, first edition, 1997.
- [14] G. Bruylants, J. Wouters, and C. Michaux. Differential scanning calorimetry in life science: thermodynamics, stability, molecular recognition and application in drug design. *Current Medicinal Chemistry*, (17).

- [15] M. S. Celej and G. G. Fidelia. Protein stability induced by ligand binding correlates with changes in protein flexibility. *Protein Science*, 12:1496–1506, 2003.
- [16] W. W. Christie. What is a lipid? <http://lipidlibrary.aocs.org/Lipids/whatlip/index.htm>, November 2013.
- [17] Mayo Clinic. Diseases and conditions of lyme disease <http://www.mayoclinic.org/diseases-conditions/lyme-disease/basics/symptoms/con-20019701>, May 2014.
- [18] B. R. Copeland and H. M. McConnell. The rippled structure in bilayer membranes of phosphatidylcholine and binary mixtures of phosphatidylcholine and cholesterol. *Biochimica et Biophysica Acta*, 599(1):95–109, 1980.
- [19] George Cordoyiannis, Chandra Shekhar Pati Tripathi, Christ Glorieux, and Jan Thoen. Order of phase transitions and tricriticality in mixtures of octyloxycyanobiphenyl and nonyloxycyanobiphenyl liquid crystals: A high-resolution study by adiabatic scanning calorimetry. *Phys. Rev. E*, 82(3):031707, 2010.
- [20] H. G. Dobereiner, J. Kas, D. Noppl, I. Sprenger, and E. Sackman. Budding and fission of vesicles. *Biophysical Journal*, 65(4):1396–1403, 1993.
- [21] M. Eeman and M Deleu. From biological membranes to biomimetic model membranes. *Biotechnology, Agronomy, Society and Environment*, 14(4):719–736, 2009.
- [22] T. N. Estep, D. B. Mountcastle, R. L. Biltonen, and T. E. Thomson. Studies on the anomalous thermotropic behavior of aqueous dispersions of dipalmitoylphosphatidylcholine-cholesterol mixtures. *Biochemistry*, 17(10):1984–1989, 1978.
- [23] N. C. Garbett, C. S. Mekmaysy, C. W. Helm, A. B. Jenson, and J. B. Chaires. Differential scanning calorimetry of blood plasma for clinical diagnosis and monitoring. experimental and molecular pathology. *Experimental and Molecular Pathology*, 86:186–191, 2009.
- [24] N. C. Garbett, M. L. Merchant, J. B. Chaires, and J. B. Klein. Calorimetric analysis of the plasma proteome: identification of type 1 diabetes patients with early renal function decline. *Biochimica et Biophysica Acta*, 1320:4675–4680, 2013.
- [25] N. C. Garbett, J. J. Miller, A. B. Jenson, and J. B. Chaires. Calorimetry outside the box: A new window into the plasma proteome. *Biophysical Journal*, 94(4):1377–1383, 2008.
- [26] A. Genz, J. F. Holzwarth, and T. Y. Tsong. The influence of cholesterol on the main phase transition of unilamellar dipalmytoylphosphatidylcholine vesicles. A differential scanning calorimetry and iodine laser T-jump study. *Biophysical Journal*, 50(6):1043–1051, 1986.
- [27] P. Gill, T. T. Moghadam, and B. Ranjbar. Differential scanning calorimetry techniques: Applications in biology and nanoscience. *Journal of Biomolecular Techniques*, 21(4):167–193, 2010.
- [28] X. M. He and D. C. Carter. Atomic structure and chemistry of human serum albumin. *Nature*, 358:209–215, 1992.
- [29] T. Heimburg. *Thermal Biophysics of Membranes*. Wiley-VCH, Weinheim, 2007.
- [30] L. S. Hirst, P. Uppamoochikkal, and C. Lor. Phase separation and critical phenomena in biomimetic ternary lipid mixtures. *Liquid Crystals*, 38(11-12):1735–1747, 2011.

- [31] J. Hjort Ipsen, G. Karlstrom, O. G. Mouritsen, H. Wennerstrom, and M. J. Zuchermann. Phase equilibria in the phosphatidylcholine-cholesterol system. *Biochimica et Biophysica Acta*, 905(1):162–172, 1987.
- [32] F. R. Julicher and R. Lipowsky. Domain-induced budding of vesicles. *Physical Review Letters*, 70(19):2964–2967, 1993.
- [33] A. Kamps. How do LDL and HDL differ structurally and functionally? <http://healthyeating.sfgate.com/ldl-hdl-differ-structurally-functionally-2003.html>, June 2013.
- [34] J. J. Kelly. Review of thermodynamics. Technical report, University of Maryland, 2002.
- [35] D. P. Kharakoz, M. S. Panchelyuga, E. I. Tiktopulo, and E. A. Shlyapnikova. Critical temperatures and critical chain length in saturated diacylphosphatidylcholines: 20 calorimetric, ultrasonic and Monte Carlo simulation study of chain-melting/ordering in aqueous lipid dispersions. *Chemistry and Physics of Lipids*, 150(2):217–228, 2007.
- [36] Dr. Rumiana Koynova and Dr. Boris Tenchov. Phase transitions and phase behavior of lipids <http://www.springerreference.com/docs/html/chapterdbid/319207.html>, March 2014.
- [37] J. Leys, P. Losada-Pérez, E. Slenders, C. Glorieux, and J. Thoen. Investigation of the melting behavior of the reference materials biphenyl and phenyl salicylate by a new type adiabatic scanning calorimeter. *Thermochemica Acta*, 582:68–76, 2014.
- [38] D. Liden and J. Walker. What are the functions of lipids in the body? <http://www.wisegeek.com/what-are-the-functions-of-lipids-in-the-body.htm>, December 2013.
- [39] L. A. Liotta and E. F. Perticoiu. Serum peptidome for cancer detection; spinning biologic trash into diagnostic gold. *The journal of clinical investigation*, 116(1):26–30, 2006.
- [40] E. Lloyd. An introduction to protein molecules: The building blocks of life <http://www.brighthub.com/science/medical/articles/6050.aspx>, May 2014.
- [41] P. Losada-Pérez, K. L. Jiménez-Monroy, B. van Grinsven, J. Leys, S. D. Janssens, M. Peeters, C. Glorieux, J. Thoen, K. Haenen, W. De Ceuninck, and P. Wagner. Phase transitions in lipid vesicles detected by a complementary set of methods: heat-transfer measurements, adiabatic scanning calorimetry, and dissipation-mode quartz crystal microbalance. *Physica Status Solidi (a)*, page Published online, 2014.
- [42] P. Losada-Perez, N. Mertens, B. De Medio-Vasconcelos, E. Slenders, J. Leys, M. Peeters, B. van Grinsven, J. Gruber, C. Glorieux, J. Thoen, and P. Wagner. Phase behavior of binary lipid mixtures: a combined study by adiabatic scanning calorimetry and quartz crystal microbalance with dissipation. 2014.
- [43] Patricia Losada-Pérez, Chandra Shekhar Pati Tripathi, Jan Leys, Claudio A. Cerdeiriña, Christ Glorieux, and Jan Thoen. The Yang–Yang anomaly in liquid–liquid criticality: Experimental evidence from adiabatic scanning calorimetry. *Chem. Phys. Lett.*, 523:69–73, 2012.
- [44] H. Lowen, M. Watzlawek, C. N. Likos, M. Schmidt, A. Jusufi, J. Dzubiella, C. von Ferber, E. Allahyarov, A. Thuneman, and I. D’Amico. The hard physics of soft matter. *Advances in Solid State Physics*, 40:809–817, 2000.

- [45] S. Mabrey, P. L. Mateo, and J. M. Sturtevant. High-sensitivity scanning calorimetric study of mixtures of cholesterol with dimyristoyl- and dipalmitoylphosphatidylcholines. *Biochemistry*, 17(12):2464–2468, 1978.
- [46] S. Mabrey and J. M. Sturtevant. Investigation of phase transitions of lipids and lipid mixtures by high sensitivity differential scanning calorimetry. *Proceedings of the National Academy of Sciences of the United States of America*, 73(11):3862–3866, 1976.
- [47] S. Mabrey and J. M. Sturtevant. Investigation of phase transitions of lipids and lipid mixtures by sensitivity differential scanning calorimetry. *Proceedings of the National Academy of Sciences of the United States of America*, 73(11):3862–3866, 1976.
- [48] S. Marcelja. Chain ordering in liquid crystals. 1. even-odd effect. *The Journal of Chemical Physics*, 60(1):3599–3604, 1974.
- [49] R. McElhany. The use of differential scanning calorimetry and differential thermal analysis in studies of model and biological membranes. *Chemistry and Physics of Lipids*, 30:229–259, 1982.
- [50] T. P. W. McMullen, R. N. A. H. Lewis, and R. N. McElhany. Differential scanning calorimetric study of the effect of cholesterol on the thermotropic phase behavior of a homologous series of linear saturated phosphatidylcholines. *Biochemistry*, 32(2):516–522, 1993.
- [51] T. P. W. McMullen and R. N. McElhany. New aspects of the interaction of cholesterol with dipalmitoylphosphatidylcholine bilayers as revealed by high-sensitivity differential scanning calorimetry. *Biochimica et Biophysica*, 1234(1):90–98, 1995.
- [52] H. Mehling and L. F. Cabeza. *Heat and cold storage with PCM*. Springer Verlag, Berlin, 2008.
- [53] G. Milano, T. Kawakatsu, and A. De Nicola. A hybrid particle–field molecular dynamics approach: a route toward efficient coarse-grained models for biomembranes. *Physical Biology*, 10(4):1–16, 2013.
- [54] O. G. Mouritsen. *Life - As a matter of fat*. Springer, Berlin, 2000.
- [55] R. Nave. PvT surface for a substance which contracts upon freezing <http://hyperphysics.phy-astr.gsu.edu/hbase/thermo/pvtsur.html>, November 2013.
- [56] T. X. O’Connell, T. J. Horita, and B. Kasravi. Understanding and interpreting serum protein electrophoresis. *American Family Physician*, 71(1):105–112, 2005.
- [57] C. E. Ophardt. Denaturation of proteins <http://www.elmhurst.edu/~chm/vchembook/568denaturation.html>, April 2014.
- [58] A. Raudino, M. Grazia Sarpietro, and M. Pannuzzo. The thermodynamics of simple biomembrane mimetic systems. *Journal of Pharmacy and Bioallied Sciences*, 3(1):15–38, 2011.
- [59] D. J. Recktenwald and H. M. McConnell. Phase equilibria in binary mixtures of phosphatidylcholine and cholesterol. *Biochemistry*, 20(15):4505–4510, 1981.
- [60] L. Robles, D. Mondieig, Y. Haget, and M. A. Cuevas-Diarte. Review on the energetic and crystallographic behaviour of n-alkanes. ii. series from C₂₂H₄₆ to C₂₇H₅₆. *Journal de Chimie Physique et de Physico-Chimie Biologique*, 95(1):92–111, 1998.

- [61] V. E. Sahini, G. Csire, C. Popa-Tilimpea, and A. Tirsoaga. Kinetic study of the pH influence on bsa thermal denaturation. *Analele Universitatii Bucuresti*, pages 127–132, 2002.
- [62] D. V. Schroeder. *An introduction to Thermal Physics*. Addison Wesley Longman, United States, first edition, 2000.
- [63] E. J. Shimshick and H. M. McConnell. Lateral phase separations in binary mixtures of cholesterol and phospholipids. *Biochemical and Biophysical Research Communications*, 17(2):446–451, 1973.
- [64] E. B. Sirota, H. E. King, D. M. Singer, and H. H. Shao. Rotator phases of the normal alkanes: An x-ray scattering study. *Journal of Chemical Physics*, 98(7):5809–5824, 1993.
- [65] E. B. Sirota and D. M. Singer. Phase transitions among the rotator phases of the normal alkanes. *American Institute of Physics*, 101(12):10873–10882, 1994.
- [66] P. F. Sullivan and G. Seidel. Steady-state, ac-temperature calorimetry. *Physical Review*, 173(3):679–685, 1968.
- [67] J. Thoen. Adiabatic scanning calorimetric results for the blue phases of cholesteryl nonanoate. *Phys. Rev. A*, 37(5):1754–1759, 1988.
- [68] J. Thoen. High resolution adiabatic scanning calorimetry and heat capacities. In E. Wilhelm and T. M. Letcher, editors, *Heat capacities: liquids, solutions and vapours*, pages 287–306. The Royal Society of Chemistry, London, 2010.
- [69] J. Thoen, G. Cordoyiannis, and C. Glorieux. Investigations of phase transitions in liquid crystals by means of adiabatic scanning calorimetry. *Liquid Crystals*, 36(6-7):669–684, 2009.
- [70] J. Thoen, H. Marynissen, and W. Van Dael. Temperature dependence of the enthalpy and the heat capacity of the liquid-crystal octylcyanobiphenyl (8CB). *Phys. Rev. A*, 26(5):2886–2905, 1982.
- [71] H. van der Hoorn. Waterkoeling en casemodding guide, deel 2 [http://tweakers.net/reviews/258/2/waterkoeling-en-casemodding-guide-deel-2-werking-peltier-\(1\).html](http://tweakers.net/reviews/258/2/waterkoeling-en-casemodding-guide-deel-2-werking-peltier-(1).html), March 2014.
- [72] B. Van Roie. *Studie van faseovergangen in complexe vloeistoffen en vloeibare kristallen met Adiabatische Scanning Calorimetrie*. PhD thesis, Laboratorium voor Akoestiek en Thermische Fysica, Departement Natuurkunde en Sterrenkunde, Katholieke Universiteit Leuven, 2005.
- [73] M. R. Vist and J. H. Davis. Phase equilibria of cholesterol/dipalmitoylphosphatidylcholine mixtures: deuterium nuclear magnetic resonance and differential scanning calorimetry. *Biochemistry*, 29(2):451–464, 1990.
- [74] WebMD. Diabetes health center <http://www.webmd.com/diabetes/tc/symptoms-of-high-blood-sugar-topic-overview>, May 2014.
- [75] L. Yang, M. E. Biswas, and P. Chen. Study of binding between protein A and immunoglobulin G using a surface tension probe. *Biophysical Journal*, 84(1):509–522, 2003.
- [76] U. Zammit, M. Marinelli, F. Mercuri, and S. Paoloni. Analysis of the order character of the RII-RI and the RI-RV rotator phase transitions in alkanes by photopyroelectric calorimetry. *The Journal of Physical Chemistry B*, 114(24):8134–8139, 2010.

DEPARTEMENT NATUURKUNDE EN STERRENKUNDE

Celestijnenlaan 200d bus 2412
3001 HEVERLEE, BELGIË
tel. + 32 16 32 71 24
fys.kuleuven.be

